

# TreeBio - Preliminary study on traceability of tree logs using digital log end images

## Masterarbeit

Zur Erlangung des Mastergrades

Diplom-Ingenieur

an der Naturwissenschaftlichen Fakultät der  
Paris-Lodron-Universität Salzburg

Eingereicht von

B.Eng. Rudolf Schraml

Gutachter:

Univ.-Prof. Dr. Andreas Uhl

Fachbereich:

Computerwissenschaften

Salzburg, Juni, 2013

Rudolf Schraml  
Wildmoosweg 13  
A-5020 Salzburg

Hiermit versichere ich, dass ich die von mir vorgelegte Arbeit selbstständig verfasst habe, dass ich die verwendeten Quellen, Internet-Quellen und Hilfsmittel vollständig angegeben habe und dass ich die Stellen der Arbeit – einschließlich Tabellen, Karten und Abbildungen –, die anderen Werken oder dem Internet im Wortlaut oder dem Sinn nach entnommen sind, auf jeden Fall unter Angabe der Quelle als Entlehnung kenntlich gemacht habe.

Salzburg, den 17.Juni 2013

---

Rudolf Schraml

# Acknowledgement

First, I would like to thank my advisor Prof. Andreas Uhl for his patient guidance. He gave me the opportunity to write my master thesis in the field of wood imaging. Nearly a decade after I have finished the higher technical school for forest industry, I got the chance to contribute to the development of a new technology for the wood industry. I am very grateful for his support and for giving me the chance to succeed in all my different endeavours.

Special thanks to Maria for the countless hours of discussions about the sense or non-sense of academic publishing. Without her experience and suggestions for academic writing it would have been more difficult. I would also like to thank Sepp who provided me with the opportunity to focus on this work. Thanks to my friends who always managed to successfully distract me from work – thanks for the unforgettable hours in our beautiful mountains.

Most importantly, I want to say thank you to my parents Franziska and Rudolf Schraml. Your support and encouragement have made everything I have done in the last years possible. As promised seven years ago, I will finish my studies before turning 31 ;-). This work is dedicated to you.

# Abstract

This thesis focuses on the biometric traceability of wood logs. Biometric log traceability is at an early stage and present research treats traceability in the sawmill. State-of-the-art systems use Radio Frequency Identification (RFID) or plastic batches to reach log traceability from forest site to further processing companies. This work is a preliminary study on biometric log traceability using digital log end images. Digital images can be taken at little cost and at almost every stage in the log processing chain. Similar to a human fingerprint or iris the annual ring pattern of a cross-section shows a specific texture pattern containing biometric features.

The study is subdivided into a theoretical and a practical part. In the theoretical part basics of log traceability and biometric systems are considered. Furthermore, a comprehensive literature overview on cross-section imaging and biometric systems in other fields of applications forms the basis for the practical part of this study.

In the practical part an initial scheme for a biometric log recognition framework (TreeBio) is introduced. By treating pith estimation and cross-section segmentation in rough log end images this work contributes to the development of the TreeBio framework. For both tasks, computational approaches and experiments are presented. The practical part highlights the difficulties of biometric log recognition. This makes it possible to present considerations on future work.

**keywords** image analysis, wood logs, log traceability, pith estimation, cross-section segmentation, cross-section analysis

# Zusammenfassung

Diese Masterarbeit beschäftigt sich mit der Rückverfolgbarkeit von Holzstämmen. Vorhandene Methoden, die sich mit der biometrischen Rückverfolgbarkeit von Holzstämmen beschäftigen, befinden sich noch im Entwicklungsstadium und beschränken sich auf die Rückverfolgbarkeit im Sägewerk. Diese Arbeit ist eine vorausgehende Studie, die sich mit biometrischer Rückverfolgbarkeit anhand digitaler Bilder von Holzstammenden beschäftigt. Bilder von Holzstammenden können fast überall in der Verarbeitungskette kostengünstig erfasst werden.

Die vorliegende Studie behandelt das Thema theoretisch sowie in praktischer Hinsicht. Im praktischen Teil wird das Thema "Rückverfolgbarkeit von Baumstämmen" bearbeitet und theoretische Grundlagen von biometrischen Systemen werden behandelt. Eine Literaturliste über Bildverarbeitungsmethoden zur Querschnittanalyse von Holzstämmen und Biometrischen Systemen in anderen Anwendungsgebieten bildet die Grundlage für die Überlegungen im praktischen Teil der Studie.

Im praktischen Teil wird ein biometrisches Framework (TreeBio) schematisch skizziert. Diese Studie trägt zur Entwicklung des TreeBio Frameworks bei, indem Lösungen und Experimente zur Mittenerkennung und Querschnittsegmentierung präsentiert werden. Die Experimente zeigen praktische Probleme auf. Dies macht es möglich Überlegungen bezüglich weiterer Entwicklungsschritte zu präsentieren.

# Contents

<b>1</b>	<b>Introduction</b>	<b>1</b>
1.1	Research gap . . . . .	3
1.1.1	Contributions . . . . .	4
<b>I</b>	<b>Theoretical Background</b>	<b>5</b>
<b>2</b>	<b>Traceability of wood logs</b>	<b>6</b>
2.1	Traceability definition . . . . .	6
2.2	Log supply chain - LSC . . . . .	6
2.3	Traceability methods . . . . .	7
2.3.1	Manual labels . . . . .	7
2.3.2	Badge labels . . . . .	8
2.3.3	Transponders . . . . .	8
2.4	Biometric systems . . . . .	10
2.4.1	System characteristics and classification categories . . . . .	10
2.4.2	System performance . . . . .	13
2.4.3	Biometric systems in other fields of applications . . . . .	15
2.4.3.1	Recognition of animals . . . . .	15

<i>CONTENTS</i>	IV
2.4.3.2	Recognition/ classification of plants, fruits or vegetables . . . 18
2.4.3.3	Recognition of industrial products and goods . . . . . 19
2.5	Research on biometric recognition of logs . . . . . 23
<b>3</b>	<b>Log image processing</b> . . . . . <b>26</b>
3.1	Wood basics . . . . . 27
3.1.1	Wood anatomy . . . . . 27
3.1.2	Wood - measurement and grading . . . . . 30
3.1.2.1	Wood properties . . . . . 30
3.1.2.2	Log measurement and grading . . . . . 31
3.2	Cross-section analysis . . . . . 32
3.2.1	Pith estimation . . . . . 33
3.2.1.1	Literature Overview . . . . . 33
3.2.2	Annual ring analysis . . . . . 38
3.2.2.1	Literature Overview . . . . . 38
3.2.3	Further literature on cross section analysis . . . . . 44
3.2.3.0.1	Further wood properties: detection and analysis . . . 48
<b>II</b>	<b>Implementation</b> . . . . . <b>49</b>
4	TreeBio framework . . . . . 50
5	Pith estimation . . . . . 53
5.1	Local Fourier Spectra analysis of annual ring blocks . . . . . 55
5.1.1	Local orientation estimation . . . . . 55

5.1.2	Fourier Spectra of annual ring sections . . . . .	55
5.1.3	Fourier Spectrum analysis methods . . . . .	57
5.1.3.1	Fourier Spectrum Preprocessing . . . . .	57
5.1.3.2	Peak Analysis - PA . . . . .	58
5.1.3.3	Least Squares Regression - LSR . . . . .	58
5.1.3.4	Weighted Least Squares Regression - WLSR . . . . .	59
5.1.3.5	Principal Component Analysis - PCA . . . . .	59
5.2	Pith estimation algorithms . . . . .	60
5.2.1	Block area selection - BAS . . . . .	60
5.2.2	Pointwise block selection - PBS . . . . .	61
5.3	Experiments . . . . .	63
5.3.1	Image test sets . . . . .	64
5.3.2	CT-IS experiments . . . . .	65
5.3.3	RLE-IS experiments . . . . .	67
5.4	Summary . . . . .	71
<b>6</b>	<b>Cross-section segmentation</b>	<b>72</b>
6.1	Histogram thresholding of cross-section images . . . . .	74
6.2	Texture analysis of cross-sections . . . . .	76
6.2.1	Texture analysis . . . . .	76
6.2.2	Cross-Section texture . . . . .	76
6.3	Theoretical Background . . . . .	78
6.3.1	Intensity Histograms . . . . .	78
6.3.2	Local Binary Patterns (LBPs) . . . . .	78

<i>CONTENTS</i>	VI
6.3.3 Histogram Distances . . . . .	81
6.4 Cross-section segmentation algorithm . . . . .	83
6.4.1 Seed block selection . . . . .	84
6.4.2 Cluster growing algorithm . . . . .	85
6.4.2.1 Cluster initialisation . . . . .	85
6.4.2.2 Growing procedure . . . . .	86
6.4.3 Shape estimation . . . . .	88
6.5 Experiments . . . . .	90
6.6 Summary . . . . .	99
<b>7 Discussion</b>	<b>101</b>

# Chapter 1

## Introduction

The timber-industry is among the top 10 industries measured by its industrial output in Austria. Consequently high amounts of wood have to be felled each year. Forests cover about 50 % of Austria's landscape and the Austrian forest law (§1 Sustainability - [www.ris.bka.gv.at](http://www.ris.bka.gv.at)) guarantees that the annual growth of wood has to be higher than the annual felling amount. Despite this precondition of sustainable forest management, it is prodigious that in 2010 - 17,82 million cubic-meter wood were felled. Alone the Austrian Forestry Service ([www.bundesforste.at](http://www.bundesforste.at)) (OBF) felled about 1,82 million cubic meter. Symbolically the annual felling amount of 2010

	2005	2006	2007	2008	2009	2010
total	16.5	19.1	21.3	21.8	16.7	17.8
softwood	85 %	85 %	87 %	87 %	84 %	86 %
hardwood	15 %	15 %	13 %	13 %	16 %	14 %

**Table 1.1:** Annual felling amounts in million cubic - metre

would equal 7,9 million wood stems where each stem would have a diameter of 30 cm and a length of 8 metre. 28% of the total felling were destructed or damaged wood and the softwood proportion on the total felling was 86%. On average 50% were processed by sawmills and further 17,5% were processed by other wood processing industries. Every year 2/3 of the annual felling are exported and about 7 million cubic-metre wood are imported additionally. This import-export activity leads to a high logistical effort. Round wood cubic-metre prices are between 35 and 90 Euro. Consequently, the traceability of each cubic-metre wood becomes very important for the involved companies. Also social aspects of traceability have become more important in the last twenty years. In times of rain-wood clearings, illegal loggings and

the ecological rethinking environmental sustainability increased in importance. So-called wood certificates are a must have for all end-sellers. Customers are very sensitive and sustainability certificates like Pan European Forest Certification ([www.pefc.at](http://www.pefc.at)) (PEFC) and Forest Stewardship Council ([www.fsc.org](http://www.fsc.org)) (FSC) can be found on nearly all timber products. Especially in East Asia and the Pacific region, the prevention of illegal logging combines social and economical aspects as nowhere else (Dykstra et al., 2003).

With respect to the above stated certificates the term Chain of Custody (CoC) has to be mentioned. CoC is the process that provides traceability through the complete wood supply chain (Dykstra et al., 2003). In difference to the whole CoC this thesis deals with traceability at the beginning of the wood supply chain and is restricted to the Log Supply Chain (LSC) (see section 2.2).



(a) Pan european forest certificate (PEFC)



(b) Forest stewardship council (FSC)

**Figure 1.1:** Sustainability certificates

Currently used traceability systems make it necessary to use traceability methods where each log is physically marked. Dykstra et al. (2003) described traceability methods that are qualified to enable wood tracking. Current used traceability methods can be classified into three groups. The first group incorporates the set of **Manual labels** where identification labels are applied manually. Here spray-cans, knives, hammers or chalk are used to apply a marking. Depending on the kind of freehand label it is possible to assign additional data in form of digital information or paper documents to each log. Due to the simpleness **Manual Labels** are commonly used by forest smallholders and for traceability systems that are not highly industrialised. The second group of methods involves all kinds of plastic, paper and metal labels and is called **Badge labels**. Predominantly badges are made of plastic and can be printed with bar-codes, numbers and logos. Unlike Manual Labels, scanners can read **Badge Labels** and guarantee automation and industrial usage. **Transponders** belong to the third group and involve all kinds of transponders than can be applied on a wood log. Nowadays industrial LSC traceability systems making use of RFID transponders are state-of-the-art. RFID transponders can be scanned without visual contact to the transponder and they are much more secure against

counterfeits in comparison to the other methods.

The Indisputable Key project (2006 - 2010 Uusijärvi (2010b)) searched for possibilities to provide traceability through the CoC. Therefore the research group enhanced the RFID method to fulfil the requirements of the LSC. In order to close the traceability gap that arises in the sawmill when the logs are cut, a second traceability method allowing to print 2D codes on wood surfaces has been developed. At the same time, the Fraunhofer Institute presented new transponders that mainly consist of lignin (Fraunhofer, 2010). Lignin is an integral part of the wood structure. Commonly transponders have to be removed before the logs are further processed in the sawmill. Lignin transponders include a minimal metal concentration that is not problematic for further processing.

Dykstra et al. (2003) already mentioned chemical and genetic fingerprint methods to examine the genetic and chemical composition of a material. The authors expected that these methods could be available within 3 - 10 years. From 2003 to 2008 the Lulea University of Technology presented several biometric approaches which relied on the assumption that logs have separate identities with unique biometric features (see Section 2.5). In these works traceability for wood logs within the sawmill were presented. Therefore 2D and 3D scanners were used to extract geometric wood properties. Another approach used Computer Tomography (CT) scanners to enable traceability between wood logs and the cut boards. Here knots were used as biometric features. Beside insufficient recognition rates these methods also require 2D and 3D scanning devices. The usage of Laser, CT, or Multi Resolution Imaging (MRI) scanners at forest sites and other wood processing industries is too complicated and entails high costs. Biometric fingerprint or iris and retina recognition systems are using sensors which are quite cheaper and also smaller. For example Iris images can be simply captured with digital cameras using infra-red light to enhance the texture quality. Thinking of a human fingerprint, the annual ring pattern of a log shows similar features and can also be captured with digital cameras. Perhaps it is possible to use annual ring patterns to develop a biometric log recognition system and further to reach traceability in the LSC.

## 1.1 Research gap

The biometric approaches (see Section 2.5) for traceability use existing equipment, e.g. 2D or 3D scanners, in order to reach traceability in the sawmill. These approaches show too low recognition rates for log traceability and require expensive capturing devices. For traceability in

the LSC a connection between the forest based industries and wood processing industries has to be established. Conventional methods implement marking/reading methods (see Section 2.3) to establish this connection. In order to realize a biometric approach, a biometric characteristic that can be recorded at the forest site as well as in processing companies is required.

Similar as for human recognition using fingerprints, it is assumed that annual ring patterns of wood logs can be used to identify/ recognize wood logs. Images of the log end face can be captured by digital cameras at forest sites and processing companies. Digital cameras are not expensive and do not influence existing process steps. For our research we assume that captured annual ring patterns can be used to extract biometric features of logs. Recognition of wood logs with digital images could then be implemented nearly everywhere in the LSC.

### 1.1.1 Contributions

This master thesis is a preliminary study on biometric log traceability using log end images. The study contributes to the development of a biometric log recognition approach by treating theoretical and practical aspects. The theoretical part of this work creates a solid basis for the considerations on a biometric log recognition framework using log end images. After introducing the components and processes of this framework two required image analysis tasks are considered in detail. For this purpose methods for estimating the pith position and cross-section segmentation in images of rough log ends are presented and examined. Computation of the pith position and the cross-section boundary are required to perform image registration. Image registration is a major task which has to be performed prior to feature extraction. Additionally, the relation between the pith position the cross-section boundary is a biometric feature of a cross-section. By treating pith estimation and cross-section segmentation this study contributes to the development of the biometric framework. To my knowledge, so far no work on cross-section segmentation in rough log end images has been published. Finally, this study presents considerations on future work to promote the further development of the biometric framework.

# PART I

---

## Theoretical Background

The first part of this thesis contains a theoretical work-up which points out several aspects of traceability using biometric characteristics of rough log ends. In Chapter 2 a possible definition for log traceability (Section 2.1) is introduced first and second an overview on common and state-of-the-art traceability methods (2.3) is presented. The chapter concludes with an introduction into biometric systems (Section 2.4) and presents applications and research in other fields of applications (Section 2.4.3) as well as for recognition of logs and sawn boards (Section 2.5). Finally, Chapter 3 first presents an overview on wood basics (Section 3.1) before a literature review on cross-section analysis (Section 3.2) is given.

# Chapter 2

## Traceability of wood logs

### 2.1 Traceability definition

There are various definitions for traceability. Some of these definitions originate from research and are therefore more or less related to a research topic. Others are defined by ISO quality standards and are adapted to the scope of an application. Most of the literature available focuses on part productions and on single companies (Kvarnström and Oghazi, 2008).

Like (Kvarnström and Oghazi, 2008, p.5) we use the definition from Töyrylä (1999) which suits the continuous processes: *"Traceability is the ability to preserve and access the identity and attributes of a physical supply chain's objects."* Kvarnström and Oghazi (2008) introduce the terms "traceability system" and "traceability methods". Thereby the ability of traceability is built up on a traceability system, which uses traceability methods to link process and object data.

### 2.2 Log supply chain - LSC

The above presented definition restricts traceability to the supply chain for predefined objects. Consequently it is necessary to define the process or time span in which traceability of wood logs as objects should be enabled. Päivinen and Lindner (2006) use the term Forest Wood Chain (FWC) to collect processes in which forest resources are converted into services and products. The author's focus is on the assessment of sustainability in Forest-Wood Chains. So Päivinen and Lindner (2006) are aware of the fact, that there are a lot of different FWCs.

In each of these FWCs logs are required as raw material. Logs have to be cut in the forest and transported to a sawmill, pulp mill or another processing company. This sub-chain can easily be defined as a supply chain called LSC. In general the LSC is restricted to the lifetime of a log. This lifetime starts when a single tree is felled and length cut into a number of logs. The lifetime ends when a log is further processed e.g. by cutting and therefore stops existing to be a single object. The term "LSC" indicates the objects and the time span for which we want to enable traceability. It mainly involves forest based and processing industries like sawmills or pulp mills.

## 2.3 Traceability methods

The introduction classifies three groups of traceability methods: Manual Labels, Badge Labels, Transponders. These groups represent current methods used for traceability systems in the LSC. Industry and many small sized companies make use of these methods. It depends on the application of each method if it's possible to identify each object in the supply chain. For sustainability issues it would be sufficient to know the origin of each object. All methods rely on a marking/reading principle and require additional equipment.

### 2.3.1 Manual labels

The simplest and oldest methods are conventional paint (Fig. 2.1b), hammer and chisel labels. While chisel labels are markings that are engraved with knives, conventional paint labels are simply applied with spray cans or chalk. Another method is the use hammers with special stamps to create brands at the log end faces. Although these practices are very old and simple, forest smallholders prefer them. The major advantage of these methods is that they are very cheap and resistant to abrasion and damaging. Normally these methods are used to verify the origin of a log and not to identify it. Depending on the application these methods allow identification of each individual log. There are good solutions which show that these basic methods can be improved for industrial usage. The company Otmetka ([www.otmetka.com](http://www.otmetka.com)) has developed a method where the harvester punches a set of hammer brands on the cross section. This unique punching label is then used as an identity code and can be scanned automatically (Fig. 2.1a). Otmetka enhanced hammer brands to fulfil the requirement of identification of each log.



(a) Punching Label by Otmetka.  
(Image source: [www.otmetka.com](http://www.otmetka.com))



(b) Marking with spray.  
(Photo by Schraml)

**Figure 2.1:** Manual labels

### 2.3.2 Badge labels

The second group of methods uses badge labels, consisting of paper, plastic or metal. These labels can be printed with different varieties of bar-codes, numbers or logos and provide the possibility to integrate additional information. Badges can be applied manually or automatically and are readable via scanning devices. Depending on how these labels are applied on the wood logs, major disadvantages are damages, fall offs and high prices compared to manual labels. In sawmills or pulp-mills metal badges and plastic labels can lead to problems in some processing steps. Therefore plastic badges consisting of a special plastic material are used. These are not detected by metal sensors and dissolve when they come in contact with paper base.



**Figure 2.2:** Plastic badges from Latschbacher. (Image source:[www.signumat.com](http://www.signumat.com))

### 2.3.3 Transponders

This group of labels contains all kind of transponders which can be applied on wood logs. A major advantage is the fact, that transponders transponders can be scanned automatically without having visual contact. Disturbances (e.g. snow or dirtiness) do not influence the scanning quality and additional processing data can be transferred on the transponder. Therefore RFID is used as technology. Data readers can access data stored on a transponder. When a transponder enters the electromagnetic field of a data reader, data can be exchanged by radio

waves. RFID transponders can be active or passive and can be further distinguished by the frequency range they use. Active RFID transponders need a power supply like a battery. Passive ones are non-volatile and do not need any power supply to store data. Passive transponders receive the required submission energy from radio waves via the antenna of the transponder. Depending on the frequency range different reading ranges result. While Low Frequency (LF) transponders have a reading range of a few centimetres, High Frequency (HF) transponders have a reading range up to 1.5 metres. Ultra High Frequency (UHF) transponder reach reading ranges of several metres. Consequently, higher frequencies reach a better reading range and enable bulk reading, but they are more sensitive to dielectric material like metals or liquids (Kvarnström and Oja, 2008).



**Figure 2.3:** Different transponders:

- a)** Nail and Chip LF RFID Transponder. (Image source: Korten and Kaul (2008))
- b)** UHF RFID Transponder presented by Uusijärvi (2010a)
- c)** RFID Transponder in batch format by Latschbacher. (Image Source: [www.signumat.com](http://www.signumat.com))
- d)** Lignin RFID Transponder by Fraunhofer (2010)

The two EU-projects Lineset and Indisputable Key propose RFID transponders in the LSC as traceability method. In the Lineset project the use of LF RFID transponders has been studied and pilot-tested. The image in Fig.2.3 a) shows typical LF RFID tags. Because of higher reading ranges, the Indisputable Key project studied the use of UHF RFID transponders in which a special UHF RFID tag has been designed. These transponders promise higher reading ranges and rates as well as lower costs compared to LF RFID transponders. The most promising transponder with a reading range of 2 meter is shown in Fig. 2.3 b). This

transponder is applied at the cross section. In doing so mechanical damaging is low. Another UHF RFID transponder is shown in Fig. 2.3 c) and is presented as preview by the company Latschbacher in Austria. It promises reading ranges up to 4 metres. It depends on the transponder material and the costs whether it is necessary to remove a transponder before a log is further processed. The Fraunhofer Institute presented a RFID Transponder which mainly consists of lignin. Lignin transponders have a low metal concentration and provide the possibility to save a single number (Fraunhofer, 2010). Bulk reading ability and no disruption of further processing steps make these transponders very interesting for future applications.

## 2.4 Biometric systems

With the significant changes in society and economy human recognition became a major task in our life. Related to human recognition the term **Biometrics** stands for the study of behavioural or physiological characteristics to identify living people. Biometric systems are almost always computer aided systems for biometric recognition of humans. Currently used biometric systems use characteristics like fingerprints, iris, retina, handwriting, face, gait and many more to extract biometric features of living persons. Beneath biometric systems for human recognition - approaches treating recognition of vegetables, plants, animals or products were presented.(Wayman et al., 2005)

These approaches are based on the theoretical background and concepts from human recognition to explore biometric systems for new fields of applications. Subsequently, an introduction to biometric system characteristics (Section 2.4.1) and the performance evaluation of biometric systems (Section 2.4.2) is given. In section (Section 2.4.3) an outline of biometric approaches in other fields of applications is presented.

### 2.4.1 System characteristics and classification categories

In this section characteristics and classification categories of biometric systems are considered in detail. For this purpose categories and modes of biometric systems as described in Maltoni et al. (2009) are presented.

**Verification vs. Identification mode** Commonly, biometric systems are either classified as identification or as verification systems, whereat **recognition** is used as universal term

regardless of the operation mode. Both modes require that humans become enrolled into the system (see Fig. 2.4). Depending on the used biometric characteristics specific sensors are used to capture/ digitize the related characteristics. Next, the biometric system extracts features from the captured characteristics. Out of these features a compact and comparable representation, called *template* is generated. Commonly, biometric applications store the template together with personal information (e.g. an ID or name) into a database or data carrier.

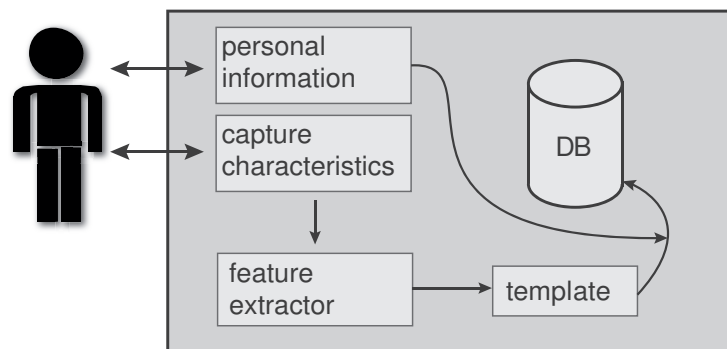


**Figure 2.4:** Biometric system - enrolment schemata

The two operation modes can be distinguished regarding the recognition procedure of the system:

- **Verification** systems are based on one-to-one comparison. A person requesting authentication by the system has to announce the claimed identity to the system using personal information (e.g. ID, PIN, magnetic cards, ...). The system then compares the biometric characteristics of the person to those from the pre-stored template of the claimed person in the system database. Consequently, the system can accept or reject the claimed identity. The term *authentication* is likely used as synonym for verification, as verification confirms or negates the claimed identity of a person.
- **Identification** systems perform one-to-many comparisons. For each request of a person the system compares all pre-stored templates in the system database to the template generated from the biometric characteristics of the person. The system has to make a decision if the person is enrolled in the system. Consequently, a single template in the database has to be selected as the person's template. If there is no corresponding template available, the system fails and rejects the claim for identification.

Beside the basic classification into verification or identification systems a biometric system can operate in further modes:

- **online vs. offline**

Recognition can be performed immediately or with a long delay response. Online systems are almost always fully automatic, while off-line systems are likely to be supervised semi-automatic systems.

- **positive vs. negative recognition**

A system that operates in positive recognition mode tests if a person is already enrolled. Thereby the system checks if the claimed (explicit or implicit) identity is correct or not. Consequently, it prevents different users from using the same identity. In the negative recognition mode the system checks if the person is not enrolled in the system. It prevents a single user from using multiple identities. Positive recognition can be performed in identification or verification systems. Due to the fact that all templates have to be checked, negative recognition can only be established in an identification system.

**Application taxonomy:** Additionally to these basic classifications biometric systems can be described using application-dependent categories (Wayman et al., 2005):

- overt vs. covert
- standard vs. non-standard environment
- habituated vs. non-habituated
- public vs. non-public
- attended vs. non-attended
- open vs. closed

**Biometric characteristics quality:** The development of a biometric system relies on the quality of the selected biometric characteristics. The quality of a biometric characteristic can be assessed considering a set of criteria (Maltoni et al., 2009):

- **universality** - is the characteristic available for each person?
- **distinctiveness** - is it possible to receive a strong variation between a set of individuals?
- **permanence** - is it invariant against change over time?
- **collectability** - can it be captured or digitized with sensors?
- **performance** - different measures that describe the accuracy, robustness and speed of the system using the characteristic (see Section 2.4.2)

- **acceptability** - is it tolerated by the individual to capture or digitize the characteristic?
- **circumvention** - is it possible to defraud the biometric system?

Compared to the other criteria, performance, acceptability and circumvention are criteria used to evaluate and describe the biometric system. The other criteria describe the quality of the biometric characteristic itself.

## 2.4.2 System performance

This section describes (error) measures that are used to assess the performance of biometric systems as described in Maltoni et al. (2009). Each time a biometric system compares two templates, a matching algorithm computes a matching score ( $s$ ) ranging between 0 and 1. The closer to 1 the higher is the certainty that the templates are from the same person. The decision if two templates are said to be from the same person depends on a threshold ( $t$ ). If the matching score between two templates is lower than the system's threshold, the two templates form a non-matching pair, otherwise they form a matching pair. Out of this, two biometric system errors are derived:

- **False match or false acceptance**  
denotes a matching pair where the compared templates are not from the same person
- **False non-match or false rejection**  
denotes a non-matching pair where the compared templates are from the same person

It has to be noted that the terms "false acceptance" and "false rejection" have different meanings in positive or negative recognition mode. Instead, false match and false non-match have the same mode-independent meaning. Nevertheless, in practical use the terms "false match" and "false non-match" are preferably used. The performance evaluation of a biometric system is based on the computation of the false match rate (FMR) and the false non-match rate (FNMR). These rates can be determined considering the impostor and genuine distribution of the system:

- **Impostor Distribution**  
of the matching scores of each enrolled template of a single person to all templates of the other enrolled persons - can also be denoted as interclass variance.
- **Genuine Distribution**  
of the matching scores between several templates generated from the biometric characteristics of a single person - can also be denoted as intraclass variance.

Figure 2.5 illustrates how the FMR and FNMR are determined for a certain threshold and given impostor and genuine distributions of a biometric system. For a positive recognition system the FMR describes the percentage of comparisons that would be accepted by the system although the templates are from different persons. The FNMR gives the percentage of comparisons that would be rejected although the templates are from the same person. Consequently, the

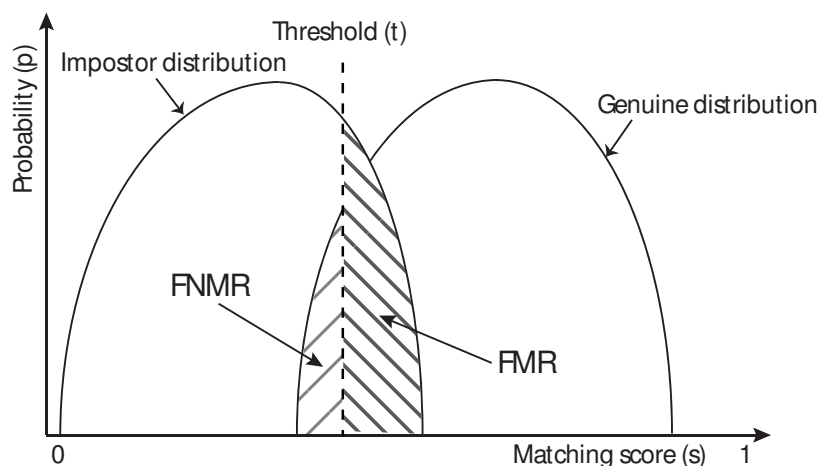
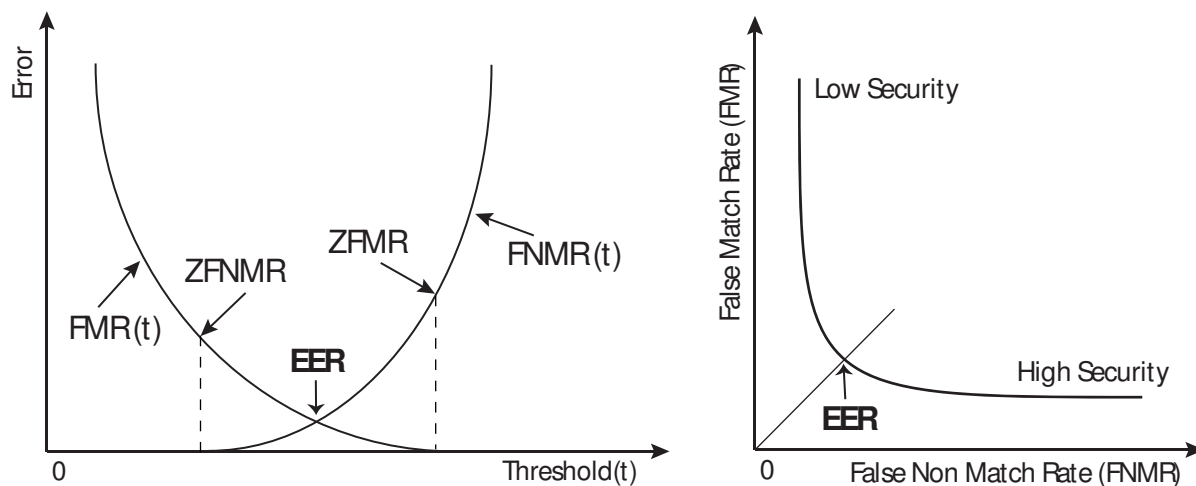


**Figure 2.5:** Biometric errors: FMR and FNMR for given impostor and genuine distributions at a certain threshold ( $t$ ). (Template: Maltoni et al. (2009))

selection of the threshold influences the performance of the biometric system. For example, a high security application will choose a high threshold, taking into account that the system denies access for a higher percentage of actually authorized persons - increasing FNMR and decreasing FMR. Alternatively, tolerant systems use lower thresholds to ensure that a high amount of authorized persons are accepted and so decreasing the FNMR. A further important measure, denoted as equal error rate (EER), is the error rate at the threshold value where FMR and FNMR are equal. EER is likely used as measure for the comparison of different biometric systems. Because FMR and FNMR are depending on the threshold value they can be described as functions  $FMR(t)$  and  $FNMR(t)$  as illustrated in the plot in Fig.2.6a. This plot offers further points of interests like the zero false match rate (ZFMR) and the zero false non-match rate (ZFMNR).

Another possibility to get an overview on the performance of a biometric system is to analyse its receiver operating characteristic (ROC). This curve visualizes the dependency of the FMR on the FNMR for changing system thresholds. Figure 2.6b depicts a sample illustration for a ROC curve and the resulting use cases using different thresholds. It is shown that low security applications (e.g. forensic applications) require a low FNMR and therefore take a higher FMR into account. High security applications have to ensure that they can only be accessed by

authorized people and so they require a low FMR. On the other hand a lower FMR implies a higher FNMR and so the amount of actually authorized people that are not recognized by the system increases.



(a) Equal error rate estimation - Illustration of the FMR(t) and FNMR(t) curves and the corresponding points of interest.

(b) Illustration of a receiver operating characteristic and the corresponding use cases (ROC).

**Figure 2.6:** Biometric performance curves. (Templates: Maltoni et al. (2009))

### 2.4.3 Biometric systems in other fields of applications

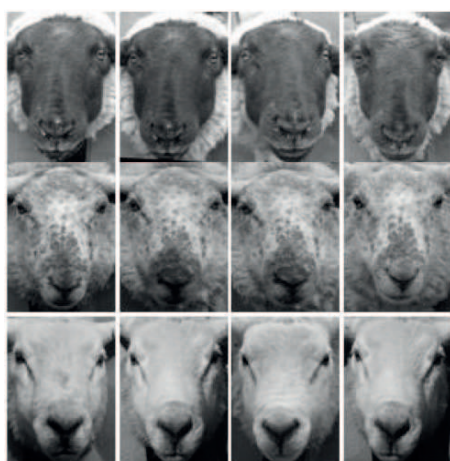
The idea of using biometric characteristics for human recognition has been carried to the recognition of plants, vegetables, animals and industrial products. Subsequently, an overview on biometric approaches divided into three categories is provided.

#### 2.4.3.1 Recognition of animals

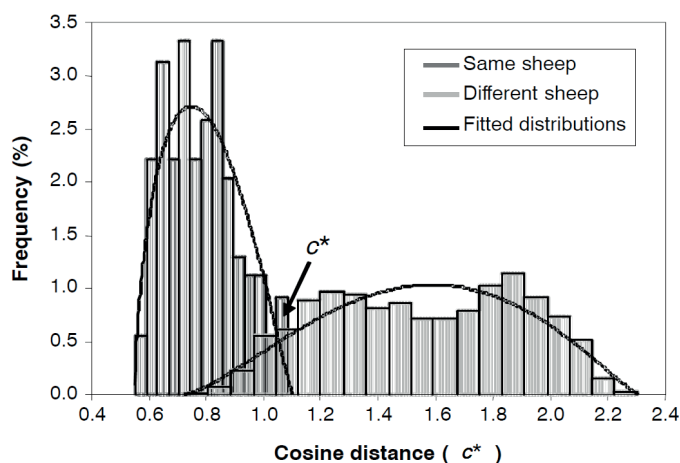
Like humans, animals show biometric characteristics that can be used to enable biometric recognition. Some of the biometric characteristics like iris, retina or the face used for human recognition can also be found at animals. In the past several manual biometric approaches for livestock identification have been presented. For some of these approaches like muzzle recognition in cattle, automated solutions were proposed and new automated biometric approaches came up. In the current section, a selection of current literature is pointed out to get an insight on used biometric characteristics and the performance of automated animal recognition. The Bioresources Research Centre from the University of Dublin contributed to

the biometric recognition of farm animals (compendium of recent publications - Ward et al. (2009) ). Investigations on biometric recognition in sheep treating retinal recognition and face recognition are presented in Gonzales-Barron et al. (2008), Gonzales Barron et al. (2008) and Gonzales-Barron et al. (2007a), respectively. An innovative biometric approach using the avian comb of poultry is introduced in Corkery et al. (2009).

For the purpose of face recognition the authors of Gonzales-Barron et al. (2007a) used independent component analysis (ICA) and the cosine distance transform as matching score between two sheep faces. The authors captured four face images from 50 sheep over a period of five weeks (see Fig.2.7a). The best results outperformed the results from the same method applied to human faces by reaching a recognition rate of 96% compared to 88%. The higher recognition rates can be explained due to the more constant face expression of a sheep. The genuine and impostor distributions in Fig.2.7b show that face recognition is a potential method for sheep recognition (threshold  $c^*=1.06$ , FMR=7.74%, FNMR=0.80% ).



(a) Sheep face images



(b) Sheep face recognition - Impostor and genuine distribution based on cosine distances

**Figure 2.7:** Investigation on face recognition in sheep (images source: Gonzales-Barron et al. (2007a))

The investigations for retina recognition in sheep were performed using the Optireader device ([www.optibrand.com](http://www.optibrand.com)). This device can be used to capture retina images and provides a built in matcher. The matcher compares two retina images and returns a matching score between 0 and 100.

In Gonzales-Barron et al. (2008) two experiments evaluating the impact of ageing are presented. One experiment deals with retina images from lambs captured in the first 22 weeks after birth. This resulted in 13 different data sets, where the last three ones were used as

basis sets. The matching scores between the early age data sets and the basis data sets indicated structural changes of the retina at the beginning of a lamb's life. With increasing age the matching scores increase up to an age of 8 weeks until they reach an upper bound for the matching score (approximately 94 to 96). However, the overall impostor and genuine distribution can be separated from each other and so retinal recognition in sheep is robust and accurate beginning from the birth of a lamb. The second experiment evaluated the matching scores of 2 to 3 year old sheep in a time span of 5 months. Their results showed that the matching scores are not influenced by ageing. Finally, in Gonzales Barron et al. (2008) experiments with changing capturing parameters (different operators and lighting conditions - indoor and outdoor) showed that there is nearly no impact on the matching performance. Additionally, the authors suggested to use both retina of sheep and to combine the matching results to a final matching score. For this case the FMR and FNMR became zero for the evaluated test set.

Poultry recognition using the avian combs of chicken is introduced by Corkery et al. (2009). For this purpose forty 45-week old hens were side captured. For each chicken four images were taken. The stages for the extraction of a chicken comb profile are illustrated in Fig.2.8a. Avian comb extraction is done using colour indexing and is based on the assumption that the comb is red coloured. The line bounding the comb area (see Fig.2.8a - top right) was selected manually. Finally, the avian comb is extracted and aligned using binarization, morphological image processing and the preselected line. Fourier descriptors are used to extract shape features from the avian comb outlines. For the matching procedure linear discriminant analysis using the extracted harmonics of each comb and additional template matching were performed. With a recognition rate of 84% for 40 chicken it can be concluded that recognition using avian combs is a meaningful approach. The genuine and impostor distributions of the experiments are illustrated in Fig.2.8b .

Another interesting biometric characteristic of animals are nose-prints, the pattern of which is entitled as muzzle pattern. Nose-prints are similar to human fingerprints and are commonly used for the sale and exhibition of sheep and cattle. For this purpose, the muzzle pattern is taken using ink prints and recognized by visual inspection. A feasibility study on automated muzzle pattern recognition for cattle using digital images is proposed in Gonzales-Barron et al. (2007b). First, the digital muzzle patterns are preprocessed which results in skeletonized muzzle patterns containing the central area of the pattern. The used feature extraction algorithm is based on eigenfaces as used in human face recognition. Twenty-nine cattle were video imaged, once a week over a period of three weeks. The resulting 87 images were used for the verification stage. For the training stage 10 muzzle images for each of a total of

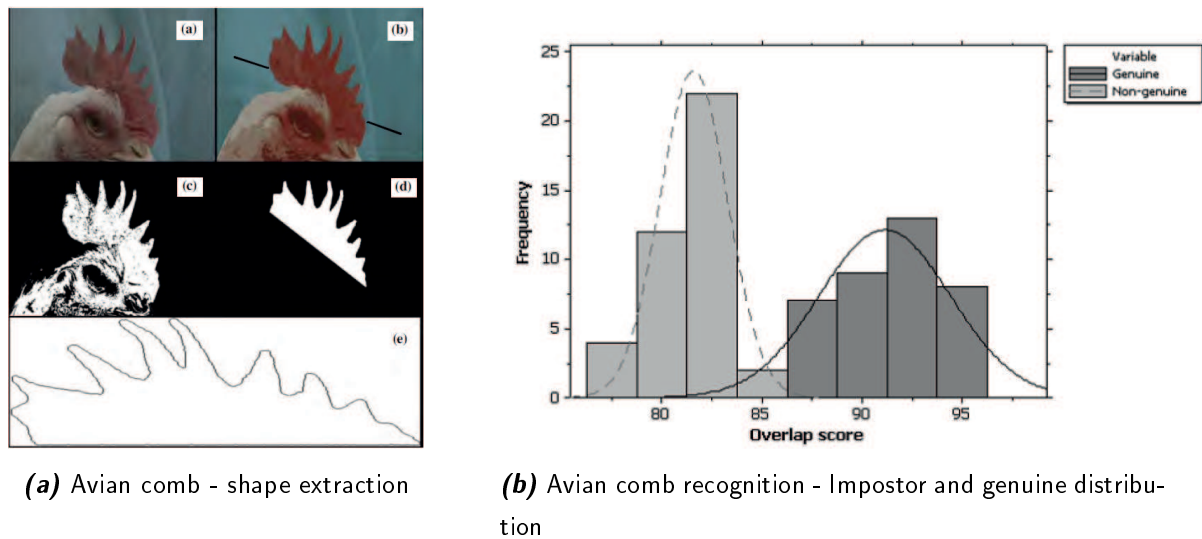


**Figure 2.8:** Investigations on poultry recognition using the avian comb (Images source: Corkery et al. (2009)).

29 cattle were captured in the first two weeks. Using 230 (of total of 290) eigenvectors a recognition rate of 98.85% could be achieved. Fewer eigenvectors and training images reduce the recognition accuracy remarkably.

Finally, one approach using the coat of animals as biometric characteristic is mentioned. In the work of Lahiri et al. (2011) the typical zebra stripes are used for biometric recognition of zebras using digital images.

### 2.4.3.2 Recognition/ classification of plants, fruits or vegetables

In case of plants, fruits or vegetables the task of recognition mostly refers to species classification. For example, tree leaves identification requires to determine the corresponding tree species using the biometric characteristics of a single leaf. A review on plant recognition and classification of plants using leaf images is presented in Bhardwaj and Kaur (2013). All described approaches use the leaf shape as biometric characteristic. Consequently, most approaches extract shape features. Biometric classification requires a training set for each plant species. The extracted features of a leaf are then compared to the features of each training set. Another approach for the classification of fruit images presented by Arivazhagan et al. (2010) uses colour and texture features. This approach may find an application in supermarkets, to automatically recognize a fruit when it is weighted by the consumer.

### 2.4.3.3 Recognition of industrial products and goods

Nowadays, there exist two major requirements for recognition of industrial products and goods. One requirement results from the high losses in sale because of counterfeiting products. Product recognition increases the safety of counterfeiting products. The second requirement is to solve a set of security issues. Identification or authentication of persons using security keys (stored on physical objects - e.g. key cards, RFID tags, ...) or the identification/ verification of hardware components or physical objects ( e.g. internet security, genuineness of documents, ...) are very important to increase security in different fields of applications. Commonly, security issues require cryptographic solutions to ensure protection against fraud. A possibility which implicates solutions for both requirements is to establish recognition of industrial products using physical characteristics. Physical characteristics are similar to biometric characteristics. In case of products or physical objects biometric methods are often denoted as "*fingerprint*" approaches.

Subsequently, an overview on research and applications for recognition of industrial objects using physical characteristics is given. This overview is based on the concept of physically unclonable functions and their applications in object recognition.

**Physically unclonable functions (PUF)** The concept of physical one-way functions was introduced in Pappu (2001) and Pappu et al. (2002). Over the past years different works contributed to the further development of this concept into different directions. Today the expression Physically Uncloneable Function (PUF) incorporates a set of cryptographic functions. The idea behind this concept and its various applications gives a good overview on measurable physical characteristics, that can be used to recognize industrial objects or goods.

In Maes and Verbauwhede (2010) a comprehensive study on PUFs is presented. Generally, a PUF is a procedure that produces a measurable output for a certain input and is not a mathematical function. Simplified, a PUF is a challenge - response function. The mapping between challenge and response depends on the physical nature of the object. Because the function depends on the complex, various physical characteristics of an object it cannot be expressed as mathematical function. Consequently, PUFs are said to be unclonable and unpredictable. PUFs are for example used in the following applications (VirginiaTech - SES Lab, 2013):

- Cryptographic key generation
- Device authentication
- Memoryless key storage
- PUF-based RFID for anti-counterfeiting

- Intellectual Property (IP) protection
- Anit-Counterfeiting

According to the study of Maes and Verbauwheide (2010), PUFs can be broadly classified into two categories referring to the nature of the considered physical characteristic: Non-electronic and electronic PUFs. Further considerations on different classification categories and concepts are listed in the phd thesis of Maes (2012a). Subsequently, both categories and selected approaches (which are of interest for object recognition) are introduced using Maes and Verbauwheide (2010), Maes (2012a) and Maes (2012b) as sources.

**Non-electronic PUFs** measure non-electronic properties of objects and are further classified regarding their constructions. For the purpose of object recognition two different constructions are of interest:

(a) *Optical PUF*

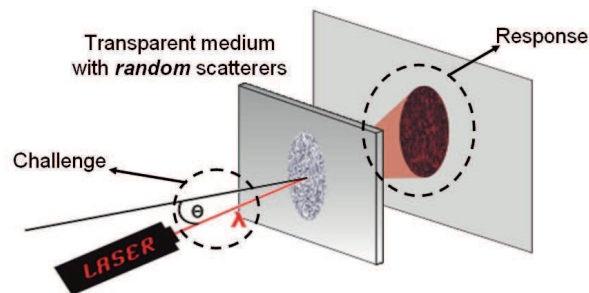
(b) *Paper PUF*

Both PUF constructions demonstrate that surfaces of industrial objects are physical characteristics, eligible to establish fingerprint recognition. Non-Electric PUFs require external devices for the measurement of a physical property. The challenge-response mechanism is not part of the PUF. Consequently, they are labelled as non-intrinsic PUF constructions.

(a) *Optical PUFs* are intended for the generation of cryptographic keys. Although optical PUFs find no application in object recognition they show an interesting approach to extract biometric fingerprints of a physical object structure. For this purpose tokens that contain a transparent micro-structure are used. This micro-structure is constructed by mixing refractive glass spheres. When these tokens are hit by a coherent beam of light (laser) a unique and unpredictable speckle pattern arises that can be captured by a digital camera. Fig.2.9a illustrates the challenge - response function of an optical PUF. As challenge the laser is directed on the token and as response the speckle pattern arises. The hash value of a token is computed applying a Gabor hash to the speckle pattern. Optical PUF systems are very sensitive because the speckle pattern will vary already with minimal changes in the capturing procedure.

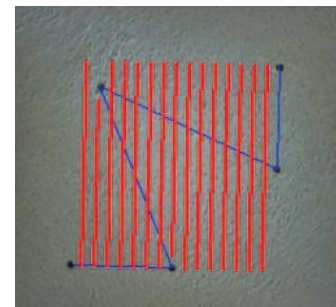
(b) *Paper PUFs* utilize the fiber structure of a material as physical characteristic. Selected fingerprint approaches for paper documents or packaging materials are presented in Metois et al. (2002), Buchanon et al. (2005), Clarkson et al. (2009).

The *FiberFingerprint* presented by Metois et al. (2002) extracts fingerprints from small marked sections ( $< 25m^2$ ) of fibre-structured materials. Figure 2.9b shows a captured section of paper.



(a) Optical PUF for cryptographic key generation: Producing a unpredictable, unreproducible speckle pattern of a transparent token.

(Image source: Maes (2012b))



(b) Paper PUF for document authentication - *FiberFingerprint* extraction from a marked paper patch.

(Image source: Metois et al. (2002))

**Figure 2.9:** Two optical PUF examples

The black dots are the markings of the section. A one dimensional signal (*FiberSignal*) is extracted along a path defined by the marking dots (blue line). The sampling frequency of the *FiberSignal* is defined by the signal path (red lines). Finally, the *FiberSignal* is quantized and used as *FiberFingerprint* template. For the experiments 30 marked sections on different pieces of paper were captured using a consumer grade camera. It turned out that there is no intersection between the genuine and impostor distribution for the test-set.

The paper PUF approach by Buchanan et al. (2005) uses a laser scanner that scans fibre-structured material across a length of 40mm at a certain position. The intensity variances from different angles are recorded using four photo-detectors which are further used as templates. The authors describe that the recognition performance is excellent even after the paper was roughly handed: screwing, baking, submerging in cold water for example (EER for paper  $10^{-72}$ ). For smoother surfaces like plastic cards or coated paper boards the recognition performance decreases remarkably (EER for plastic cards  $10^{-20}$ ).

A paper PUF that used the three dimensional surface of a document is presented by Clarkson et al. (2009). Regardless of being printed or not, the surface texture of the document is computed by scanning it in four directions with a commodity scanner. Finally, the feature vector is extracted from regions defined by a Voronoi distribution. This distribution is stored in the fingerprint which complicates the verification process. Under the best conditions an EER of  $10^{-148}$  could be achieved. Even after the document had been soaked and dried, the EER decreased only slightly.

A commercial solution for document authentication, entitled "Laser Surface Authentication" (LSA) is provided by the company *Ingenia* (<http://www.ingeniatechnology.com>). The

description on their website promotes a technology that can be used with a set of materials: paper, cardboard, plastics, metals, ceramics and textiles.

**Electronic PUFs** are based on the manufacturing variabilities of integrated circuits placed on chips. Even when two integrated circuits are manufactured in the exact same way they are not identical. Electronic PUF constructions measure electronic characteristics from integrated circuits. For the overview in this thesis silicon PUFs are introduced, which are a major subclass of electronic PUFs. Silicon PUFs are referred to as intrinsic PUFs because the measurements/fingerprint extraction can be directly performed by the embedding device of the silicon chip. Fingerprints of silicon chips can be used for device recognition or cryptographic issues. Silicon PUFs can be classified based on their working principles. The main two working principles are (a) *delay-based silicon PUFs* and (b) *memory-based silicon PUFs*.

(a) *Delay-based PUFs* measure the random delay of a digital circuit on a silicon device. An example for a delay-based PUF is an arbiter PUF. In Fig. 2.10 the challenge - response function of an arbiter PUF is illustrated. For the delay measurement two symmetrical delay lines are used. These lines are concatenations of switch elements. Each switch transfers two inputs straight or crosses them, depending on a one bit parameter. For  $n$  - switches there exist  $2^n$  different path configurations. Both delay lines are triggered at the same moment. It depends on the delay of each switch and the corresponding bit parameters of a certain configuration which line is the fastest. The arbiter detects the fastest line and returns a one-bit result. Each configuration produces a different delay. Using  $n$  different challenge vectors results in a  $n$  - bit code.

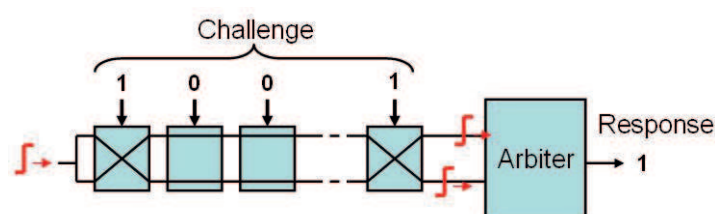


**Figure 2.10:** Arbiter PUF - Challenge Response Illustration. (Image source: Maes (2012b))

(b) *Memory-based PUFs* utilize variabilities of memory cells. For example Static Random Access Memory (SRAM) PUFs use random variabilities of SRAM cells to produce a fingerprint. A SRAM cell is a circuit constructed by two cross-coupled logic inverters that resides in one of two possible states. SRAM cells require a certain voltage to remain in a stable state.

SRAM PUFs use the state of a cell when it powers up. In case of equal inverters a set of

SRAM cells would have the same power-up state. Again, manufacturing variabilities cause a mismatch between two inverters of a single SRAM cell. The mismatch between two inverters of a single cell determines the power-up state of a cell. By addressing  $n$  cells on a chip (challenge) their power-up state (response) produces a  $n$ -bit fingerprint of the chip.

## 2.5 Research on biometric recognition of logs

In the last section of this chapter an overview on research in the field of biometric log recognition is given. As described in Section 2.3.3 state-of-the-art log traceability approaches propose the usage of RFID technology. Nonetheless, the works of Chiorescu and Grönlund (2003), Chiorescu and Grönlund (2004), Flodin et al. (2007), Flodin et al. (2008a) and Flodin et al. (2008b), Peterson (2009) focus on biometric recognition of wood logs and sawn boards. By analogy to human recognition, these works are based on the assumption that wood logs are unique entities which can be recognized using biometric log characteristics.

The approaches introduced in Chiorescu and Grönlund (2003) and Chiorescu and Grönlund (2004) utilize measurement data from the outer shapes of logs as biometric characteristics. Therefore, the log shapes were captured with a two-axis log scanner and a three-dimensional log scanner, respectively.

With the intention to use existing environment to enable log traceability Chiorescu and Grönlund (2003) presented preliminary investigations on biometric recognition for wood logs. For this purpose, the on-bark shape of 879.571 logs (spruce and pine) was scanned using a 2-axis scanner. Out of this data seven biometric features (length, diameter, bumpiness, taper, butt, bow and ovality) were computed and stored into a database. In a first step the whole dataset was used to find the most discriminative feature set, considering different combinations of features. Results show that the best feature combination consists of four features: diameter, length, taper and bumpiness. Using these features approximately 98% of the logs are recognized as unique individuals. The second step investigates the measurement accuracy of the utilized 2D-axis scanner. Hundred logs were measured five times at random rotational positions. The standard deviations for each feature are used to assess the measurement robustness. Based on the insights of the previous investigations a tree-based searching algorithm is introduced. The recognition rate for the proposed matching algorithm is evaluated by a simulation. Therefore a second test-set is created. This test-set is derived from the measured log features and incorporates measurement deviations caused by the scanner. The simulation

indicates that the utilized 2-axis scanner is too inaccurate to accomplish a recognition rate over 34%. The authors assessed that the scanner measurement accuracy and the recognition algorithm have a major impact onto the recognition rate.

As a consequence of the previous insights Chiorescu and Grönlund (2004) used a three-dimensional scanner. This scanner is normally used for optimal positioning of the logs into the headrig and is able to create a complete three-dimensional shape model of a log. Out of this model 27 parameter for optimal sawing are calculated. Nine of them were selected as biometric features. They were chosen with regard to their measurement robustness (volume, length, area minimum diameter, middle diameter, log taper, top taper, bumpiness, relative taper and bow). As test set 772 debarked logs were divided into three diameter classes and each log was scanned three times. The first scan was performed after the log was debarked. Further two scans were performed after storing periods of two weeks and two months. For the recognition procedure two different algorithms were proposed and tested. The first algorithm is a further development of the search algorithm in Chiorescu and Grönlund (2003). It is an one-variable procedural search based on a robustness ranking of the features. The robustness was estimated regarding the measurement accuracy of the scanner during the repeated scanning of a set of logs. Compared to this, the second algorithm uses all features concurrently based on multivariate principal component analysis and a nearest neighbour search. Recognition rates ranged between 80% and 95% depending on the diameter, matching algorithm and the time span between the scan cycles. Chiorescu and Grönlund (2004) advise that future work has to pay attention of the influence of bark on the recognition rate. In most Swedish sawmills, logs get debarked/ butt end reduced and scanned before they are processed by the headrig. It follows that the first scan at the log sorting station is done with bark and the second scan is done debarked and possibly butt-end reduced.

In the work of Flodin et al. (2008a) the authors take up the suggestion for future work in Chiorescu and Grönlund (2004). The authors present investigations on traceability from the log sorting station to the saw intake. Therefore, a special three dimensional scanner is used at the log sorting station. In bark suppression mode, the scanner is able to differentiate between clear wood and bark using the so-called tracheid effect of wood. For the experiments the logs were scanned at the log sorting station and before the saw intake. The test-set is divided into two diameter specific groups, each consisting of 50 logs. At the log sorting station, each log was scanned three times with bark suppression and once without bark suppression. The scan at the saw intake (each log got debarked and butt-end reduced) was done a month later. For each scanned log 11 biometric outer shape features were extracted. Further, the features were used to compute intra-measurement differences between the three bark-suppression log

scans and the inter-differences between scans from the log sorting station and the saw intake. By analogy to the previous works the measurement differences are used to rank the features regarding to their robustness and reliability for a fingerprint approach. Like in Chiorescu and Grönlund (2004), the matching is based on multivariate principal components analysis. The recognition rate was computed comparing each log from the saw intake to all logs from the log sorting station of the respective diameter group. For small sized logs and bark suppression a recognition rate of 91.8% and without bark suppression 77.6% could be achieved. Large-sized logs were hardly influenced by the butt-end reducer and consequently a recognition rate of 63.6% - bark suppression and 54% - no suppression could be reached. The authors concluded that the achieved recognition rates are not applicable for a traceability system.

Further two publications from Jens Flodin (Flodin et al. (2007), Flodin et al. (2008b)) focus on traceability between logs and cut boards. Each log was scanned with an x-ray and an optical log scanner. The log length as well as the knot positions and lengths were extracted as biometric features. After sawing, a surface scanner was used to determine the board lengths and knot positions plus lengths of each board. These biometric features were used to match each board to all logs of the test-set. Results show that this approach reaches a correct matching for approximately 90% of all boards.

Finally, the master thesis Peterson (2009) presents a feasibility study on using end-grain characteristics to enable traceability between sawn wood and their parent log. Sixty Douglas fir trees were cross cut at both ends which led to 120 cross section slices. Each slice was captured in a studio - three times over a period of three days. On each cross section reference points were used to capture three equally aligned cross section images from each cross section. The cross section images were then manually cropped and subdivided into cants and boards simulating end grain images of sawn wood. As a matching score the ratio of the correlated pixels between two images is used. No features were extracted and no image processing was performed. In the experiments board images were matched against cant images and cant images against cross section images. The matching was performed between images from different days. All matching configurations reached recognition rates between 83% to 98%. Although the presented work is thematically closely related to this work, the detailed results are less meaningful due to the oversimplified approach and experimental settings.

# Chapter 3

## Log image processing

The increasing industrialization of sawmills in the 1990's presented new challenges to existing processes. Requirements such as higher process speeds, better yields and lower costs contributed significantly to the development of new methods. Until today log grading and the decision, how to best process each single log, is still predominantly done by humans. Optical scanners and the improvement of x-ray technology offer new possibilities. While optical scanners enable optimal measurement of logs and detection of external wood properties, x-ray or nuclear magnet resonance scanners additionally allow detecting internal wood properties in a non-invasive way. The exact measurement and knowledge of external and internal wood properties offer many possibilities to improve log processing. Log scanners support or automate processes. Automation is mainly based on the development of image processing systems making use of captured data. There are two common approaches how to implement image processing systems: New scanning or capturing devices implicate new solutions and applications; or there is an idea or problem which should be realized or solved. In the past 15 years several log image processing systems and research approaches were successful. Regarding the sawmill industry, the use of automatic measurement and grading devices increased significantly. Although measurement systems have been developed for the forest based industries, mechanical and manual measuring methods are mainly used. Log scanning devices cause high costs and are subjected to large companies rather than small wood owners and small sawmills.

The next section presents wood basics and available scanning devices. Subsequently, relevant cross-section image processing methods are considered.

## 3.1 Wood basics

This section presents facts on wood as raw material. An introduction into the anatomy of wood provides an overview and describes special material features. Although European and Austrian tree species share some basic anatomic features, their cross section surfaces can look completely different. The development of an image analysis approach, using cross section images, has to be aware of these differences. It would be a drawback to specialize on a single tree species or a group of tree species with the same features. This part also focuses on wood measurement/ grading and the related properties. Measurement/ grading of logs is based on wood properties. Consequently, general wood properties are summarized before the basics of measurement/ grading of wood logs are introduced. Wood properties are biometric features of wood logs and can be used to enable biometric log traceability (see Section 2.5). Furthermore these properties are of interest with respect to a multi-biometric approach using cross section images as well as conventional measurement data.

### 3.1.1 Wood anatomy

Worldwide more than thousand tree species are known. In Austria, about twenty-five tree species are of economic interest. Generally, Austrian and European tree species are subdivided into softwood and hardwood tree species. Macroscopic and microscopic features identify each tree species. Microscopically there are major differences between the anatomy of hardwood and softwood. Following, some macroscopic features and related basic information will be presented.

Standing trees can be easily classified according to their leaves. Hardwood trees typical wear broad leaves and softwood trees scale-like leaves also known as needles. These leaves are essential for the tree to grow, as they collect sunlight and carbon dioxide which are necessary for photosynthesis.

**Annual Rings/ Growth Rings** Each year a tree, independent of its species, produces new sap conducting tissue in shape of an annual ring. These annual rings record the age of a tree. Due to our climate and the seasons, an annual ring consists of two ring-like bands. Earlywood/ springwood is produced at the beginning of the growing season and is mostly light-coloured, -weight and soft tissue. The dark coloured, stronger and harder tissue is formed in the period from summer to the end of the growing season and is called latewood/ summerwood. In

most tree species annual rings and the two different tissue bands are clearly visible. In regions without major climatic changes and seasons there are less differences between earlywood and latewood. Especially in subtropical/ tropical regions trees form several rings each year, which are called growing rings. The number of growing rings depends on wet and dry periods. The growing of annual rings and growing rings depends on weather and other environmental conditions. Dendrochronology uses annual ring patterns for tree dating (Crossdating) in order to draw conclusions about ecological conditions in the past (ProHolz, 2007).

**Pith** The pith represents the innermost point of of a tree stem. As a tree starts growing or grows higher the first annual ring is formed around the pith. The thickness of a single annual ring varies within itself due to different influences, like wind or pressure. As a result the annual ring pattern is not a real circular concentric pattern. So the pith is not the geometric center (gc) of a tree stem. A pith which is located wide outside of the geometric center acts as an indicator for reaction wood.



(a) The pith is located slightly outside due to compression wood in the bottom left of the cross section. (Image source: [http://commons.wikimedia.org/wiki/File:Reaction\\_Wood\\_of\\_Picea\\_Abies.jpg](http://commons.wikimedia.org/wiki/File:Reaction_Wood_of_Picea_Abies.jpg))



(b) The pith is located near to the geometric center (gc). (Image source: RLE-IS see Section 5.3.1)

**Figure 3.1:** Examples for different pith locations

**Heartwood/Sapwood** As a tree grows and becomes older only the outer zones transport water and nutrients (sap) stem-upwards. This causes the inner zone dying and it gets embalmed in tannins and resins. The resulting heartwood is commonly darker than sapwood and has different mechanical properties.

**Tracheids/ Pores and Vessels** Sap transport differs in soft- and hardwood. In softwood tracheids are responsible to transport sap upwards and can only be seen microscopically. Hardwood is often referred to as porous wood. Huge vessels appearing as holes or pores conduct sap upwards. Depending on the hardwood species, these pores are distributed differently and can be recognized macroscopically on sanded log end faces or cross-sections. The distribution of the pores is used to subdivide hardwood species into three different categories (further reading - Fellner et al. (2006)).

**Vascular/ Medular Rays** To transport sap in horizontal direction so-called vascular or medular rays are formed. For some tree species these rays are very distinctive and visible. Maple is well known for its distinct texture caused by these rays leading to a mirror effect at the tangential surface.

**Bark** Bark is the outermost layer of a tree stem. At the inner side of the bark there is a special layer called xylem. Xylem is supported by vascular rays with sap and produces fresh wood cells. Phloem is the outer side of the bark and protects the tree stem from environmental damages.

**Knots** Each tree develops branches laterally from the tree trunk. Branches accommodate leaves and needles which collect sunlight. In the wood stem and on the wood surface branches can be seen as knots. Generally it can be distinguished between inter-grown and encased or loosed knots. Inter-grown knots are formed by healthy branches and get encased when branches die and fresh wood is surrounding them. Encased knots are not disturbing the wood texture/ grain as much as inter-grown knots (Wiedenhoeft, 2010).

**Reaction Wood** When a tree is physically (eg. by wind, snow, slate subsoil) stressed he tends to form reaction wood to counteract these influences. Softwood tree species react by producing compression wood on the inner side of the load while hardwood species produce tension wood on the rear side of the load. Macroscopically reaction wood can be identified by narrower and darker annual rings in contrast to their surrounding. Branches always cause mechanical stress at the tree trunk and so lead to the production of reaction wood. Unfortunately, reaction wood has a strong negative impact on the mechanical and physical properties of wood. Consequently reaction wood is evaluated very negatively and mostly restricted by grading rules.

**Diseases and Vulnerabilities** Trees can be affected by diseases or attacked/ injured by animals and micro-organisms. Some of them cause colour changes or wood structure damages. A list of common diseases and vulnerabilities is involved in the presentation of the log properties (see Section 3.1.2.2).

### 3.1.2 Wood - measurement and grading

Measurement of an object is always based on the object's properties. Measurement of wood properties is further used for wood grading. Depending on the field of wood industry different properties are measured for description and grading. Measurement and grading determines the quality and applicability of a piece of wood for a defined usage. Generally wood and wood-product properties can be subdivided into three groups: Geometric Properties, Object Properties and Physical Properties. The following description is very general due to the diversity of measurement and grading in wood industry.

#### 3.1.2.1 Wood properties

**Geometric properties** are used to describe the outer shape of a piece of wood.

**Object properties** These properties involve most of the wood features which were described in Section 3.1.1. The appearance, quantity and the size of these features are essential for wood grading and sorting. It depends on the usage of the piece of wood which features are essential. While some features have an impact on mechanical properties of wood, others are wanted or unwanted due to their visual appearance.

**Physical properties** Density, moisture content and shrinking/swelling are very important physical properties of wood. The moisture content affects density and causes shrinking and swelling of wood. For specific density values, normal-density and oven-dry density are commonly used. Normal-density is determined in an atmospheric climate of 20 degrees and 65 percent humidity. Wood with a moisture content of zero percent is defined as oven-dry. Like density, shrinking and swelling values are also different among the wood species and products.

**Mechanical properties** Hardness, durability and strength-properties are of high interest. Mechanical properties indicate which wood species or wood products are convenient, in terms

of solidity, for different fields of applications.

### 3.1.2.2 Log measurement and grading

Measurement and grading are very important tasks for trading and processing of round timber. The forest based industries allocate round wood to different wood processing industries by defining sorts and classes. This allocation is based on measurement and grading of round timber by using its specific properties. The wood processing industries use measurement and grading to optimize round wood/log processing and to increase the economic output and yield. Moreover, predefined measurement and grading rules ensure fair trading of round wood and logs for all parties involved. The specific properties of round wood/logs used for various measurement and grading purposes are listed on the basis of the general wood properties (see Section 3.1.2.1).

**Geometric properties** describe the dimension and shape of round wood or a log like different diameters (butt-end diameter, middle diameter), taper, stem curvature, log length, average ring width, pith position, etc.

**Object properties** most of them are defined as wood defects: branches, compression- and tension wood, spiral grain, fungal attack, resin-pockets, insect infestation, cracks, diseases (blight bark disease, rot disease,...), decay, ring shake and much more.

**Physical properties:** density, moisture-content

In Austria the trading of round and sawn timber is regulated by the Oesterreichische Holzhandelsussancen - Austrian Wood Trading Rules (OHHU). The OHHU regulate how wood/ log properties are measured and which properties are applicable to allocate round wood/ logs to several sorts. The major round wood/ log sorts are sawmill round wood, industry- or pulpwood, energy wood and veneer wood. Furthermore sorts like instrumental wood and some others are defined. The highest demand is for sawmill round wood followed by industry wood. Some wood sorts are further divided into sub-sorts and quality classes. It depends on the sort of round wood which properties are essential for trading and for determining the economic value. Compared to sawmill wood (which is sold piecewise calculating the cubic metre of each log) industry wood is traded by the weight of a delivery.

**Devices** As already mentioned measuring/grading is used for trading for optimizing round wood processing. Therefore it depends on the grade of industrialization which devices are used. At forest site manual as well as automatic methods are used in practice. State of the art measuring devices at forest site are placed on harvesters or implemented on mobile measuring stations. These systems are used to collect geometric properties. Devices which are placed on harvesters mostly use contact-methods collecting the dimension of each tree while processed by the harvester head (Deere, 2011). The company Woodtech offers mobile gates which use laser scanners and promise measurement of complete truck loads (Nylinder et al., 2008). Another interesting system is offered by the Swedish company Dralle. A mobile unit which is placed on a car uses cameras to capture the end faces of a log stack. In combination with the log lengths a 3D model of the log stack is calculated. In these sawmills mainly 3D laser scanners are used to create a 3D profile of the log shape. 3D profiles enable automatic measurement of log dimensions and can be used to improve log sawing. Additionally video cameras are used for visual inspection by an operator. In future scanners the use of computer tomography and magnet resonance imaging will be state of the art. These scanners capture cross section images from a log in predefined resolutions and enable to create 3D models of logs. Other wood processing industries like pulpmills do not require 3D scanners for log processing.

## 3.2 Cross-section analysis

Current research defines this section as log end face analysis. This caption does not fit with the further presented methods because some of them make use of CT or MRI technology which captures cross-section images along the length axis of a log. These images have specific features but the wood properties are quite the same as from log end images. Compared to conventional log end face images, CT or MRI cross section images are prevented from disturbances due to cutting or dirt. Since the middle of the 19th century cross section analysis is used in the field of dendrochronology for tree dating (ProHolz, 2007). The first known approach which uses computers for cross section analysis was presented by McMillin (1982). The author presented a semi-automatic image analysis system which requires an operator who mainly performs image or camera enhancement. A scanner unit was used to produce an analogue video signal from sanded pine samples. This signal was then displayed to the operator who adjusted the region of interest, gray levels and threshold values before the signal could be binarized and processed. 13 basic measurements including annual ring measurements like growth rate per inch or late and early wood measurements have been implemented. Therefore, the current feature that should be measured had to be emphasized by setting the threshold

adequately. He also presented measurements of microscopic features like the fibre length or some cell measurements of specially prepared pine samples. Finally geometric measurements of a CT cross section slice were shown. McMillin (1982) already proposed the advantages of internal log scanning regarding the sawing of a log.

In the next three subsections an overview on present research until 2012 is provided. The present literature on cross-section analysis can be subdivided depending on the analysed macroscopic feature. Pith estimation and annual ring analysis tasks are the most common cross-section analysis tasks. For both tasks a literature overview and selected state-of-the-art algorithms will be presented in detail in the two subsequent sections (see Section 3.2.1 and Section 3.2.2). In the last subsection an overview on literature treating further cross-section analysis tasks is presented.

### **3.2.1 Pith estimation**

Pith detection/ estimation is very important for cross section imaging. Anatomically the pith is the growth centre of a tree stem. At the cross section of the tree stem the pith is the innermost point surrounded by annual rings. Annual rings and the pith are the only features that are always present. Thus, the pith is a unique point on a cross section. In determining the wood quality the pith position has two main functions: First, it is an indicator for the presence of other wood properties like compression or reaction wood. Second, it represents a reference point for further analysis like annual ring measurements. Pith estimation is fundamental for cross section analysis.

In some cases it can be impossible to determine a ground truth for the pith location, whether by visual inspection or an image analysis application. In combination with the fact that all pith detection/ estimation approaches rely on a probability match it is appropriate to speak of pith estimation rather than pith detection.

#### **3.2.1.1 Literature Overview**

The existing literature can be subdivided into approaches based on annual ring analysis or local orientation estimation. Both rely on the assumption that annual rings are concentric circles the center point of which is the pith position. Annual ring analysis focuses on finding and identifying annual rings or arcs. The detected annual rings or arcs are then used to compute orthogonal vectors pointing towards to the pith or to compute annual ring/ arc centre points

representing votes for the pith position. Local Orientation estimation utilizes the fact that small annual ring sections represent an oriented texture. Equal as orthogonal vectors from annual rings/arcs local orientation estimates from annual sections point towards the pith. With intersection of the local orientations the pith position can be determined.

Regarding the capturing device, the most approaches were developed for images from polished/sanded cross sections or ct-images. The main advantage of these images is that they are free of distortions caused by sawing or dust and that annual ring borders are slightly emphasized. Pith estimation approaches treating ct-images are presented in Bhandarkar et al. (1996), Andreu and Rinnhofer (2001), Longuetaud et al. (2004), Entacher et al. (2008).

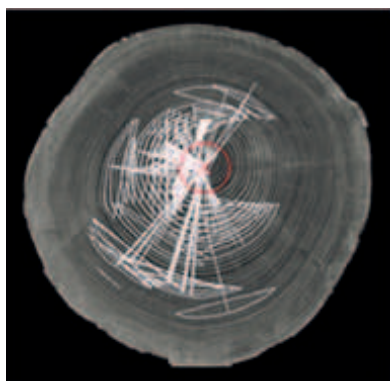
In Bhandarkar et al. (1996) a system to detect internal log defects using ct-image slices of a log is presented. Sobel edge detection and a subsequent threshold are used to extract the annual rings and their gradients. For each detected annual ring point the values inside of an accumulator array are raised in a certain range of the corresponding gradient vector. It is assumed that the maxima in the accumulator array is the location of the pith. The computational demand was reduced by only considering a sub-area around the geometric center of the image.

For enhancing the annual ring pattern in ct-images Andreu et al. (2002) used contextual Gabor filters. The proposed pith estimation algorithm utilizes the assumption that the orthogonal line of an annual ring cord through its bisect passes the pith. After preprocessing the annual rings are expressed as pixel chains. Each pair of pixels from a pixel chain defines a chord. An accumulator array sums up the intersections of the orthogonal vectors and the maximum is assumed to hold the pith position.

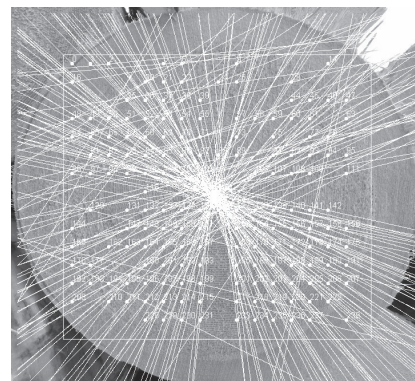
Longuetaud et al. (2004) presented an algorithm to detect the pith in a set of ct-slices from a scanned log. Like Bhandarkar et al. (1996) gradients and an intersection image are used to determine the pith position for a single slice. Additional information of the pith location in the previous slice is used to speed up and to improve the accuracy of the algorithm. The algorithm in Boukadida et al. (2012) is a successor of this work and shows improved results by applying adaptive thresholds and an optional reversion of the ct-slice order to improve the accuracy in case of branch forks. The authors performed experiments on 125 logs from 17 different tree species. It is shown that the proposed algorithm performs very accurate with an overall mean error of 1.69 mm.

Entacher et al. (2008) made a comparison between 6 different pith estimation methods. The main focus was on keeping the computational effort low. In addition to the pith estimation

methods the influence of different preprocessing methods was evaluated. Except one method (Poincare (Poi) - well known from fingerprint recognition - see Maltoni et al. (2009)) all methods are annual ring analysis methods. The other methods use the circle equation (CE) or gradient estimation methods (GM). For CE and GM two different variations are presented respectively. The first variation for the circle equation - CEeg (equal gradients) uses the Kirsch operator to compute gradients for all pixels. Sets of adjacent pixels are used to determine annual ring arcs. For the second variation CErt (ring tracing) the entire image or a sliding window is cut at different positions and ring tracing is performed along the cut edge (indicated by white pixels). For both variations each pair of points  $(x_i, x_y), (x_j, x_y)$  on an annual ring arc is used to determine the coordinates of the circle centre  $(x_0, y_0)$ . The centre points are used as votes for an accumulator array, where the maximum is assumed to represent the pith position. The two GM variations use a sliding window and ring tracing to detect annual ring arcs. One variation - GMi (intersection) determines the bisects of the previously localised annual ring arcs. The second variation - GMrl (radial length) additionally uses the radial lengths of the bisects and finally the centre point candidates are used to calculate a pith estimate. For pith estimation GMi intersects all gathered bisects and GMrl uses the point candidate as votes in an accumulator array. The fifth method - Curvature(Cur) uses the fact that the annual ring arc curvature increases towards the pith. Therefore CERl and two thresholds are used to choose annual ring arcs that are close to the pith. The estimated pith position is used to perform a local circle HT. The experiments show that CERt, GMi and especially CEeg are very accurate. Poi and Curv are not suitable for pith estimation.



**(a)** Intersection using the radial length of detected arcs. (Image source: (Entacher et al., 2008))



**(b)** Intersection using local orientations gathered by Fourier Spectrum analysis. (Image source: Pith Estimation see Chapter 5)

**Figure 3.2:** Intersection images

Pith estimation approaches for digital images are presented in Wu and Liew (2000), Hanning et al. (2003), Österberg et al. (2004) and Norell and Borgefors (2008).

While Wu and Liew (2000) basically applied the approach presented by Bhandarkar et al. (1996), in Hanning et al. (2003) two methods with the intent to fulfil the requirements of EN 1310 were presented. This European norm defines rules for visual ring width measurements on cut wood, where the pith position is a required feature. The main focus was on unpolished board end images because polishing or sanding of end faces would be too expensive in an industrial usage. One approach is based on finding annual ring structures from which gradients through their barycentre are computed. This is done by local quantization and clustering of neighboured pixels. In this case local connectivity components are defined as local long structures of adjacent pixels, similar to annual rings. In Fig. 3.3 a) the result of the local connectivity step is shown. The second approach uses the peak of the local Fourier spectrum as local orientation estimate of an annual ring section. The entire picture is subdivided into 32x32 or 34x34 windows. For each window or window position the local orientation of the annual ring section is determined by local Fourier Spectrum analysis. This is established by searching the peak in the corresponding Fourier Spectrum. For both methods the final pith estimate is computed by intersecting the gradients or local orientation estimates. This work was probably the first which uses local orientation estimation instead of annual ring analysis for pith estimation.

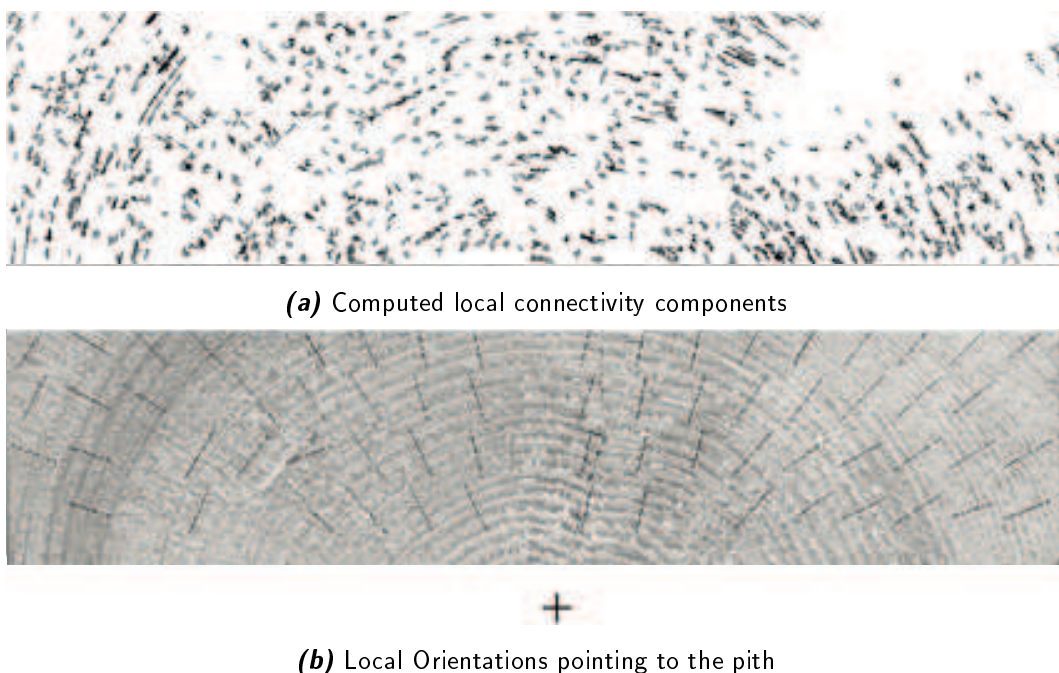


**Figure 3.3:** Pith estimation in images of rough log end boards. (Image source: Hanning et al. (2003))

Österberg (2009) presented experiments using Fourier Spectrum analysis for well prepared and under perfect light conditions captured cross section discs. Instead of moving a window over

the entire image an interesting algorithm for pith estimation was introduced. The principle of this technique is that first two points around a reference point are chosen. Initially, the geometric center of the image is used as first reference point. Two further points are chosen, so that an angle of 90 degrees is formed. The distance from the starting point to the two other points is equal to the half-distance between the image border and the starting point. Then, two local orientation estimates are calculated for the annual ring sections around these points. The intersection of the two local orientations is used as next guess for the pith position. This one represents the new starting point for the next iteration. At each iteration the distance between the pith estimate and the other two points is reduced by a factor  $<1$ . The procedure stops after a certain number of iterations or if the new reference point is close to the old one. The concept of this technique is based on the assumption that annual rings close to the pith are more circular. Optimally the pith estimate accuracy increases after performing several iterations.

The authors of Hanning et al. (2003) and Österberg (2009) conclude that pith estimation using local Fourier Spectrum analysis could also be applied on images from rough log ends. So far the only work focusing on the treatment of images of rough log ends has been presented by Norell and Borgefors (2008). The authors use two local Fourier spectrum analysis methods suggested in Knutsson and Granlund (1983) and Bigun (1992). Both methods determine local orientations by convolution of filter kernels in the spatial domain. Log end images from a sawmill yard, including several disturbances, were used for the experiments. Both methods use a sliding window. The first method uses quadrature filter whereby 3 filters ( tuned to a certain frequency range in different directions) are applied in the spatial domain. By combining the filter outputs a local orientation estimate and certainty value are computed (see Knutsson and Granlund (1983)). Norell and Borgefors (2008) computed a local orientation estimate for each pixel. Subsequently for  $8 \times 8$  pixel blocks one estimate is chosen to represent the block orientation. With these orientations an intersection image is created. The intersection image is smoothed and the maximum is assumed to hold the preliminary pith position. A second iteration in a smaller section around the first estimate and a rotation filtering step is used to improve accuracy. The second method uses the concept of linear symmetry and Laplacian pyramids, presented in Bigun (1992). This approach uses the fact that frequencies with equal orientations are distributed over a straight line in the Fourier Spectrum. The more the image deviates from being a simple image, the more the Fourier Spectrum deviates from being a straight line. Orientation estimation is then a typical line fitting or Principal Component Analysis (PCA) problem. In the Fourier Spectrum line fitting is established by calculating the Inertia matrix. The eigenvectors and eigenvalues of the matrix are utilized to extract a

dominant orientation and its certainty. In Bigun and Granlund (1987) it is shown that line fitting can be established in the spatial domain. For pith estimation Norell and Borgefors (2008) computed a Laplacian pyramid with two levels. With each level the high frequencies are reduced. As in the case of the first method local orientation estimates are computed for each pixel and the intersection step is performed similarly. First, the intersection image is computed with the results of pyramid level 2. If the standard deviation is too high the intersection image is computed for level 1 as well. Subsequently the intersection image with the lower standard deviation is used to compute the pith position. Finally the validity of the pith estimation is computed using a smoothed intersection image by analysing the standard deviation and the mean.

Along with the described methods, a few other approaches are presented in Som et al. (1993), Som et al. (1995), Chalifour et al. (2001), Sliwa et al. (2003) and Flood et al. (2003). These methods are not examined in detail because these papers are not available to us. A structured review about these methods is presented in Longuetaud et al. (2004).

### 3.2.2 Annual ring analysis

Beneath the pith as the growth centre annual rings are the only constant features that are present in each cross section. As described in Section 3.1.1, each year a tree produces a new annual ring around the existing annual rings of a tree stem. Depending on climatological and physical conditions the annual ring widths differ each year. Small annual ring widths indicate a low growth rate and high strength. Consequently, annual ring width measurement and annual ring counting are tasks to determine the strength of a log. Furthermore, these measures are used for log grading in several European countries (see Section 3.1.2.2). The vast majority of literature contributes to the field of dendrochronology. In dendrochronology, the early-/ latewood proportion as well as the annual ring width are of interest (see Fig. 3.4). Compared to industrial annual ring width measurements, high resolution images are necessary to determine the exact early-/ latewood proportion as well as the exact singular annual ring widths.

#### 3.2.2.1 Literature Overview

The focus in this thesis is on literature treating unprepared log end images and images from unprepared cross section discs. For the sake of completion, the literature overview approaches

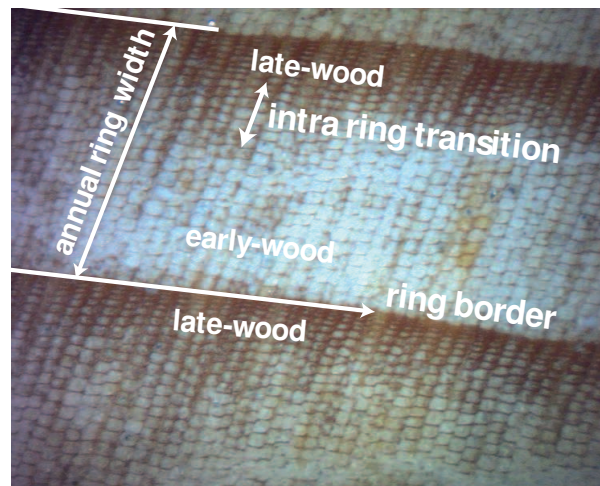


**Figure 3.4:** Microscopic view of an annual ring from a picea abies (spruce). The image depicts the smooth intra transition between early- and late-wood and the sharp transition between two annual rings from late- to early-wood. (Image adapted from: [http://commons.wikimedia.org/wiki/File:Earlywood-latewood\\_PCAB.jpg](http://commons.wikimedia.org/wiki/File:Earlywood-latewood_PCAB.jpg))

treating ct-images or images from well prepared log end faces/ cross section discs are described first.

**Tree Ring Analysis in Dendrochronology** A big part of literature focuses on image analysis to support dendrochronological tree ring analysis tasks. High resolution images of cross section slices are analysed and almost always sanded and probably polished before they are captured. A major task in dendrochronology is to generate tree ring profiles for tree ring dating which is denoted as crossdating. For crossdating tree ring profiles are matched with other profiles. Another aspect is to analyse the climatological circumstances over the tree life time using its tree ring profile sometimes depicted as dendroecology. Consequently, dendrochronological tree ring analysis approaches analyse radial vectors from the pith outwards to the border and generate 1-dimensional tree ring profiles. All known approaches are semi-automatic and require that the pith is moved to the geometric image center or marked by an operator.

The first approach on tree ring analysis by McMillin (1982) is described in Section 3.2. Further approaches for annual ring detection and annual ring width measurement are presented in Rauschkolb (1994), Smith (1995a), Conner (1999), Vaz et al. (2004), Laggoune et al. (2005).

In the master thesis of Rauschkolb (1994) approaches to identify and measure annual rings in high resolution images (400 dpi) of sanded log ends are introduced. The thesis focuses on detecting annual ring boundaries which arise between early- and late-wood. Basically, there

are two boundaries that belong to a single annual ring. A slight border arises at the intra ring transition between early- and late-wood. After winter, the annual ring growth starts with fresh early wood and forms the real annual ring border. Then a strong and sharp crossover between dark coloured late-wood and light coloured early-wood is produced (see Fig.3.4). As final algorithm the author introduced the "Hybrid Edge Detection from Center". For this algorithm the pith position has to be moved to the geometric image center. For each radius on a radial vector a set of 30 pixels is analysed. 15 pixels are taken from the left and right side respectively. The 30 pixel values of each radius along the radial vector are stored in a matrix. Each column represents a neighbour radial vector. Subsequently, the radial vectors in the columns of the matrix are analysed. For edge detection central differences between two pixels on a radial vector are computed. Only pixel with a positive slope (transitions from dark to light) are marked as edge pixels. Finally, the average slope is computed and marked edge pixels smaller than the average are disregarded. Now the matrix is analysed and the edge pixels of each row are summed up. Finally a histogram is produced. The peaks are defined as being ring boundaries. This procedure is repeated four times for initially defined radial vectors with  $\pi/2$  angular distance to each other.

Smith (1995b) described an algorithm which requires perfect annual ring patterns without disturbances or interruptions. The algorithm starts from the outside towards the pith and detects ring boundaries by contour tracing. Subsequently, the area between two boundaries is calculated and assumed to be the annual ring area. As termination condition a flood fill procedure was introduced. This procedure relies on the fact that the innermost area is the smallest.

At the University of Arizona master theses regarding "TREES: computer assisted dendrochronology" are presented by Conner (1999), Giribalan (2000) and Engle (2000) (<http://www.ltrr.arizona.edu/pub/trees/>). The developed semi-automated system for dendrochronology of Conner is also addressed in Conner et al. (1998) and Conner et al. (2000). The system analyses an assembled set of images that are captured under a microscope from the pith outwards to the bark (see Fig. 3.5). For annual ring border detection, the Canny edge detector (Canny, 1986) was utilized. Non maxima suppression was performed by comparing the gradient magnitudes of the neighbours into the gradient direction. This ensures that edge borders are only one pixel wide. Additionally, the system uses the knowledge of the orientation of the captured annual ring section. Edges where the gradient is orthogonal to the annual ring section orientation are disregarded. At last, only transitions from late to early-wood (dark to light) are considered for the final edge image, so intra-ring transitions are disregarded as well. After linking the found edges, the ring widths are measured by counting and averaging pixel distances among them.

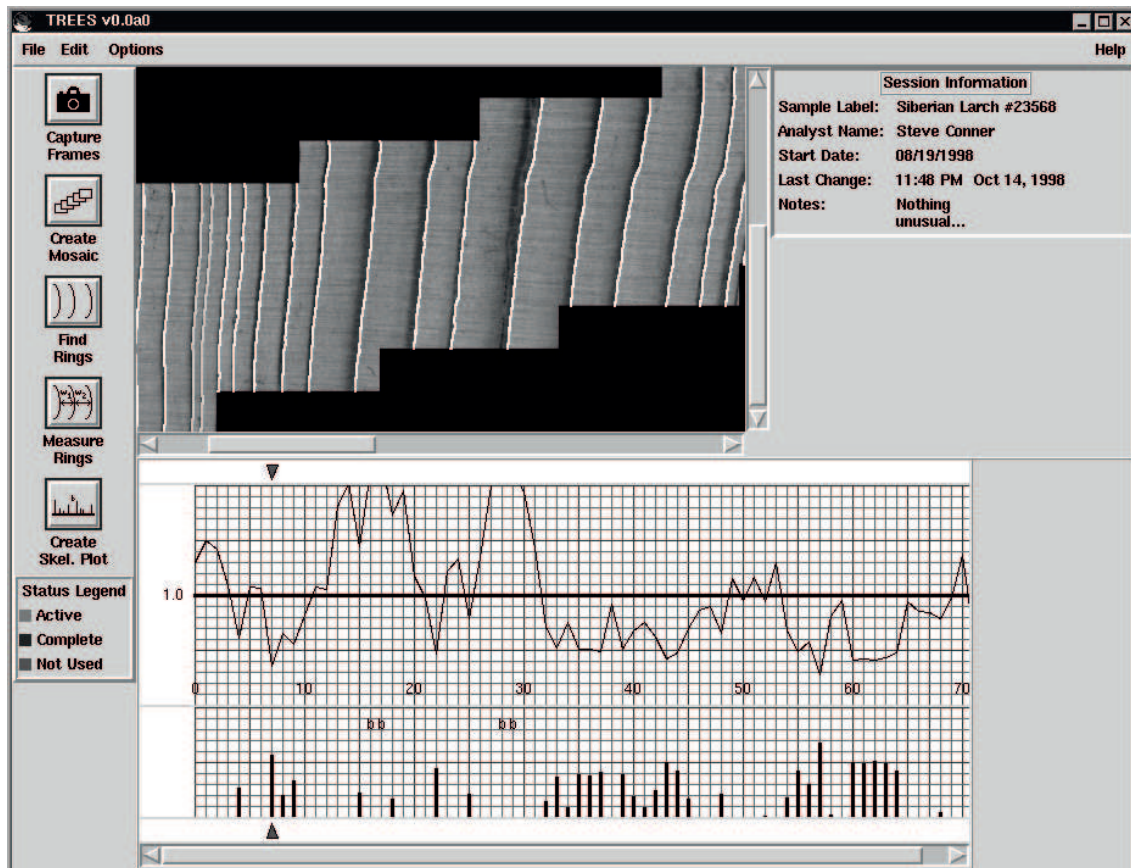


**Figure 3.5:** GUI of the TREES software for dendrochronology. (Image source: Conner (1999))

Several approaches to overcome problems with narrow ring widths are introduced in Vaz et al. (2004). As a solution, the image scale (represented by the annual ring width) is determined prior to annual ring detection. For this purpose, it is assumed that the gray value profile of an annual ring in radial direction can be modelled by a Gaussian profile. Gaussian kernels with different scales are applied to radial vectors. The extrema for each scale are used to determine annual ring centres of all annual rings lying on a radial vector. As intermediate step the signal of the radial vector is analysed and false maxima and minima are removed. Finally, transitions between early and late-wood are determined. First, the original signal of the radial vector is reconstructed with cubic polynomials and a cross-entropy similarity measure between both is used to map the gray levels of a single annual ring into two classes. The border of the two classes defines the intra ring transition and the annual ring borders (see Fig. 3.6).

Laggoune et al. (2005) paid attention to the image quality and proposed an edge detection filter adopted to noisy images. The test images were captured with a grayscale flat bed scanner (600 dpi). After edge detection thinning and thresholding is performed. Now the annual ring contours are searched analysing the neighbours into the gradient direction. Contours whose

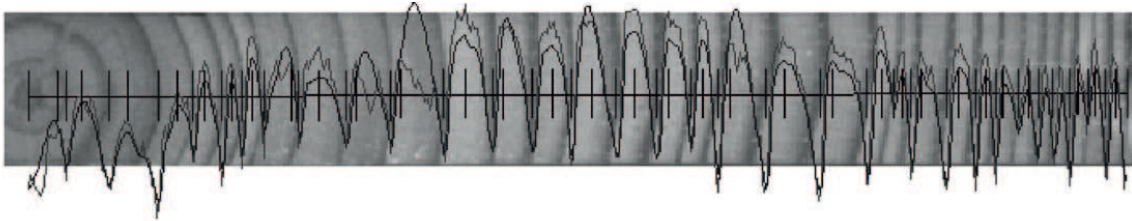


**Figure 3.6:** Estimation of intra- and annual ring borders. (Image source: Vaz et al. (2004))

length are below a certain threshold are eliminated. At last, the found annual ring contours are used to reconstruct a 3D model.

**Industrial Annual Ring Analysis Approaches** Annual ring analysis approaches for images from rough log end ends/ cross section discs are presented in Hanning et al. (2003), Cerda et al. (2007) and Norell and Lindblad (2008), Norell and Borgefors (2008).

In the work of Hanning et al. (2003) an approach to determine the average annual ring width of rough log end boards is presented. With the intention to fulfil the requirements of DIN 4074 the pith position is required to determine the average annual ring width from the pith position to one of the border corners. The pith estimation approach is described in Section 3.2.1. Determining the annual ring width is performed by computing the main frequency of windows positioned along the line between the pith and the border edge. Some unacceptable outliers indicate that the method requires further investigation for an industrial usage.

An algorithm to approximate annual rings on a cross section with closed polygons is described in Cerda et al. (2007). The pith position and the outer shape as polygon are required as input. First, the Canny edge detector is applied to the input image. Using the pith position and the intensity of each detected edge point, dark-to-light edges are determined for further processing. Now polygons of different scales ( $k$ ) (each polygon can be represented as a function of the outer shape and the pith position) are computed (see Fig. 3.7). Each detected edge point is assigned to the closest polygon of a given scale. This results in an accumulator array where each assigned edge point represents a vote for a certain polygon with scale  $k$ . The polygons with local maxima in the accumulator array are assumed to represent an annual ring (see Fig. 3.7).

The first approach for a full automated ring width measurement system on images from rough log ends was proposed by Norell (2009a). The system utilizes the pith estimation presented in Norell and Borgefors (2008). The log end images were captured in a Swedish sawmill and 20

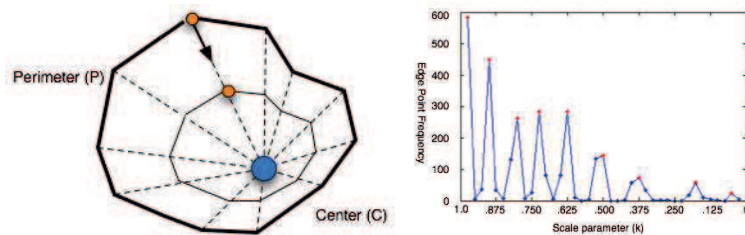


**Figure 3.7:** Polygons with different scale based on the outer shape and the pith position (left). Based on the accumulator array local maxima are chosen to represent annual rings (right). (Image source: Cerda et al. (2007))

images with clearly visible annual rings were used for the experiments. Additionally, a synthetic set of log end images was produced for evaluation (Synthetic Log End Images - Norell (2009b)). After preprocessing and pith estimation the algorithm determines a proper region for annual ring counting. For this purpose, the image is divided into  $N$  circle sectors using the estimated pith position as center point. For all pixels at the cross section, a local orientation estimate is computed. In each sector, the sum of errors between the computed local orientation and the pixel orientation relative to the pith is computed. Next, the contrast of the sector with the lowest error is enhanced. In this sector, annual rings are detected in a radial range between 1 and 9 centimetres from the pith using the grey weighted polar distance transform (GWPDT) presented in Norell et al. (2007) (see Fig. 3.8). Grey weighted polar distance transform can be

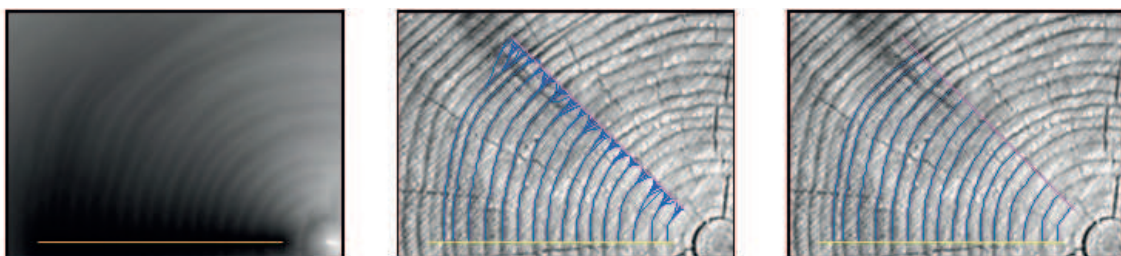


**Figure 3.8:** Illustration of the gray weighted polar distance transform. The left image shows the distance image computed with GWPDT. The image in the middle illustrates computed paths from the angular to the horizontal line. Finally in the right image the shortest paths between the two lines are selected. (image source: (Norell et al., 2007))

used to compute circular and approximately circular paths in grayscale images. For the chosen sector two distance images are computed using the two sector borders as starting lines. Finally, the two distance images are analysed along a radial vector placed at the mean sector direction, which results in two one-dimensional vectors. Local minima in these vectors correspond to annual rings. Before counting the annual rings, elastic registration is used to best match the signals of the two one-dimensional vectors. After registration, the local minima of the registered signals are utilized to count the annual rings. The experiments on the synthetic

images show that eccentric annual rings, small ring widths as well as disturbances result in considerable errors. The experiment on the real log end images are less meaningful because the test set was very small. One conclusion is that the proposed algorithm tends to count less rings than counted by visual inspection. Results for counting annual rings on 75 Scots pine logs are presented in Norell (2010). The approach is identical as the one proposed in Norell (2009a), except that marks from un-even sawing were removed by Fourier Spectrum filtering. The results showed that the proposed approach performs acceptable in a range from 12 to 20 rings. The author concluded that counting annual rings in a sawmill environment is a very difficult task mainly influenced by sawing disturbances.

Similar to Hanning et al. (2003), in Österberg (2009) local Fourier Spectrum analysis is used for pith estimation and several other algorithms (e.g. thickness fields, annual ring counting) are applied to images from well prepared cross section discs. The pith estimation algorithm is described in Section 3.2.1. For annual ring counting, a sliding window is moved along a predefined radial vector where the rings are to be counted. For each pixel on the line the local Fourier Spectrum is calculated using an appropriate window size. The dominating frequencies of the Fourier Spectrum of each pixel are determined and in combination with the line length the amount of annual rings is determined.

### 3.2.3 Further literature on cross section analysis

Further literature on cross section analysis mainly focuses on ct-cross-section images. A stack of ct-cross-section slices from an entire wood log enables the non-invasive analysis of the internal log structure. The analysis of the internal log structure is required for two reasons. First, automated internal log defect detection systems promote the development and the standardisation of automated log grading systems. Second, internal log defects influence the physical properties and the visual appearance of the final wood products. The knowledge about internal log defects is used to improve the saw intake which increases the yield and the value.

Several wood properties and features visible on ct-cross-section images are labelled as wood defects. In case of analysing the internal log structure such defects are entitled as internal log defects (e.g. knots, resin pockets, cracks, spiral grain and compression or reaction wood). Beside the detection of internal log defects approaches for the detection of further wood properties not labelled as defects have been presented.

Subsequently, an overview on the most common literature treating log defect detection and the detection of further wood properties (bark detection and the detection of the hard- and sapwood boundary) is presented.

**Log defect detection and analysis** Except spiral grain all defects are detectable due to their specific gray values, geometric shapes and their location/orientation in ct-cross-section images. The majority of the related literature first determines defect regions in each ct-cross-section slice using different segmentation and clustering techniques. In case of ct-cross-section images it is assumed that different wood defects are represented by grayvalues in a certain grayscale range. By combining the information of all ct-cross-section slices a 3D model of each detected defect is generated. Eventually, each 3D model is assigned to a certain wood defect using different approaches and techniques. The present literature mostly differs in the procedure how the detected objects are assigned to a certain wood defect.

Spiral grain detection works in a different way. The detection of spiral grain can only be established by comparing a set of longitudinal neighboured annual ring structures extracted from the ct-cross-section stack.

The first algorithm for defect detection in ct-cross-section slices is described in Funt (1985) and Funt and Bryant (1987). This algorithm aims to segment and cluster similar gray-scale coloured regions and to classify the kind of defect based on 2D features of the previously segmented regions. Segmentation is based on histogram multi-thresholding. Each pixel is assigned to a certain class representing a set of possible defects. For example, knots are considered to be represented by the darkest pixels. In a further step the pixels of each class are clustered. Eventually, 2D information like size and orientation criterion's are used to validate if a cluster represents a certain defect. For example, knots have an elliptical shape and are longitudinal aligned into the direction of the pith position.

At the beginning of the 1990s different groups of researchers presented various approaches for internal log defect detection. Australian researchers presented ct-cross-section defect detection approaches in Wells et al. (1991), Som et al. (1993), Som et al. (1995). As noted in the literature overview on pith estimation (see Section 3.2.1.1), these publications are not available to us and cannot be examined. Further information on these works can be found in the literature review on knot detection by Longuetaud et al. (2012).

Many publications on log defect detection are published by researchers from the Virginia Polytechnic Institute and State University. For example, in Zhu et al. (1996) a prototype for

analysing ct-slices of hardwood logs is presented. This prototype is the final result of a set of earlier published works (see literature review in Longuetaud et al. (2012)). It consists of a segmentation module and a scene analysis module. The segmentation module first applies the Unser filter to remove annual rings from the ct-cross-section image. In the next step, similar as in Funt and Bryant (1987) adaptive histogram multi-thresholding is utilized. According to the Ph.D.-thesis of Zhu (1993), the pixels are assigned to three different classes. For example, knot and bark pixels are in the same class and are separated by the scene analysis module. Morphological operations are applied to determine 2D regions representing wood defects. Finally, a 3D model is generated by clustering of the 2D areas of all slices together. For each detected object, geometric features and color features are computed. Finally, the Dempster-Schafer theory of evidential reasoning is used to classify the kind of wood defect of each object. For this, basic knowledge about the shape, color and location/ orientation of each wood defect is utilized.

Further publications published by researchers from the Virginia Polytechnic Institute and State University focus on artificial neuronal networks (ANNs) used to classify internal log defects (see Li et al. (1996), Schmoldt et al. (1997), Schmoldt et al. (1998) and Schmoldt et al. (2000)). A prototype system based on the noted previous works on ANNs is presented in Sarigul et al. (2003a) and Sarigul et al. (2003b). These publications provide a good overview on log defect detection using ANNs.

Further research on log defect detection has been published by researchers from the University of Georgia. In Bhandarkar et al. (1996) and Bhandarkar et al. (1999) the system CATALOG (Computer Axial Tomography for Analysis of LOGs) is described. The system uses 3D shape parameters to classify and 3D render internal log defects. In recent two publications, Bhandarkar et al. (2006) and Bhandarkar et al. (2008) presented a new approach based on Kalman filter tracking algorithms.

Further recent approaches are presented by Rojas et al. (2006), Wei et al. (2009), Baumgartner et al. (2010), Breinig et al. (2012), Longuetaud et al. (2012) and Cristhian A. Aguilera (2012).

In Rojas et al. (2006) two supervised classification algorithms (minimum distance classifier and maximum likelihood classifier) for wood defect detection are introduced and evaluated. The work of Wei et al. (2009) evaluates the applicability of a back propagation artificial network and the maximum likelihood classifier for wood defect detection in sugar maple and black spruce. In Baumgartner et al. (2010) the main focus lies on knot detection just in the heartwood region. For this purpose, the sapwood–hardwood boundary was detected in polar transformed cross sections using the pith as pole.

A knot-detection (3DKnotDM) software package and exhaustive experiments and tests on the accuracy and timing performance are presented by Longuetaud et al. (2012). Additionally, this work includes a well-structured literature review on knot-detection in ct-images. Finally, in Cristhian A. Aguilera (2012) the idea of using active contours to detect internal log defects using a-priori information is introduced and evaluated.

So far, the listed literature treats the general task of internal log defect detection or specialises on knot detection and analysis. Furthermore, a few other publications focused on the detection or analysis of a particular log defect. Approaches for crack detection in ct-cross-section images are published by Bhandarkar et al. (2005), Li and Qi (2007) and Wehrhausen et al. (2012). In Bhandarkar et al. (2005) Sobel-like filters are used to detect annual rings and cracks which are aligned orthogonal to the annual ring structure. A recent approach presented by Wehrhausen et al. (2012) also uses directional filters and focuses on the evaluation of the approach. A novel approach based on fractal dimension is presented by Li and Qi (2007).

Another wood defect is compression wood or reaction wood. The only found work treating automated compression wood detection in ct-images or digital images is presented by Nystrom and Hagman (1999). It seems that there is no further literature on compression/ reaction wood detection.

Literature on spiral grain detection using ct-image slices of logs are presented in Sepúlveda (2001), Sepúlveda et al. (2002), Ekevad (2004) and Entacher et al. (2007). The approach presented by Sepúlveda (2001) manually analyses streaks in surfaces that are generated by cutting the ct-cross-section image stack concentrically around the pith. The streak inclination relative to the longitudinal axis corresponds to the spiral grain. In Sepúlveda et al. (2002) the authors tried to predict spiral grain based on variables extracted from cross-section images (e.g. knot volume and heart/sapwood relation). The results indicated that prediction of spiral grain should be possible.

Another algorithm to determine spiral grain is presented by Ekevad (2004). Principal directions of inertia of spheres that are distributed along the longitudinal axis of a log or wood board can be used to compute local fibre-directions which represent the local spiral grain angle.

Eventually, the applicability of motion estimation algorithms for spiral grain detection is evaluated in Entacher et al. (2007). For this purpose, the ct-cross-section image stack is interpreted as video data and three different motion estimation techniques are assessed. The results are too irregular and it is not clear if the detected movements are correlated to spiral grain in wood.

**3.2.3.0.1 Further wood properties: detection and analysis** The group of wood properties that are not labelled as defects and which are relevant for cross-section analysis tasks is formed by the pith, annual rings, heart- and sapwood and the bark. Annual ring analysis and pith estimation were treated in Section 3.2.1.1 and Section 3.2.2, respectively. Subsequently, the most common literature treating detection and analysis of bark and heart-/sapwood is quoted.

For heart- and sapwood detection, approaches based on heat sensitive infra-red images (Gjerdum and Høibø (2004)) and ct-images (Longuetaud et al. (2007)) were published. In Gjerdum and Høibø (2004) an approach to detect heartwood in Scots pine using heat infra-red images of log ends is introduced. Due to the different physical structure of heart- and sapwood their moisture contents differ which results in different temperatures. Consequently, heart- and sapwood can be clearly identified in heat infra-red images of log ends.

The heart-/sapwood boundary detection algorithm proposed by Longuetaud et al. (2007) uses the pith position and analyses the gray values of 360 radii. For each radii the first pixel exceeding a certain threshold is chosen as boundary point.

At last, bark detection is considered. Automated bark detection enables to determine the exact volume of a wood log without debarking it. For some wood species it is critical to remove the bark for longer periods - e.g when storing it on the sawmill yard. Basically, no research focuses on the particular task of bark detection. However, most of the approaches in the literature on log defect detection are able to detect and analyse the bark in ct-cross-section images. An industrial solution for bark detection is provided by the company Microtec (<http://www.microtec.eu/de>). A scanner entitled TOMOLOG automatically creates a 3D profile of the log with and without bark. In Baumgartner et al. (2007) results for automatic bark measurements using the TOMOLOG scanner are presented.

# PART II

---

## Implementation

The second Part of this thesis addresses two practical issues of the development of a biometric log recognition framework, named as *TreeBio* framework. This part is subdivided into four chapters. In the first Chapter, (Chapter 4) the *TreeBio* framework is introduced and the main issues of a biometric log recognition system using log end images are pointed out. Subsequently, in Chapters 5 and 6, approaches and experiments for pith estimation and cross-section segmentation are presented. Eventually, this part concludes with a discussion and an outlook on future work for the further development of the *TreeBio* framework.

# Chapter 4

## TreeBio framework

This chapter presents considerations for a biometric recognition framework for wood logs using digital log end images. For this purpose, schemes of the enrolment and the recognition procedures are presented and discussed. As integral parts of the TreeBio framework, the importance of pith estimation and cross-section segmentation is emphasized.

Analogous to biometric systems using fingerprints or iris images as biometric characteristics, different tasks have to be performed to generate a biometric template of a single log. A biometric template is a compact and fast comparable representation of the features extracted from the biometric characteristic which is stored into the database of the biometric system. Figure 4.1 illustrates an exemplary enrolment scheme for tree logs.

As described in Section 2.2, a tree log is a sub-part of a tree. For an industrial application, harvesters could be used to capture both ends of a single log after the log end is cut by the harvester head. Due to the growth of a tree, it can be assumed that the two ends of a single log are different and so their biometric templates will differ. To establish traceability in the LSC, it is required to recognize each log independent of the captured log end.

In the enrolment stage, additional data is added to the template of each log. For example, the harvester operator can assign data like source, owner, date of cutting and other relevant information for log processing to each log template. Another possibility is to assign data captured by the harvester head. Only in combination with additional data a single log gets an identity.

Before generating biometric templates, two basic steps have to be performed. In a first step, different image analysis/ processing tasks are performed. With respect to this thesis pith

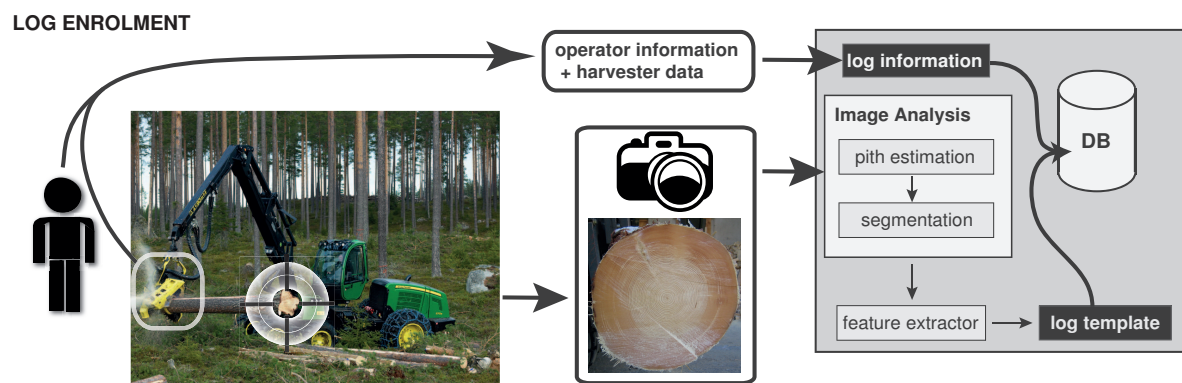


**Figure 4.1:** Exemplary illustration of an enrolment scheme for the TreeBio framework

estimation and cross-section segmentation are listed as image analysis tasks in the schematic enrolment illustration (Fig. 4.1). Second, appropriate feature extraction methods are required.

The theoretical part of this work shows that the pith is a unique reference point and its location represents a unique feature of a log end. Consequently, pith estimation is an integral component of the TreeBio framework. The estimation of the relative pith location with respect to the cross-section requires to determine the cross-section boundary. These considerations show that cross-section segmentation is a further integral part of the framework. Additionally, the cross-section shape is a further feature of the log end.

Before continuing with feature extraction, image registration techniques have to be applied to the segmented log end face. Image registration enables a system which is invariant against rotation, scaling and different angles of the captured cross-sections. Again, the pith position and the cross-section boundary are required to solve image registration issues. Finally, methods for feature extraction on cross-sections are required. As noticed, the pith position and cross-section boundary of the log end can be used as features. Furthermore, methods from fingerprint and iris recognition can be applied to log end images to extract a set of features. Finally, the extracted features have to be transformed to a compact and fast comparable representation – the biometric template. Together with the collected log information it is then stored into the database of the TreeBio system. The tree log is now enrolled in the system.

A scheme for log recognition is shown in Fig. 4.2. Industrial applications for log traceability require a system that operates in identification mode. In some cases the template space can be reduced by using additional information, like the source of a bulk of trees or shape features.

Log recognition starts by capturing a log end anywhere in the LSC. In Fig. 4.2 two examples for possible capturing places are depicted. However, the log end image is passed to the image

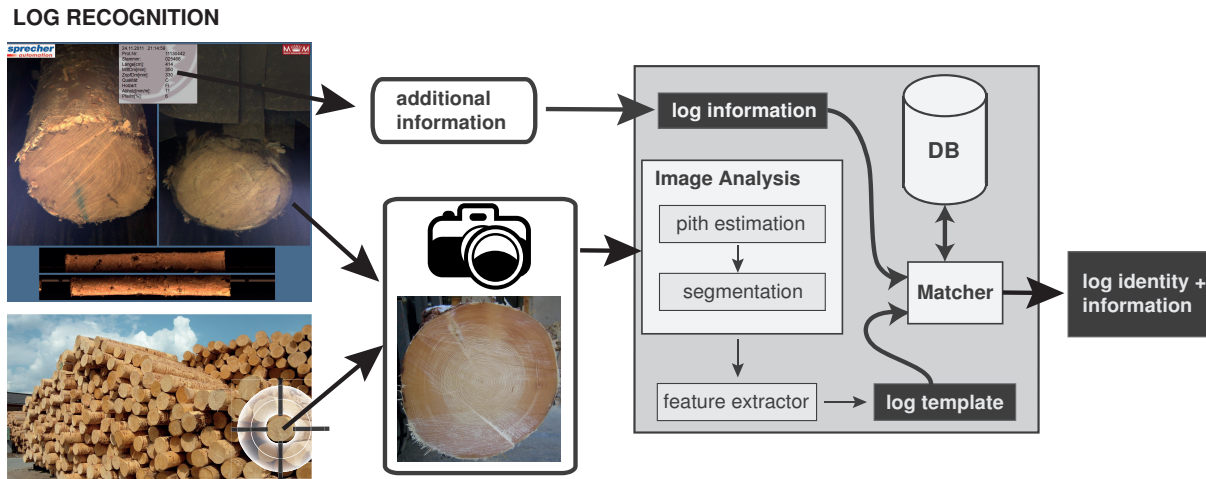


**Figure 4.2:** Exemplary Illustration of the log recognition scheme for the TreeBio framework

analysis module. As mentioned, additional information simplifies the recognition procedure. Like in the enrolment, a biometric template is generated. The template is passed to a matching module which is crucial for log recognition. The matcher compares the received template with all or a subset of templates in the database. Finally, the matcher has to decide whether or not a corresponding template in the database exists. In the positive case the matcher returns the identity information of the log which was added in the enrolment stage.

# Chapter 5

## Pith estimation

The considerations in the previous chapter outlined the requirements for pith estimation in the TreeBio framework. In this chapter a comprehensive study on pith estimation in rough log end images is presented. Parts of this chapter have been published in Schraml and Uhl (2013) before this thesis has been finished.

As introduced in Section 3.2.1 pith estimation is fundamental for cross section analysis. Previous approaches for analysing cross section images mostly rely on images from polished/sanded cross sections or ct-images. Ct-images are free of distortions caused by sawing or dust and the annual ring borders are slightly emphasized. Approaches treating ct-images rely on annual ring analysis. Due to the distortions annual ring analysis approaches are not applicable to images of rough log ends.

Local orientation estimation approaches for pith estimation are shown in Hanning et al. (2003), Österberg et al. (2004) and Norell and Borgefors (2008). The former two use local Fourier Spectrum analysis for pith estimation on rough log end boards and on well prepared cross section discs, respectively. The authors use the peak of the local Fourier spectrum as local orientation estimate of an annual ring section. Pith estimation approaches rely on the assumption that annual rings are concentric circles. Consequently, local orientation estimates point towards the pith. With intersection of the local orientations the pith position is determined. The experiments of Hanning et al. (2003) indicate that pith estimation using local Fourier Spectrum analysis could also be applied on images from rough log ends. So far the only work focusing on the treatment of images of rough log ends was presented by Norell and Borgefors (2008) utilizing two local Fourier Spectrum analysis methods suggested in Knutsson and Granlund (1983) and Bigun (1992). Both methods determine local orientations by convolution

of filter kernels in the spatial domain. Results of Norell and Borgefors (2008) show that the second method ( Laplacian pyramids and linear symmetry) is more robust to disturbances. Even though Norell and Borgefors (2008) provides first important insights into pith estimation of rough log ends, the authors of Norell and Borgefors (2008) noticed that the used image test set is not appropriate to draw conclusions about the performance of pith estimation for rough log ends of a sawmill yard.

This work contributes to pith estimation by treating images from rough log ends of a sawmill yard. By treating images of rough log ends, this work presents first insights on different pith estimation methods applicable in the TreeBio framework. For this purpose the Peak Analysis Method ( Hanning et al. (2003) and Österberg et al. (2004)) and further three Fourier Spectrum Analysis methods are used to compute local orientations of small sections from cross section images, denoted as annual ring sections. Contrary to Norell and Borgefors (2008) it is shown that local orientation estimation in the Fourier domain is applicable for annual ring sections from rough log ends. For estimating the pith position two different algorithms for selecting annual ring sections and intersecting the gathered local orientations are assessed. One of these methods is based on the pith estimation algorithm presented in Österberg et al. (2004). To the author's knowledge, no study so far has focused on the influence of the annual ring section size and selection on the pith estimation accuracy and timing. Thus, this work additionally contributes to existing literature by showing that the size, the amount and the selection of annual ring sections influence the accuracy and timing of the proposed methods for pith estimation.

The empirical study compares two different sets of cross section images. One image set consists of 109 images of rough spruce log ends from a sawmill yard. The other set is equal to the ct-image set used in the experiments of Entacher et al. (2008). The results of the experiments of the ct-image set are compared to the results for pith estimation using annual ring analysis methods presented in Entacher et al. (2008). The results of the proposed methods on the rough log end images are compared to those from Norell and Borgefors (2008).

Section 5.1 introduces the basics of local orientation estimation (subsection 5.1.1) and presents considerations about Fourier Spectra of annual ring sections (subsection 5.1.2). Subsequently three Fourier spectrum analysis methods for local orientation estimation of annual ring sections are introduced (subsection 5.1.3). Two pith estimation algorithms for selecting annual ring sections and computing a pith estimate are presented in Section 5.2. Finally, Section 5.3 describes and assesses the experiments on the two image sets.

## 5.1 Local Fourier Spectra analysis of annual ring blocks

All pith estimation approaches using annual ring analysis or local orientation estimation methods rely on the assumption that annual rings are concentric circles the center point of which is the pith position. Annual ring analysis focuses on finding and identifying annual rings. The detected annual rings or arcs are then used to compute orthogonal vectors pointing towards the pith or to compute annual ring/ arc centre points representing votes for the pith position. Regardless of using gradient operators, edge detectors or other methods to extract annual rings or arcs, it becomes impossible to extract valid data with increasing disturbances (see Section 5.1.2). Local orientation estimation methods show higher reliability in case of disturbances.

### 5.1.1 Local orientation estimation

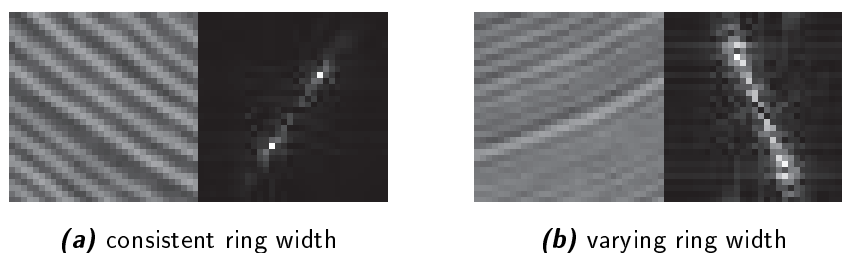
Local orientation estimation is a widely used technique in image processing systems and especially in texture analysis. In Bigun and Granlund (1987) and Granlund and Knutsson (1995) the terms "linear symmetry" and "simple neighbourhood" are introduced, respectively. These terms are based on images where the grey values are equal along lines and only change in one direction. Such images are called simple images. The direction in which the grey values vary is defined as the image orientation, denoted as a unit vector  $\hat{n}$ . A simple neighbourhood can be represented by a 1-dimensional function  $f(x, y) = g(x) = g(x^T \hat{n})$  where  $x^T \hat{n}$  denotes the scalar product Jähne (2005). Images that are not simple can be divided into image sections, which (approximately) fulfil the property of simple images. Image orientations of such simple image sections are referred to as local orientation. The Fourier Spectrum of a simple image is represented by a single line that is equally oriented as the simple image orientation. If the simple image can be described as a sinusoidal function it is represented by two points in the Fourier spectrum. The more the simple image deviates from being simple the more the Fourier Spectrum spreads.

### 5.1.2 Fourier Spectra of annual ring sections

The energy distribution of annual ring sections in the Fourier Spectrum is influenced by the capturing device (ct-scanner, digital or infra-red camera, ...), the wood species (different wood species show different annual ring structures), wood properties visible at the cross section (e.g. knots), the wood surface (sanded or rough - chainsaw or circular saw), and several other

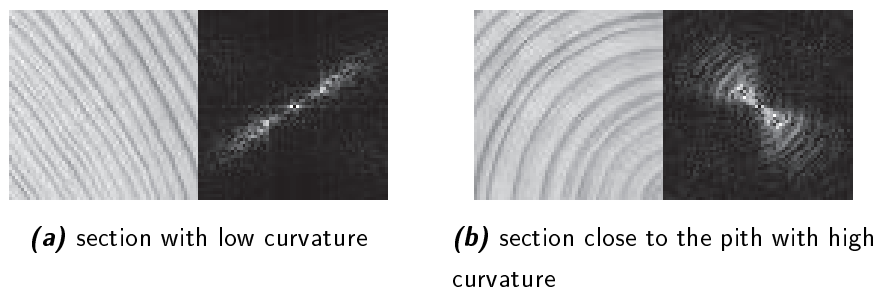
disturbances (light conditions, soiling and dirt, cracks, ...).

Annual ring sections of ct-cross section images are nearly free from distortions and have similar properties as images from sanded/ polished log ends. Compared to images from rough log ends they show less cracks and no cutting distortions (compare the annual ring sections in Fig. 5.2 and Fig. 5.3).



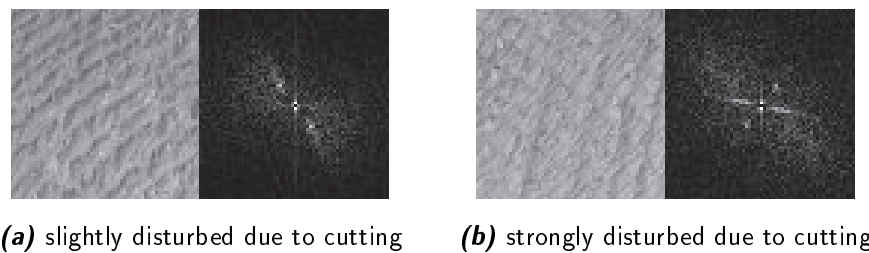
**Figure 5.1:** Annual ring sections from a ct-cross section image and their Fourier Spectra

Fig. 5.1 shows two annual ring sections from a ct-cross section image. The annual rings in Fig. 5.1a are consistent in width and are slightly curved. As a result the Fourier spectrum is concentrated around two points that reflect the main annual ring width and the annual ring orientation. In Fig. 5.1b the annual ring widths vary more strongly and the Fourier spectrum spreads from a point to a straight line. The annual ring sections in Fig. 5.2 are from a sanded



**Figure 5.2:** Annual ring sections from a sanded cross section and their Fourier Spectra

log end face, captured under perfect light conditions. Apart from the inverted colour (late wood is bright and early wood is dark) these annual ring sections are similar to those from ct-cross section images. Fig. 5.2a and Fig. 5.2b demonstrate the influence of the annual ring curvature on the Fourier Spectrum. The stronger the curvature, the more the line spreads and forms two circle sectors. The annual ring sections in Fig. 5.3 are from a rough log end image. It is obvious that the noise increases in the spatial domain as well as in the Fourier domain. While in Fig. 5.3a the dominant annual ring orientation is clearly visible, in Fig. 5.3b two different orientations are present. This typically occurs when the cutting pattern, cracks, knots or light shadows disturb the annual ring section. Commonly, many annual ring sections



**Figure 5.3:** Annual ring sections from a rough log end image and their Fourier Spectra

from a rough log end image are disturbed in such a way, so that no annual ring orientation can be determined.

Subsequently, different approaches for local annual ring orientation estimation using Fourier Spectrum analysis are presented. All presented methods utilize the Fourier Spectrum of a given annual ring section as input. As results, all methods deliver an estimate of the orientation and if possible a certainty value of the estimate. For this purpose the size of the annual ring section in conjunction with the image resolution has to be chosen carefully. Basically, a higher image resolution provides more detailed information about the cross section, but on the other hand it suffers from additional noise in the Fourier Spectra of the annual ring sections. The size of the annual ring section determines the amount of included annual rings. The bigger the annual ring section, the higher the probability of a stronger annual ring curvature and a variation in width. These observations also affect the performance of the following methods to some extent.

### 5.1.3 Fourier Spectrum analysis methods

In this subsection the Peak Analysis method (c.f. Hanning et al. (2003) and Österberg et al. (2004)) and additionally three methods for local orientation estimation using Fourier Spectrum analysis are described. First, two approaches for Fourier Spectrum preprocessing of annual ring sections are described.

#### 5.1.3.1 Fourier Spectrum Preprocessing

Two circumstances require a filtering of the Fourier Spectrum. First, it can be expected that the annual ring texture of an annual ring section is assigned to a certain bandpass in the Fourier Spectrum. Consequently, a bandpass filter, filtering low and high frequencies, is used to filter out insignificant frequencies. Second, annual ring sections from images of rough log

ends cause a very noisy Fourier Spectrum. A simple threshold is used to determine frequencies with a high magnitude. The threshold is calculated by determining two peaks of the Fourier Spectrum. If the ratio between them exceeds a certain value (e.g. 0.6) the threshold is set to  $T = \text{max. peak} \cdot \lambda$ , where  $\lambda$  is chosen in a range between 0.6 - 0.9. Otherwise it is assumed that the annual ring pattern is represented by the max. peak and just the maximum peak is further processed.

### 5.1.3.2 Peak Analysis - PA

PA is a very simple technique to gather a local orientation estimate. Linear symmetry assumes that the Fourier Spectrum of a simple image is aligned along a straight line. Disregarding the DC coefficient the maximum frequency should also lie on this line. Especially in the case of annual rings and appropriate section sizes, it can be assumed that the annual ring growth is approximately regular. The more uniform the local annual ring pattern is, the more the Fourier Spectrum converges to a single point. PA for pith estimation was introduced by Hanning et al. (2003) with the intention to count existing annual rings on rough log end boards from the two top end board edges into the direction of the pith. For this purpose, the presence of the pith on the board is not required. In this work the scope is to determine the exact pith position in images of rough log ends. For implementation a simple maximum search in one half-plane of the Fourier Spectrum has to be performed. The line through the Fourier Spectrum origin and the maximum coefficient of the preprocessed Fourier Spectrum is used as the local orientation estimate.

### 5.1.3.3 Least Squares Regression - LSR

Regarding the concept of linear symmetry, linear regression analysis is most qualified for orientation estimation. Linear regression methods enable the fitting of a line into a point cloud. Regardless if one or more explanatory variables describe one independent variable, simple or multivariate linear regression models are utilized. For linear symmetry analysis in the Fourier Spectrum the X and Y coordinates can be used alternatively as explanatory or independent variable.

The method of least squares regression is the best known method for fitting a regression line into a point cloud. Since LSR reduces the summed squared error (SSE) of the dependent variable it is necessary to determine the correlation coefficients of the X and Y values. If one

axis shows a dominant correlation coefficient it is used as independent variable for the LSR. As certainty value the absolute coefficient of determination  $|R^2|$  is computed and ranges between 0 and 1. For similar correlation coefficients (ratio  $> 0.8$ ) LSR is computed with both axes as independent variables. Subsequently, the results are combined and the certainty value is set to 1. Finally the slope of the regression line, representing the local orientation estimate and the certainty value, are received as results.

#### 5.1.3.4 Weighted Least Squares Regression - WLSR

Due to the quadratic error weighting, LSR is very sensitive to outliers. A simple method to overcome the problem, that outliers from less significant frequencies influence the accuracy of LSR, is to utilize the magnitudes of the frequencies as weights. Due to the weighting - the frequencies with a high magnitude have more impact on linear regression than those with a low magnitude.

$$\beta = \frac{\sum(X_i \cdot Y_i \cdot W_i)}{\sum(X_i^2 \cdot W_i)} \quad (5.1)$$

As weight ( $W_i$ ) for a given point in the Fourier Spectrum ( $X_i, Y_i$ ) the square root of the related frequency magnitude ( $M_i$ ) is used  $W_i = \sqrt{M_i}$ . Except from using weights, WLSR is performed in the same way as LSR to compute a local orientation estimate and the related certainty value.

#### 5.1.3.5 Principal Component Analysis - PCA

PCA for texture orientation analysis using local Fourier Spectrum analysis was presented by Josso et al. (2005). In addition to determining a local orientation estimate PCA, can be used to make an assertion about the isotropy/ anisotropy of the analysed texture. Computationally PCA, is based on the Eigendecomposition of the covariance matrix for the XY coordinates. Eigendecomposition of the covariance matrix leads to two eigenvectors that represent the given points of the Fourier Spectrum. These two vectors are perpendicular to each other. The eigenvalues of the eigenvectors provide the information about the isotropy/ anisotropy. Anisotropy is used as a measure of the certainty of the orientation estimate. The more one eigenvector dominates, the more anisotropic is the distribution of the frequencies in the Fourier Spectrum. This means that an anisotropic distribution is an indicator of a simple image. For local orientation estimation the dominating eigenvector is utilized as the local orientation

estimate. The ratio

$$\lambda = \frac{l_1 - l_2}{l_1} \quad (5.2)$$

between the eigenvalue  $l_1$  of the dominating eigenvector and the eigenvalue  $l_2$  of the second eigenvector can be utilized as a certainty value

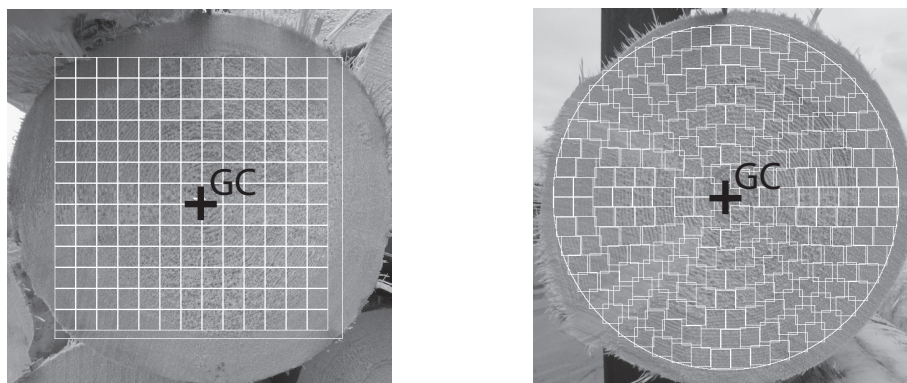
## 5.2 Pith estimation algorithms

This section describes two different algorithms for selecting annual ring sections/ image blocks and computing a pith estimate. The objective of both algorithms is to select image blocks and to compute local orientation estimates for each block. Finally, each algorithm uses the gathered local orientation estimates to perform an intersection step and to compute a pith estimate.

### 5.2.1 Block area selection - BAS

In Norell and Borgefors (2008), a rectangular area around the geometric image center is used to compute local orientation estimates for a subsequent intersection procedure. Knowledge about the cross section size and its location in the image is a precondition. Predefining an area, in which blocks are selected, is the simplest method to gather local orientation estimates for a subsequent intersection procedure. After specifying an area it is subdivided into image blocks. Overlapping image blocks or a sliding window have the advantage that more annual ring orientations can be determined. The size of the blocks depends on the image resolution and on the cross section image type. Appropriate block sizes vary between 8x8 and 128x128 pixels. The experiments indicate that a lower resolution provides some advantages. High resolution images require a large blocksize and small structures and disturbances become visible.

In Fig. 5.4, subdivided rectangular and circular areas of two rough log end images are shown. The rectangle and circle dimensions were determined using the geometric image properties of the pre-cut images of rough log ends. For all selected blocks, a local orientation estimate is computed using one of the Fourier Spectrum analysis methods. Except for the PA method, a certainty value is additionally determined. Finally, local orientation estimates with a certainty value exceeding a certain threshold are further processed, (in the case of the PA method all local orientation estimates are further processed). Similar to Hanning et al. (2003) and Norell and Borgefors (2008) an accumulator array is used to sum up the intersections of all



**(a)** Rectangular area and non-overlapping blocks (32x32 pixels)      **(b)** Circular area and non-overlapping blocks (32x32 pixels)

**Figure 5.4:** Two cross section images from the rough log end image set (RLE-IS) with two different predefined areas for BAS

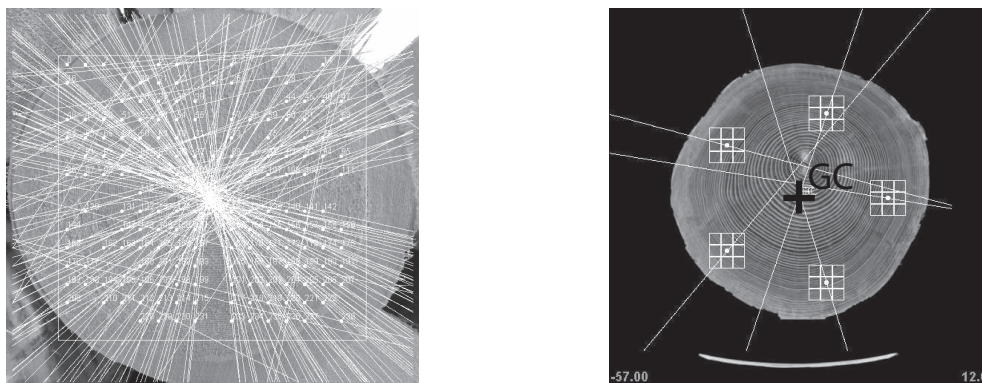
valid local orientation estimates. Finally, the accumulator array is filtered with a Gaussian smoothing kernel and the maximum accumulator value is assumed to hold the pith position. The Gaussian filter flattens local peaks and summarizes peak groups to a single peak. Fig. 5.5a shows an intersection image where a rectangular area and non-overlapping blocks with 32x32 pixels were used. It is clearly visible that the line intersections concentrate around the pith periphery. BAS can be performed with many variations. For example, Norell and Borgefors (2008) performed a second BAS choosing a rectangular section around the first estimated pith position.

### 5.2.2 Pointwise block selection - PBS

In Österberg et al. (2004), another technique that uses the geometric image center (GC) as initial reference point is presented. The principle of this technique is that first, two points around a reference point are chosen. Then, two local orientation estimates are calculated for the annual ring sections around these points. The intersection of these orientations is used as a new reference point. The procedure stops after a certain number of iterations or if the new reference point is close to the old one. The concept of this technique is based on the assumption that annual rings close to the pith are more circular. Optimally, the pith estimate accuracy increases after performing several iterations.

For the experiments Österberg et al. (2004) used images from well prepared log end images. Preliminary experiments showed that pith estimation using only two local orientation estimates (in each iteration) becomes more inaccurate the more disturbed the cross section image. In

the present work an extension of the suggested technique is introduced to overcome problems caused by inaccurate local orientation estimates. The GC is used as the initial reference point. In contrast to Österberg et al. (2004), the number of points can be chosen individually. These points are equally distributed on a circle described by a predefined radius around the reference point. Each point is used as a center point of an image block cluster. A cluster consists of an

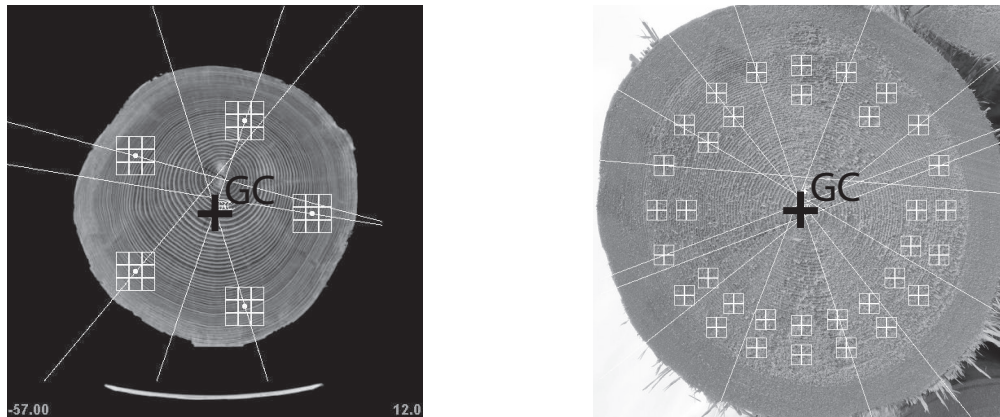


(a) BAS Intersection on a rough log end image (b) PBS/ ct-cross section image where 5 points with a cluster size of 3x3 blocks were chosen

**Figure 5.5:** Intersection Images

arbitrary number of blocks. For each block of a cluster, the local orientations and certainty values are calculated. The information of all blocks of a cluster are then used to determine whether a valid cluster orientation estimate can be calculated. If not, a new point on a reduced radius, closer to the reference point is chosen and the cluster orientation estimation procedure repeats. After a certain number of unsuccessful iterations the procedure is cancelled and it is continued with the next initially chosen point. The cluster orientation estimation procedure is performed for all initially chosen points. At least two valid cluster orientation estimates are necessary to perform an intersection procedure. Finally, the barycentre of the intersections of all valid cluster orientations is chosen as the intermediate pith position. This one is utilized as new reference point and the whole procedure is repeated with a decreased radius. The algorithm terminates if the distance between the old and new pith position is under a certain limit or if a certain number of iterations were performed. In Fig. 5.5b a ct-cross section image is depicted where one iteration of the described algorithm has been performed. Five points in a radius of 120 pixels around the GC were chosen. For all clusters a valid cluster orientation estimate could be computed. Each cluster consists of 9 - 16x16 pixel blocks. The barycentre, which is assumed to hold the pith position, is not marked. PBS has the advantage that only a few blocks have to be analysed, keeping the computational effort low. In case of images from rough log ends it is very difficult to decide if a single cluster provides a valid orientation. Although for nearly all of the 20 points a second cluster position was computed - Fig. 5.6b)

shows that for only 8 points a valid cluster could be determined.



(a) ct-cross section image where 5 points with a cluster size of 3x3 blocks were chosen.

(b) rough log end image where 20 points with a cluster size of 2x2 blocks were chosen

**Figure 5.6:** Two cross section images where the first iteration of PBS has been performed

### 5.3 Experiments

The experiments provide information about the pith estimation performance of the two pith estimation algorithms (BAS, PBS) utilizing Fourier Spectrum analysis methods for local orientation estimation. The focus is to evaluate the performance and applicability of the particular Fourier Spectrum analysis methods for analysing annual ring sections from rough log end images. Results for a ct-cross section image set (CT-IS), using the same images as in Entacher et al. (2008), show how the proposed methods perform on less disturbed images. The accuracy of the proposed methods on the rough log end image set (RLE-IS) is compared to the results presented in Norell and Borgefors (2008).

The pith estimation performance is evaluated by computing several statistical values. The mean (Mean) describes the deviation from all epp (estimated pith positions) to the corresponding mpp (measured pith positions). StDev is the standard deviation from the Mean. R is defined as the span between the maximum and minimum pith estimation deviation. #Blocks (#B) gives the number of valid blocks that exceed the certainty threshold and are finally used for the intersection step. Finally, the computation time in milliseconds [ms] specifies the demand for the whole pith estimation process, except file IO.

Subsequently, for each of the two image sets the accuracy and the timing performance for pith estimation using the two pith estimation algorithms and different Fourier Spectrum analysis

methods are presented. As a next step, the results are summarized and general conclusions about the accuracy and the timing performance of the particular configurations are drawn. All experiments were performed on an Intel Core i7-2620M processor with 2.7 GHZ and 8GB RAM, JRE 1.6.

### 5.3.1 Image test sets

For the experiments on pith estimation two different image test sets were used. One image set (CT-IS) was captured with a ct-scanner. It consists of 36 (512x512 pixels) cross section images taken from a single log. This image set was also used for the pith estimation experiments in Entacher et al. (2008). The second image set (Rough Log End Image Set / RLE-IS) consists of 109 (1024x768 pixels) spruce log end images captured with a digital camera (Samsung WB2000). Examples of both images sets are illustrated in Fig. 5.10 and Fig. 5.8. These images were taken on a saw mill yard in Austria without flash and at approximately the same distance from the log end surface to the camera (see Fig.5.7). Consequently, one pixel



**Figure 5.7:** Illustration of the capturing procedure for the RLE - image set using adjusting pliers. All images were captured at approximately the same distance and as normal as possible to the cross section surface. (Photo: Schraml)

corresponds to approximately 1.7 mm. The captured images represent log ends and their features found on a saw mill yard processing spruce logs. Log ends without any visible annual rings have been excluded. At the sorting station all log ends were cut by a circular saw. The ground truth (measured pith position - mpp) for both image sets was determined by visual inspection. Due to the approximately equal cross section size in all images of the CT-IS no localization of the cross section is necessary. The diameters of the log ends in the RLE-IS vary

between 25 and 50 cm. For simplification the images were pre-cut to the size of the log end sizes.

### 5.3.2 CT-IS experiments

For pith estimation on the CT-IS the two pith estimation algorithms (BAS, PBS) are tested with each of the four Fourier spectrum analysis methods.

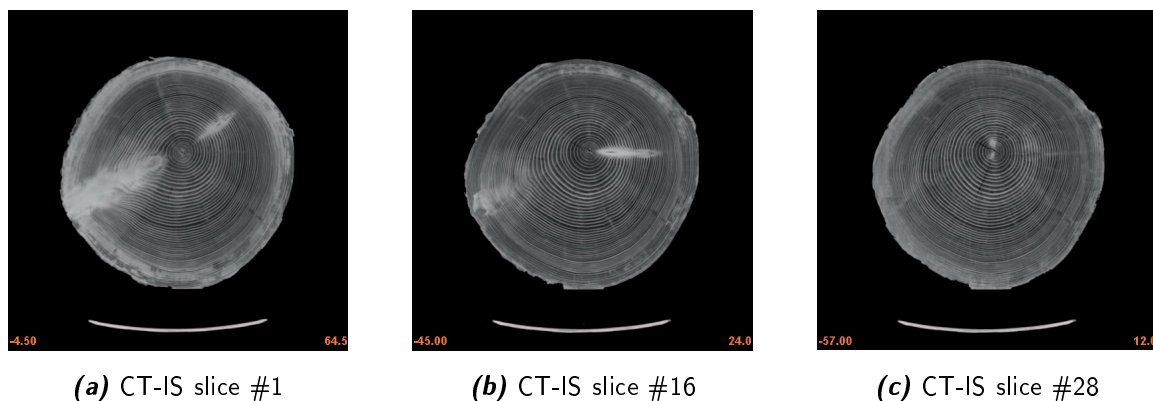


**Figure 5.8:** Computer tomography image set examples (CT-IS)

For this purpose three configurations are selected and evaluated in detail. The first configuration (CT-BAS-C1) uses non-overlapping 16x16 pixels blocks and a rectangular BAS. The second configuration (CT-BAS-C2) first applies CT-BAS-C1. Based on the assumption that annual rings close to the pith are more circular, an 80x80 pixels rectangular area around the first pith estimate is defined. Local orientation estimates closer to the pith should point more precisely to the pith position. Subsequently, a second BAS with non-overlapping 8x8 pixel blocks is performed with the newly defined area. The second pith estimate is used as the final pith estimate. For both configurations the accumulator array is smoothed with a Gaussian filter with  $\sigma = 1$ , before the maximum value is determined.

The third configuration (CT-PBS-C3) uses the PBS algorithm. Five clusters with 16x16 pixel blocks are selected at each iteration. Each cluster consists of 4 blocks and at maximum 5 iterations are performed for estimating the final pith estimate. The radius for the first iteration was set to 100 pixel and decreases by a factor of 0.6 for each iteration. As termination criteria between the results of two iterations a value of 2 pixel is used.

The particular configurations and Fourier Spectrum analysis methods are tested with different certainty thresholds in a range between 0.3 and 0.9. For each configuration and Fourier

Spectrum analysis method the most accurate result gathered with a particular certainty value is selected for the statistical analysis illustrated in Table 5.1. For PA no certainty value is computed and so #Blocks in the PA results using BAS gives the total number of selected blocks in the rectangular area. Comparing the results from CT-BAS-C1 and CT-BAS-C2, the

Config.	Method	C	Mean	StDev	#B	R	[ms]
CT-BAS-C1	PA	-	4.65	1.12	249	6	211
	LSR	0.9	4.86	1.3	234	7	196
	WLSR	0.9	4.78	1.25	243	7	202
	PCA	0.9	4.78	1.19	230	7	199
CT-BAS-C2	PA	-	3.08	1.68	346	7	303
	LSR	0.5	2.27	1.0	330	4	307
	WLSR	0.9	2.41	1.1	339	5	304
	PCA	0.7	2.46	1.35	335	6	303
CT-PBS-C3	PA	-	6.54	8.55	117	45	21
	LSR	0.9	2.16	1.75	118	8	22
	WLSR	0.9	1.86	1.3	114	5	21
	PCA	0.7	1.49	1.06	111	4	21

**Table 5.1:** CT-IS Pith Estimation - statistical analysis of three configurations. Mean, StDev and R are given as pixel values.

accuracy of all methods in the latter configuration increases remarkably. On the other hand the timing performance decreases due to the higher amount of blocks. Although the certainty thresholds are very restrictive, a high amount of blocks (compared to the total amount of blocks in the PA results) are used for the intersection procedure. This shows that in ct-images only a few blocks are too disturbed to compute a local orientation estimate with a high certainty.

Surprisingly, the best results are reached with CT-PBS-C3 using the three introduced Fourier Spectrum analysis methods. Compared to the two other configurations this method is ten times faster and uses least blocks. The PA method shows a bad performance for CT-PBS-C3. This behaviour can be explained with the missing of a certainty value. Thus, wrong orientation estimates are not sorted out and affect the pith estimation accuracy. In Fig. 5.9 the results of the most accurate method for each configuration are depicted. In the experiments of Entacher et al. (2008) the best results were reached with the method that used sets of equal gradients and the circle equation: Mean - 2.8 pixels and Timing - 16.64 seconds without preprocessing. Except the results using PA in CT-BAS-C2 and CT-PBS-C3 all methods outperform this

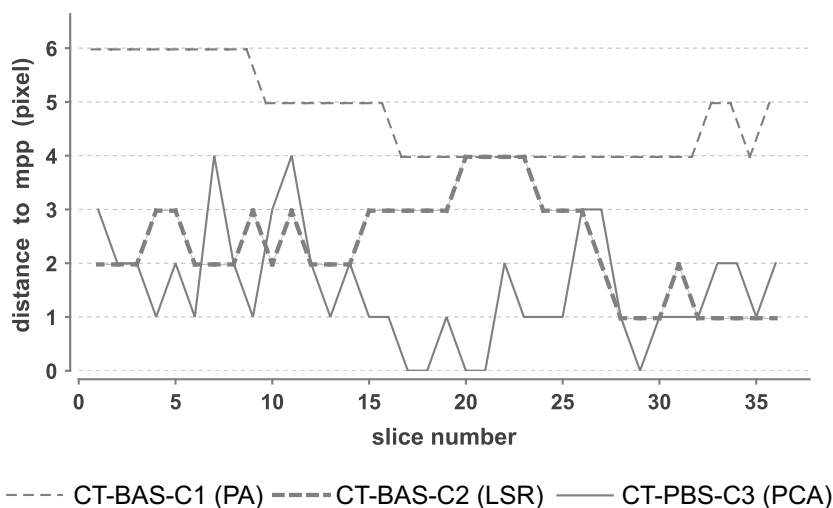


**Figure 5.9:** CT-IS | Best methods of each configuration

mean value. Considering the timing performance it is shown that the proposed methods are very fast compared to the annual ring analysis methods evaluated in Entacher et al. (2008). Additionally, no image preprocessing is required for the Fourier Spectrum analysis methods. The experiments on the CT-IS demonstrate that all proposed methods are well-suited for pith estimation on less disturbed cross section images.

### 5.3.3 RLE-IS experiments

As in the CT-IS experiments, seven configurations are selected and evaluated in detail. These configurations are divided into four groups (see Table 5.2). The first three groups present results for rectangular and circular BAS using non- and half-overlapping 16x16 pixels blocks. Circular BAS considers a larger area from the log end than rectangular BAS, which leads to a higher amount of blocks. While in the first two groups it is tried to cover a large area from the log end face (see Fig. 5.4), the third group uses a smaller 300x300 pixels rectangular area around the GC. Equal to the CT-BAS-C2 configuration the third group uses the assumption that annual rings close to the pith are more circular. Compared to the CT-IS Experiments a larger Gaussian filter with  $\sigma = 3$  was applied to the accumulator array of the BAS configurations. Finally, the fourth group presents results for pith estimation using the PBS algorithm. For this purpose 20 clusters, each cluster consisting of four - 16x16 pixel blocks, are selected at each iteration. No more than six iterations are performed with a termination limit set to a value of 4 pixels. In Table 5.2 a statistical analysis for the most accurate configurations is presented. Because all configurations achieve at least one exact pith estimate - R also gives

the most deviating pith estimate. For the configurations using BAS it can be summarized that

Config	Method	C	Mean	StDev	#B	R	[ms]	
Rectangular BAS-1	non	PA	-	5.56	4.43	710	25	1048
	over-lap-ping	LSR	0.9	6.45	5.08	643	27	1008
		WLSR	0.9	6.49	5.09	689	31	1032
	half-over-lap-ping	PCA	0.5	5.75	4.3	660	25	1036
		PA	-	3.49	2.53	2789	13	2453
		LSR	0.9	4.36	4.01	2528	24	2306
		WLSR	0.9	4.2	3.81	2709	25	2357
	Circular BAS	non-over-lap-ping	PCA	0.9	4.03	3.23	1697	15
PA			-	6.57	4.55	798	22	1053
LSR			0.9	6.0	4.7	720	27	960
WLSR			0.9	6.43	5.56	481	34	858
half-over-lap-ping		PCA	0.9	6.02	5.25	310	33	818
		PA	-	3.73	3.15	2118	20	1969
		LSR	0.9	4.43	4.39	1923	30	1888
		WLSR	0.5	4.19	4.25	2097	30	1962
Rectangular BAS-2	non-over-lap-ping	PCA	0.9	4.39	3.77	1296	25	1650
		PA	-	4.67	3.05	321	17	768
		LSR	0.9	5.91	5.1	295	33	761
		WLSR	0.5	6.46	6.7	319	45	771
	half-over-lap-ping	PCA	0.7	5.45	4.2	262	21	749
		PA	-	3.04	2.43	1284	13	1393
		LSR	0.9	3.38	3.37	1178	19	1355
		WLSR	0.3	3.01	2.49	1279	15	1396
PBS 20 - Clus- ter	PCA	0.9	3.1	2.34	785	11	1193	
	PA	0.9	6.87	7.38	417	65	150	
	LSR	0.7	8.19	9.1	390	50	178	
	WLSR	0.7	8.37	9.53	402	48	184	
PCA	PCA	0.9	6.23	7.22	299	54	229	

**Table 5.2:** RLE-IS Pith Estimation - statistical analysis of nine configurations. Mean, StDev and R are given as mm values.

configurations using PA and half-overlapping blocks entail very accurate estimates. The visual inspection of the pith estimates showed that non-overlapping blocks cause inaccuracies due to the large distances between the orientation estimates. For 16x16 pixels blocks half-overlapping blocks reduce this effect significantly (see Fig. 5.11). Additionally, it turned out that a higher



**Figure 5.10:** Rough Log End image set examples (RLE-IS)

amount of blocks, on the same area, almost always increases the accuracy and on the other hand it worsens the timing performance. For the circular BAS it was assumed that due to the optimal covering of the log end face the accuracy increases significantly. Results from Rectangular BAS-2, considering a smaller rectangular area around the GC, indicate that it is more essential to consider the area around the pith position in detail.

Overall configurations Rectangular BAS-2 using half-overlapping blocks reaches the best performance regarding the accuracy and timing performance for all methods. The best accuracy was reached with PCA (mean: 3.1 and StDev: 2.34) where all pith estimates are located within 11mm to the mpp (see Fig. 5.11).

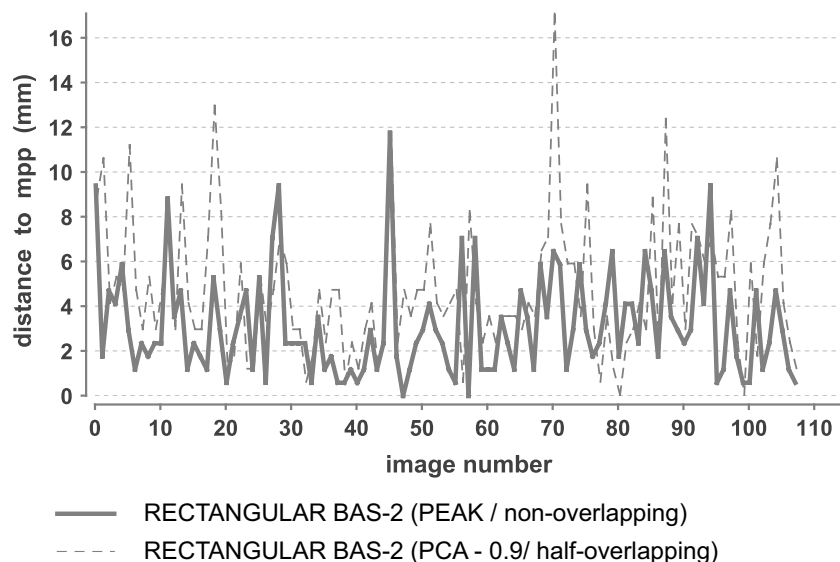


**Figure 5.11:** RLE-IS Pith Estimation accuracy - Rectangular BAS-2 with non-overlapping and half-overlapping blocks

Compared to the CT-IS Experiments the Fourier Spectrum threshold and the orientation cer-

tainty values have a major impact on the accuracy. Although the PA method assesses all blocks as valid, it is remarkable that the PA results are very accurate and robust regarding the StDev and R values. Because all blocks are valid - all blocks are used for the intersection procedure and thus slow down the pith estimation algorithm. Compared to the CT-IS experiments it can be recognised that higher certainty thresholds (C) reduce the amount of #Blocks to a higher degree. Since Fourier Spectrum preprocessing in the CT-IS and RLE-IS experiments was performed with the same parameters, the decreasing amount of #Blocks confirms that annual ring sections from rough log ends and their related preprocessed Fourier Spectra contain more disturbances. Thus, a huge amount of local orientation estimates have lower certainty values. In contrast to the PA method the introduced methods require that Fourier Spectrum thresholding filters out insignificant frequencies. Too low a threshold may have the affect that the introduced methods compute incorrect local orientation estimates and certainty values.

Comparing the PA and PCA results (Rectantgular BAS-2) it can be recognised that the PCA method assessed 500 blocks as not valid and is thus faster and additionally achieves a slightly better accuracy regarding the StDev and R values. It can be concluded that the PCA method provides reliable certainty values for all configurations using BAS and thus improves the timing performance neglecting disturbed blocks. LSR and WLSR also improve the timing performance, but they are almost always less robust regarding the StDev and R values.

Results from the fourth group show that the PBS algorithm is less suitable for rough log end images. Although the mean values are in a range between 6.23 and 8.37 pixels some unacceptable outliers are included. The best accuracy for PBS is reached with PCA (mean: 6.23 StDev: 7.22). Although the PCA method used fewest of all blocks for determining the final pith estimate it was slower than the other methods. Similar to the BAS configurations the PCA methods assess a huge amount of blocks as not valid and thus more iterations to find valid clusters are required. As for the PBS results in the CT-IS experiments the PA method is very fast since no certainty values are available and thus valid clusters are found faster.

Finally, the accuracy is compared to the results presented in Norell and Borgefors (2008) using the Ultuna image set. This one consists of 20 log end images captured from 10 logs. Except for one pith estimate all deviations were smaller than 4 mm for the approach using Laplacian pyramids and linear symmetry Norell and Borgefors (2008). Compared with the best configuration in Table 5.2 (Rectangular BAS-2 - PCA with half-overlapping blocks - mean: 3.1, stdev: 2.34) the accuracies are somewhat equivalent. Unfortunately in Norell and Borgefors (2008) no timing measurements are presented.

However, the experiments show that the proposed methods show an acceptable performance for spruce log end images of a sawmill yard. Results show that BAS and Fourier Spectrum analysis methods are well suited for pith estimation on rough log ends.

## 5.4 Summary

The experiments on the two different cross section image sets (CT-IS and RLE-IS) showed that local orientation estimation with Fourier Spectrum analysis methods are fast, robust, and very accurate in estimating the pith position. Results of the two pith estimation algorithms and the comparison of four Fourier Spectrum analysis methods highlighted the difficulties of pith estimation on images from rough log ends. The introduced PBS pith estimation algorithm achieves the best performance in the CT-IS experiments, but results show that the algorithm is inappropriate for pith estimation on images from rough log ends.

Although the PA method uses the least information of the Fourier Spectrum and provides no certainty value it reaches very accurate results for pith estimation using BAS. PCA shows a good reliability for determining valid orientation certainty values and improves the timing performance for BAS pith estimation significantly. Eventually, it was shown that it is more essential to consider sections close to the pith than to consider as much area as possible from the cross section.

Generally, it can be summarized that the block size, the distribution and amount of the blocks as well as Fourier Spectrum preprocessing are very important for pith estimation on images from rough log ends. Future research should develop more sophisticated block selection techniques.

# Chapter 6

## Cross-section segmentation

Generally, image segmentation is a fundamental image analysis task. Segmentation enables the detection of constituent regions or objects in an image. Algorithms for image segmentation can be subdivided into two categories: approaches based on discontinuity or approaches based on similarity of the pixel intensity values. Discontinuity approaches rely on boundary detection of an object or a region. Abrupt intensity value changes between neighbouring pixels indicate borders of objects or regions (e.g. edges or lines). Similarity approaches partition an image into regions based on similarity criteria (Gonzalez and Woods, 2001).

Most of the cross section analysis approaches described in Chapter 3.2 require the location of the cross-section in the image. It is thus astonishing that none of the described pith estimation approaches ( see Section 3.2.1.1) performs cross-section segmentation. Commonly, most approaches assume that the cross section is in the center area of the image. The described approaches in the literature overview on annual ring analysis (see Section 3.2.2) are either based on the same assumption or utilize a given pith position for further computations.

Some of the cross section analysis approaches treating ct-images use thresholding techniques to extract annual ring structures. Such an approach is not applicable for images of rough log ends. Examples for applying different thresholding techniques to differently captured cross-sections are illustrated in Section 6.1.

This work is the first treating cross-section segmentation of rough log ends. Cross-section segmentation is a prerequisite for industrial cross-section analysis applications. The TreeBio framework requires cross-section segmentation for several reasons. First, similar to fingerprint or iris recognition, segmentation is a preliminary step to determine/detect the biometric

characteristic, out of which the biometric features are extracted. Second, the cross-section shape/boundary represents a biometric feature. Finally, the cross-section boundary and the pith position can be utilized for image registration issues (translation, rotation, scaling).

This chapter introduces a similarity approach for cross-section segmentation in images of rough log ends. Basically, a cross-section is built up of an annual ring texture which varies strongly locally. The variations are caused by the circular alignment, different widths, colour features and disturbances of annual rings. Consequently, appropriate texture features of annual ring sections form the basis for cross-section segmentation. These considerations indicate that a two-phase procedure is required: First, detect the cross sections in an image and select representative annual ring sections which describe the texture of the detected cross section. Second, use the texture features to determine the cross-section area and its boundary for each detected cross-section or the cross-sections of interest.

The proposed cross-section segmentation approach is based on the work of Chan et al. (2007). The authors use the Earth Movers Distances as similarity measure between local grayscale histograms to establish a region-based active contours approach. For this thesis, local histogram distances between grayscale histograms and texture feature histograms are utilized.

This chapter contributes to the development of cross-section analysis applications suggesting a novel approach for cross-section segmentation. By treating images of rough log ends this segmentation approach can be utilized as preliminary component for further cross-section surface analysis. In considering the differences between ct-cross-section and rough log end segmentation, this work highlights the difficulties of the latter.

At first, Section 6.1 highlights the difficulties of segmentation in case of rough log end images as opposed to ct-cross-section images. Section 6.2 introduces the paradigms of texture analysis (Section 6.2.1) and further presents considerations about the texture of cross-sections (Sections 6.2.2). Theoretical background on the texture analysis methods used in the proposed cross-section segmentation algorithm is presented in Section 6.3. The proposed cross-section segmentation algorithm is outlined in Section 6.4. Section 6.5 describes the experimental setup and presents results for the experiments. Finally, Section 6.6 concludes the segmentation chapter and presents some considerations for future work on cross-section segmentation.

## 6.1 Histogram thresholding of cross-section images

As described in the literature overview on detection of log defects, ct-cross-section images (see Section 3.2.3) can be segmented using histogram thresholding techniques. Subsequently, an exemplary comparison on segmentation using histogram thresholding techniques is presented. For this comparison, differently captured cross-sections are used. The results give information about the differences of cross-section segmentation in ct-images compared to images from rough log ends. The applicability of histogram thresholding to segment cross-section images is assessed considering two segmentation purposes. First, segmentation is required to separate the cross-section in an image from the background. Second, annual rings are the main wood property of a cross section. Consequently, the extraction and preservation of annual rings and structures are very important for further annual ring analysis tasks.

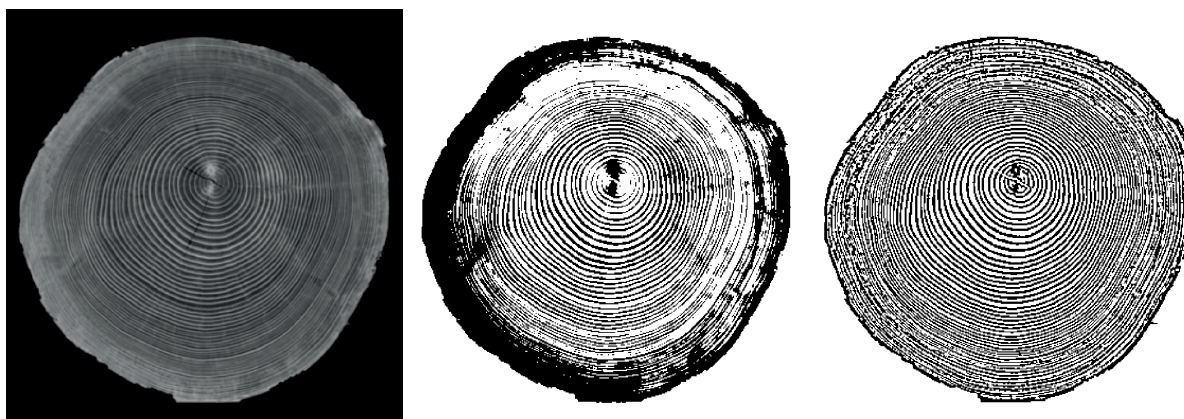


**Figure 6.1:** Two different thresholding techniques (p-tile and adaptive) applied to a ct-cross-section image

Thresholding methods are well suited for segmenting cross-sections in ct-images. In ct-images, annual rings are represented as white pixel chains and the background is dark coloured. Consequently, thresholding can be utilized for segmentation and to extract or emphasize annual ring structures and other wood features. In other words, the cross sections features are separated as foreground pixels from the background pixels. The three pictures in Fig. 6.1 illustrate the results for two different thresholding techniques applied to a ct-cross-section image. One technique is a global thresholding technique and the second one is based on adaptive thresholding. The first picture in Fig. 6.1 depicts the original ct-cross-section image. The second picture shows the result for global p-tile thresholding with an assumed foreground amount of 50 %. In the third picture, the result for adaptive thresholding is shown. For adaptive thresholding, the mean values of 15x15 pixels blocks are used as local thresholds. Both thresholding methods indicate that thresholding is an appropriate technique for ct-cross-section segmentation.



**Figure 6.2:** Two different thresholding techniques (p-tile and adaptive) applied to an image of a sanded cross-section

The same thresholding techniques using the same parameters are applied to the image of a sanded cross-section shown in the first picture of Fig. 6.2. The result for adaptive thresholding shows that this method is very sensitive to noise in the black background. However, both methods indicate that the cross-section can be separated from the background and annual ring structures can be extracted in studio-captured images of sanded cross-sections.



**Figure 6.3:** Two different thresholding techniques (p-tile and adaptive) applied to an image of the RLE-IS.

Finally, the thresholding results in Fig. 6.3 illustrate the arising difficulties using real-world images of rough log ends. In contrast to ct-cross-section images and studio captured cross-section images, the background of real world images is very heterogeneous and strongly varying in each image. Additionally, cross-section images of rough log ends are disturbed due to cutting. The results in Fig. 6.3 show that histogram thresholding is no appropriate technique to separate cross-sections from the background and to extract or separate annual ring structures in real world images of rough log ends. These simple considerations on segmentation using histogram thresholding, indicate that the segmentation of real-world images of rough log ends requires a more sophisticated approach.

## 6.2 Texture analysis of cross-sections

### 6.2.1 Texture analysis

Basically, texture analysis techniques are categorised into statistical and structural methods. Statistical methods interpret textures as statistical distributions which can be described using statistical features of the intensities and positions of the pixels. For this purpose each pixel in an image or image section is analysed. For each pixel a feature is computed to extract knowledge from the statistical distribution of the features. Statistical methods are classified as first-order (1 pixel), second order (2 pixels) and higher order statistics ( $>3$  pixels), depending on the amount of pixels which are analysed to compute the features. First-order statistics like the average and variance of the pixel intensities contain no spatial information. In second-order and higher-order statistics two or more pixels are used to compute the features, which includes spatial relationships between pixels at specific positions (Ojala and Pietikäinen, 2012)-

Structural methods use the assumption that the analysed texture is formed by micro-components, called texels. Texels can be placed regularly, randomly, with different directions, and sizes and may overlap. Structural methods create a description of the relationship between a set of texels. In case of natural textures structural methods mostly fail due to the variability and the randomness of the textures (Materka and Strzelecki, 1998).

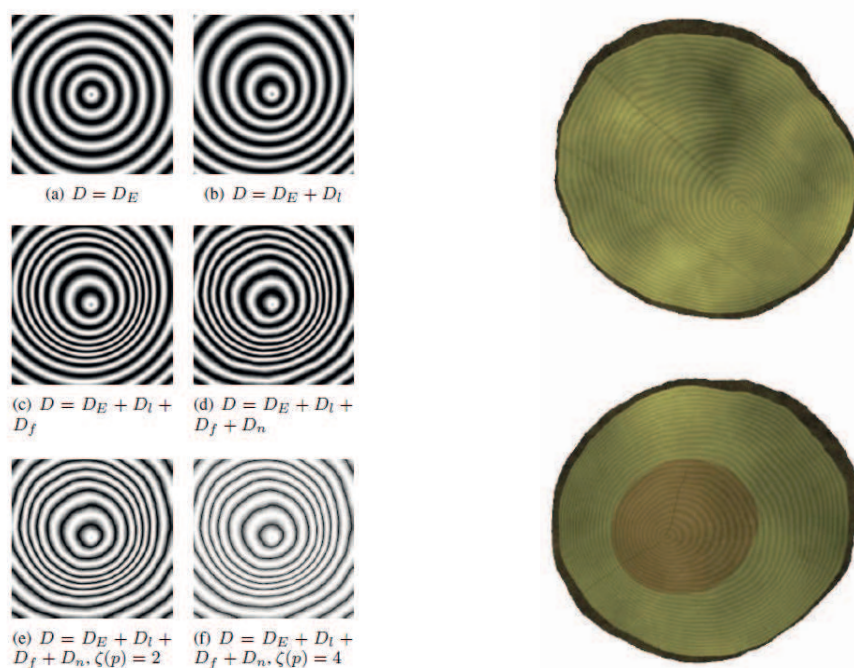
### 6.2.2 Cross-section texture

According to Davis (2008), synthetisation is a way to recognize a texture. An approach to synthesise cross-section textures (synthetic log end faces) is presented in Norell (2009b). The considerations of Norell (2009b) are subsequently used to describe typical cross-section texture features and their properties.

The proposed synthetisation procedure consists of five parts: wood, sawing, storage, light and camera position and imaging. Typical wood features are the annual ring pattern, heartwood and knots (wood features, see Section 3.1.1). As opposed to the wood features the sawing pattern, storage and imaging disturbances are externally caused features. The texture of a sanded and perfectly captured cross-section only shows wood features.

Synthetisation of wood features requires the simulation of knots, heartwood, bark, colour and annual rings. The amount and the growth of the annual ring pattern causes different cross-

section shapes and sizes. The modelling of the annual ring pattern is considered in detail. As described in Section 3.1.1, each year a new annual ring is formed. The thickness of a single annual ring is not consistent and can vary strongly. In Norell (2009b), annual rings are modelled by a circular sinusoidal pattern. This pattern is created by applying a sine function to a distance map ( $D$ ). To simulate different characteristics, the distance map is perturbed. In Fig. 6.4a the distance map function ( $D$ ) and the resulting pattern for different perturbations are illustrated. While in Fig. 6.4a-(a) a perfect circular pattern ( $D = D_E$ ) is illustrated in Fig.6.4a-(b) the uneven tree growth is simulated and added using a 2D linear function ( $D_l$ ). In Fig.6.4a-(c) a sigmoid function ( $D_f$ ) is added to vary the ring thickness. Finally, noise ( $D_n$ ) is added to simulate random perturbations (see Fig. 6.4a-(d)). The suggested noise function can be tuned to simulate early-wood with a stronger thickness than late-wood. Fig.6.4a-(e) and (f) illustrate the effect of using different parameters (2, 4). This approach for annual ring modelling illustrates that it is possible to synthesise the basic texture of a cross-section. Furthermore, Norell (2009b) introduces methods to simulate other wood features



(a) Annual ring modelling using a sine function and perturbed distance maps ( $D$ ).

(b) Two examples for synthetic log end images. The upper cross-section includes sawing disturbances and the bottom one includes heartwood.

**Figure 6.4:** Cross section texture synthesis (Images source: Norell (2009b)).

and externally caused disturbances. Referring to the introduction on texture analysis, Norell (2009b) demonstrates that the annual ring texture is basically built up on rotated, distorted

and perturbed sinusoidal texels, which are stringed together. The considerations about the Fourier Spectra of annual ring sections (see Section 5.1) indicate that local orientations can be used as texture features for cross-section segmentation. In the experiments it is shown that local orientations are less useful due to the disturbances on rough log ends.

## 6.3 Theoretical Background

The proposed region-based cross-section segmentation algorithm in this this thesis (see Section 6.4) uses two different texture analysis methods. Both methods compute texture features of annual ring sections. The first method is a statistical first-order method and simply computes local grayscale intensity histograms of annual ring sections. The second method computes feature histograms using local binary patterns. For both methods histogram distances are used as similarity measures between the intensity or LBP feature histograms of adjacent annual ring sections. Subsequently, for both methods and histogram distance some basics are presented.

### 6.3.1 Intensity Histograms

Intensity histograms are statistical first-order methods and do not extract information about the topology of the pixels. In the context of images they are simply denoted as histograms. Generally, histograms of images or image sections are probability distributions describing the frequency of each color or gray value. For example, let's consider an 8-bit grayscale image or image section. Each of the 256 gray values is represented by a single bin in the histogram. The value or height of each bin is determined by the frequency of the corresponding gray value in the image or image section. Histograms of color images or sections are mostly created computing an individual 256 bin histogram for each channel. Another possibility is to create 3D color histograms with the three axes representing the red, green and blue channel.

### 6.3.2 Local Binary Patterns (LBPs)

The concept of local binary patterns (LBPs) was first introduced in Ojala et al. (1996). In counting the frequency of micro texels in an image or image section, LBPs unify statistical and structural principles of texture analysis. Another strength of LBPs is that the detection of the micro structures is invariant to monotonic intensity variations. In the past decade several

improvements (e.g. multiscale-, multiresolution-, rotation invariant- and gradient operators) have been suggested.

**Generic LBP operator** A generic form of the original operator is shown in Ojala et al. (2002). This operator is defined by two parameters ( $N, R$ ). For each pixel in an image or image section the local binary pattern is computed by analysing  $N$  neighbours in a circular neighbourhood. These neighbours are equally distributed on a circle of radius  $R$  with the current pixel as center point. The illustrations in Fig. 6.5 show different examples for the circular neighbourhood of a pixel using different parameters. While in Fig. 6.5a the 8 adjacent pixels are selected, in Fig.6.5b and Fig.6.5c some interpolation is required to determine the pixels defined by  $R$  and  $N$ . The LBP with given parameters  $N$  and  $R$  of a pixel at location

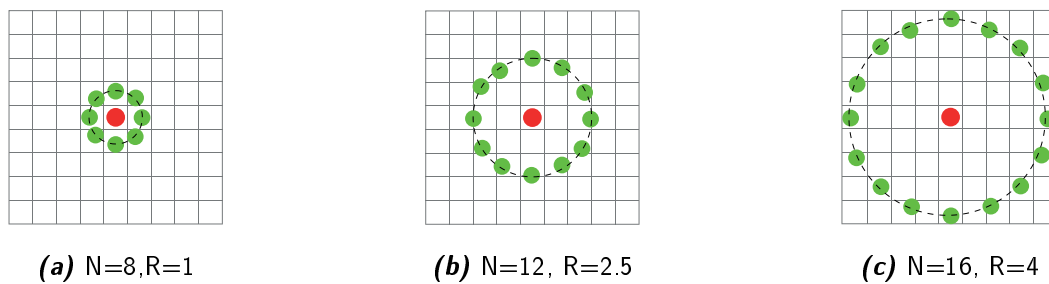


**Figure 6.5:** Selection of pixels in a circular neighbourhood based on the two parameters:  $N, R$  (Image source:[http://commons.wikimedia.org/wiki/File:Lbp\\_neighbors.svg](http://commons.wikimedia.org/wiki/File:Lbp_neighbors.svg))

$(x, y)$  and gray value  $n_c$  is then computed as:

$$LBP_{N,R}(x, y) = \sum_{i=0}^{N-1} s(n_i - n_c) \cdot 2^i, \quad s(z) = \begin{cases} 1 & z \geq 0 \\ 0 & \text{otherwise} \end{cases} \quad (6.1)$$

where  $n_i$  denotes the gray value of the currently considered neighbour pixel and  $s(z)$  is a sign function. The value of the sign function is 1 if the neighbour pixel has a higher gray value than the center pixel, otherwise the value is 0. The computation of the LBP as defined in Equation 6.1 results in an  $N$ -bit binary number given in decimal representation. Depending on the number of neighbours  $N$ ,  $2^N$  local binary patterns are available.

For texture analysis of an image or image section the LBP pattern is computed for each pixel. The occurrence of each of the  $2^N$  possible patterns is stored into a feature histogram, where each bin represents a single pattern and its frequency. Throughout this thesis this feature histogram will be denoted as LBP histogram.

Additionally to the generic formulation of the LBP operator, the authors of Ojala et al. (2002) and Mäenpää (2003) introduced three extensions for the LBP operator:

**Uniform LBPs** Uniform patterns rely on frequency observations of LBPs in natural images. The authors concluded that 90% of the LBPs in natural images are so-called uniform patterns. Uniform patterns  $U_n$  are defined by the amount of bitwise transitions from 0 to 1 or 1 to 0 in the binary LBP code.  $n$  denotes the maximum count of transitions allowed in the LBP codes of uniform patterns. In Ojala et al. (2002) uniform patterns contain maximal two transitions ( $U_2$ ). For example, the patterns 11111111 (0 transitions), 01111111 (1 transitions) and 00001100 (2 transitions) are uniform, whereas 11010100 (5 transitions) is non-uniform. In contrast to the generic formulation just the uniform patterns are used as features for LBP histograms and non-uniform patterns are neglected. Considering 8 bit LBP codes, 58 out of 256 are uniform patterns. Most of the uniform patterns correspond to features like edges, line ends, corners and spots (see (Mäenpää, 2003, p.36)).

Uniform patterns are more robust against noise, rotation and tiling. Furthermore, they enable a remarkable reduction of the number of bins in the LBP histograms. In several applications this leads to better recognition rates and timing improvements.

**Rotation Invariant LBPs** The idea of rotation invariant LBPs uses the fact that some patterns are rotated versions of a single pattern. Consequently, rotated versions are rotated back to the reference position of one reference pattern. In Ojala et al. (2002) rotation invariant codes are produced by rotating the original code until its minimum value is reached (Mäenpää, 2003). Due to this quantization, rotational information is lost and rotational invariance is established. The effectiveness of this approach depends on the amount of neighbours. In case of a 8-neighbourhood only  $45^\circ$  and in a 16-neighbourhood  $22.5^\circ$  rotations are compensated.

**Multi-scale LBPs** An approach to enlarge the spatial-support is introduced in Mäenpää and Pietikäinen (2003). The proposed multi-scale LBP extension uses Gaussian low-pass filters. For an optimal covering at each scale an appropriate radii  $R$  is chosen and the number of neighbours  $N$  is constant. At each scale and radii the low pass filter collects intensity information of a larger area and the LBPs are computed equally as in a  $3 \times 3$  neighbourhood. Finally, the feature histograms of each scale are concatenated to the final LBP histogram.

### 6.3.3 Histogram Distances

Histogram matching or comparison is a common technique in various pattern recognition and image retrieval applications. In this thesis histogram distances are used as similarity measures between intensity histograms or LBP histograms of neighbored image sections.

For two images or image sections, the corresponding intensity or LBP histograms  $H_1$  and  $H_2$  are represented by two feature vectors  $P = (x_1, \dots, x_n)$  and  $Q = (y_1, \dots, y_n)$ , where  $x_i, y_i$  denotes the bin of the corresponding color or gray value or texture feature.

The distance between these vectors is computed using a distance function  $d(P, Q)$ .  $\bar{P}$  and  $\bar{Q}$  are the mean values of the histogram vectors ( $\bar{P} = \frac{1}{N} \sum_{i=0}^n P(i)$ ,  $\bar{Q} = \frac{1}{N} \sum_{i=0}^n Q(i)$ ).

One possibility to classify different histograms distances is to subdivide them into *bin-by-bin* and *cross-bin* approaches. In the work of Pele and Werman (2010), the difference between both is described. The main advantage of bin-by-bin distances is that they can be computed very fast. Generally, the robustness of bin-by-bin comparison depends on the robustness of the represented features. In case of intensity histograms, bin-by-bin comparison is less robust because already little image variations (e.g. light changes) can strongly influence the distance. Furthermore, the robustness of bin-by-bin comparison depends on the number of bins. If the number of bins is low, the distance is robust but less discriminative. If the number of bins is high, the distance is discriminative and becomes less robust. The advantage of cross-bin comparison is that it can be robust and discriminative at the same time.

A well-known cross-bin distance is the Earth Mover's Distance (EMD) proposed by Rubner et al. (1998). For the purpose of cross-section segmentation using intensity histograms and LBP histograms, the applicability of different histogram distance have to be evaluated. In case of intensity histograms the main focus is to assess the performance of the EMD compared to common bin-by-bin distances. For this purpose and for the comparison of the LBP histograms, six bin-by-bin distances are additionally introduced. The use of the EMD for LBP histogram requires an appropriate ordering of the histogram bins which is not treated in this thesis.

Before introducing the EMD, the six bin-by-bin distances are described.

**Bin-to-bin distances** A subset of the bin-by-bin distances are  $L_p$  metrics, commonly denoted as Minkowski distances. The class of  $L_p$  distances are heuristic measures which determine the difference between two vectors (Cha and Srihari, 2002).

1.  $L_1$  - City Block distance

$$d_{CB}(P, Q) = \|P - Q\| = \sum_{i=0}^n |P(i) - Q(i)| \quad (6.2)$$

2.  $L_2$  - Euclidean distance

$$d_{Euc}(P, Q) = \sqrt{\sum_{i=0}^n (P(i) - Q(i))^2} \quad (6.3)$$

The  $L_1$  and  $L_2$  norms are likely used in image retrieval and pattern recognition. Another well known distance is the Chi-Square ( $X^2$ ) distance. Compared to the Minkowski metrics the Chi-Square distance is a probabilistic measure which describes the probability that the probability distribution of one histogram is based on the other (Cha and Srihari, 2002). Further two well-known distances are the Hellinger distance and the Battacharyya distance (Cha and Srihari, 2002).

3.  $X^2$  - Chi Quadrat Distance:

$$d_{X^2}(P, Q) = \sum_{i=0}^n \frac{(P(i) - Q(i))^2}{Q(i)} \quad (6.4)$$

4.  $H$  - Hellinger Distance:

$$d_H(P, Q) = \frac{1}{\sqrt{2}} \cdot \sqrt{\sum_{i=0}^n (\sqrt{P(i)} - \sqrt{Q(i)})^2} \quad (6.5)$$

5.  $B$  - Battacharyya:

$$d_B(P, Q) = -\ln \sum_{i=0}^n \sqrt{P(i) \cdot Q(i)} \quad (6.6)$$

**Cross-bin distance - Earth Movers Distance (EMD)** The EMD is a well-known distance used in many different fields of applications. It was introduced in Rubner et al. (1998) as metric with applications to image databases. Basically, the EMD computes the minimal cost required to transform one histogram (P) into another (Q) (Pele and Werman, 2010). In case of two one-dimensional probability distribution functions P and Q the EMD is simply given by the  $L_1$  norm between the cumulative distribution functions  $P_c(n) = \sum_{i=0}^n P(i)$ ,  $Q_c(n) = \sum_{i=0}^n Q(i)$ .

5.  $EMD$  - Earth Mover's Distance:

$$d_{EMD}(P_c, Q_c) = \|P_c - Q_c\| = \sum_{i=0}^n |P_c(i) - Q_c(i)| \quad (6.7)$$

## 6.4 Cross-section segmentation algorithm

This section presents a region-growing-based cross-section segmentation algorithm. Furthermore, some interesting insights gathered during the development are noted. This approach is based on similarity of adjacent pixels. In the case of cross-sections, similarity refers to the relation between adjacent annual ring sections. The assessment of the similarity between adjacent annual ring sections requires analysing of texture features. For this purpose, two different approaches are evaluated. First and as suggested in Chan et al. (2007), local histogram distances and particularly the EMD distance are used as main similarity measures between intensity histograms. Additionally, other distances are used to assess the performance of the EMD distance. Second, LPBs are used to assess the performance of a more sophisticated texture analysis method.

As opposed to Chan and Vese (2001) and Chan et al. (2007), no level set approach is used. Instead of using level sets, the algorithm uses a simple region growing procedure. The approach suggested in Chan and Vese (2001) uses mean gray values as criteria for the region-based level set. In preliminary tests the applicability of this approach for cross-section segmentation was assessed using the tool *OFELI* (<http://code.google.com/p/ofeli/>). Results showed that this approach is not applicable due to the varying annual ring texture of cross-sections. The proposed cross-section segmentation approach in this thesis is inspired by the EMD-region-based level set formulation in Chan et al. (2007) and is adopted to a region growing procedure.

As for the pith estimation algorithms (Section 5.2), the image is subdivided into blocks. The block size and the overlapping factor between the blocks are crucial parameters which strongly influence the segmentation accuracy and timing performance. The cross-section segmentation algorithm is subdivided into three consecutive stages:

1. **Seed block selection** (Subsection 6.4.1)
2. **Cluster growing algorithm** (Subsection 6.4.2)
3. **Shape estimation** (Subsection 6.4.3)

In the first stage seed points/blocks are selected. Next, each seed block is used as initial block to further initialise a cluster containing expected texture features of the cross-section. For each cluster, a region growing procedure is performed and the clusters are merged. Finally, in the third stage, the clustered region is used to determine the cross-section boundary. Subsequently,

the used approaches and methods for each stage are introduced and exemplarily illustrated using image #1 from the rough log end image set (RLE-IS / see subsection 5.3.1).

### 6.4.1 Seed block selection

For the selection of seed blocks, two different approaches are suggested. Both methods utilize the estimated pith position which is determined using the algorithms described in Section 5. In combination with a Hough transform which detects circular shapes, pith estimation can be used to detect seed blocks for several cross-sections in an image. For this work, we assume that the image consists of an entire cross-section and the background (which may contain parts of other cross-sections).

**Pith position-based selection** The first approach selects a predefined number of blocks (e.g. 4) which are distributed equally close around the pith position.

**Local orientation-based selection** The second approach uses the pith position and selects blocks depending on their local orientations. Local orientations are computed using the peak analysis method introduced in Section 5.1.3.2. The basic idea is to select blocks whose local orientations point close to the pith position. For this purpose, for each block the normal distance between its local orientation and the pith position is computed. Blocks where the normal distances are lower than a certain orientation threshold value  $T_o$  are selected as seed blocks. In Fig. 6.6 examples for local orientation-based selection using different thresholds  $T_o$  are illustrated.



(a) Seed blocks ( $T_o = 20$ )

(b) Seed blocks ( $T_o = 60$ )

(c) Seed blocks - ( $T_o = 100$ )

**Figure 6.6:** Local orientation based seed block selection. Three examples using different orientation thresholds  $T_o$ .

The selected blocks are used for the cluster growing procedure which is introduced in the next section.

## 6.4.2 Cluster growing algorithm

An important step prior to the cluster growing procedure is to initialise the clusters in a proper way. In the next section different ways for cluster initialisation are described. Subsequently, in Section 6.4.2.2 the growing procedure is introduced.

### 6.4.2.1 Cluster initialisation

After selecting seed blocks, the clusters are initialised in two different ways, depending on the seed point selection approach. For simplicity, the two possibilities are denoted as orientation-based and pith-based cluster initialisation approaches.

**Orientation-based cluster initialisation** In the case of orientation-based cluster initialisation, the neighbored seed blocks are merged together first. For each single seed block and each set of merged seed points, a single cluster is initialised. Next, adjacent blocks of the cluster are added, if their local orientations fulfil a similarity criterion. Therefore, a recursive neighbourhood search is performed. If the deviation between the orientation of the considered cluster block and its neighbour is below a certain deviation limit, the neighbour block is added to the cluster. Examples for this procedure are illustrated in Fig. 6.7. The three illustrations

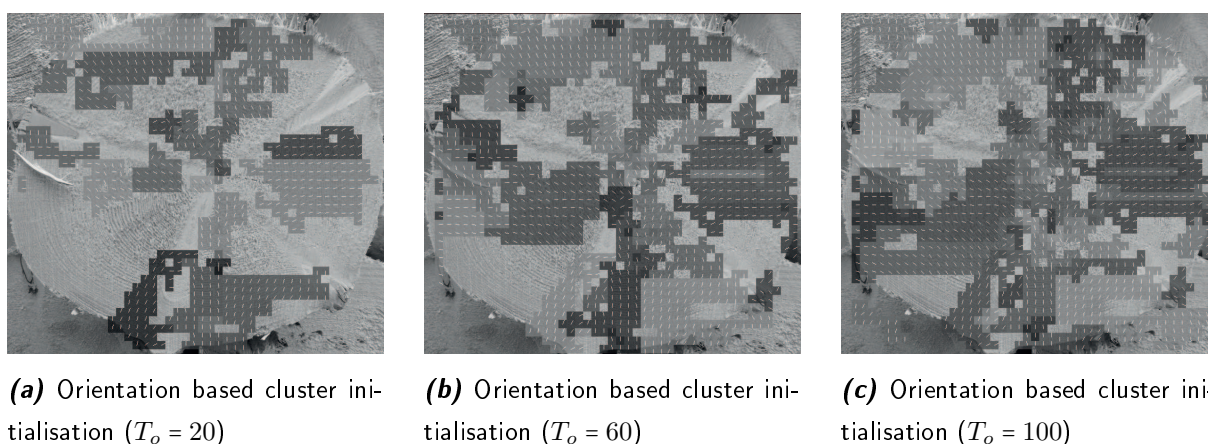


**Figure 6.7:** Orientation based cluster initialisation based on the seed blocks from Fig. 6.6 and a value of 0.3 radians as orientation deviation limit for the recursive neighbourhood search.

use the respective seed blocks shown in Fig. 6.6 as basis for the recursive neighbourhood search. For all three examples a deviation limit of 0.3 radians was used. The three examples of Fig. 6.7 and Fig. 6.6 depict that with an increasing orientation threshold ( $T_o$ ) the amount of incorrect seed points increases and the cluster initialization covers a larger share of the background.

Yet again, these examples illustrate that the orientation field of the cross-section is strongly varying due to cutting disturbances. Consequently, a segmentation approach based on the orientation field makes no sense. However, by using a low orientation threshold ( $T_o$ ) and a small orientation deviation limit, this approach is useful to initialise representative clusters which are distributed over the entire cross-section.

**Pith-based cluster initialisation** The cluster initialisation using pith-based seed block selection is very simple. For each single seed block the adjacent neighbours in a four-neighbourhood are added and then initialised as a single cluster.

The final initialisation step is performed for both approaches. Therefore, for each cluster three features describing the contained texture are computed:

- mean gray value and variance
- mean entropy and variance
- mean intensity histogram or LBP histogram distances between the blocks of the cluster and the corresponding variance

#### 6.4.2.2 Growing procedure

Before the cluster growing procedure starts, the clusters are ordered according to the minimum distance of the cluster blocks to the pith. The cluster growing procedure starts with the innermost cluster.

Then the four-neighbourhood of each border block is analysed. Only neighbours which are not allocated to a cluster are used as candidate blocks. Each candidate block is compared to the cluster which leads to a decision whether or not the block is allocated to the cluster. In Fig. 6.8 the blocks of a cluster and the decision making procedure are illustrated. For the block labelled B3 three candidate blocks (nb1, nb2, nb3) are available. The final decision whether

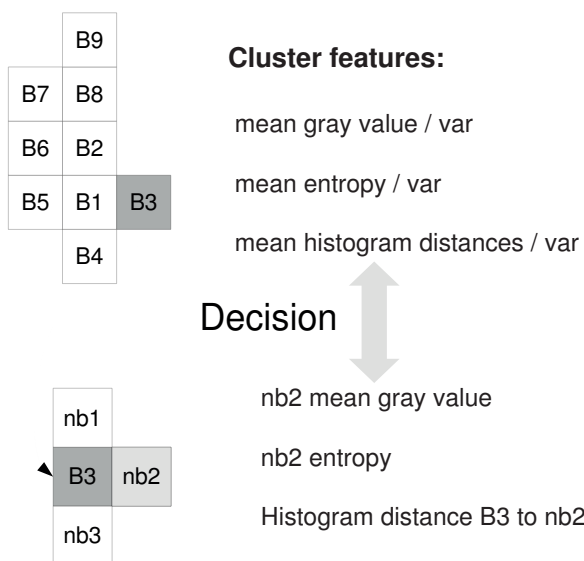
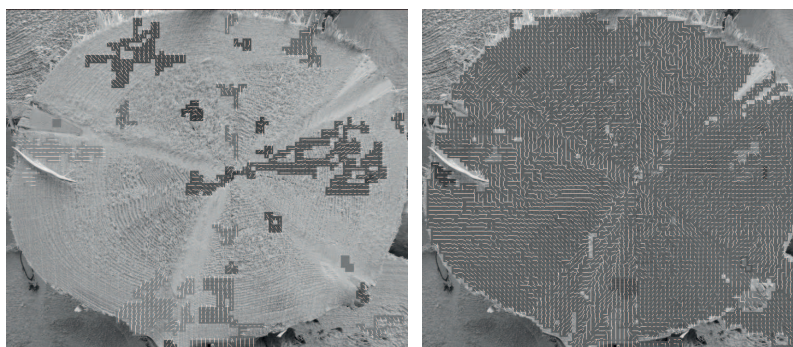


**Figure 6.8:** Illustration of the cluster growing procedure

one of the candidates (e.g. nb2) is allocated requires that each of the three comparisons satisfies predefined conditions. For example, the mean gray value of the block has to be equal to the cluster mean gray value +/- its variance. The feature-variances are used to regulate the restrictiveness of the decision making procedure. For this purpose, the variance is multiplied by a factor ranging from [-2,2]. If the block is allocated to the cluster, the cluster features are updated. The procedure continues with the next border block until no border block has further candidate blocks that fit to the cluster. Then the algorithm continues with the next cluster. The cluster-growing algorithm finishes after all clusters are processed. Finally, the clusters are merged and it is assumed that the merged cluster represents the area of the cross-section. In Fig. 6.9a, an example for the cluster initialisation result is illustrated. This example uses



**(a)** Seed block – orientation-based cluster initialisation ( $T_o = 5$ ) **(b)** Result of the cluster growing and merging procedure using the initialised clusters of Fig. 6.9a

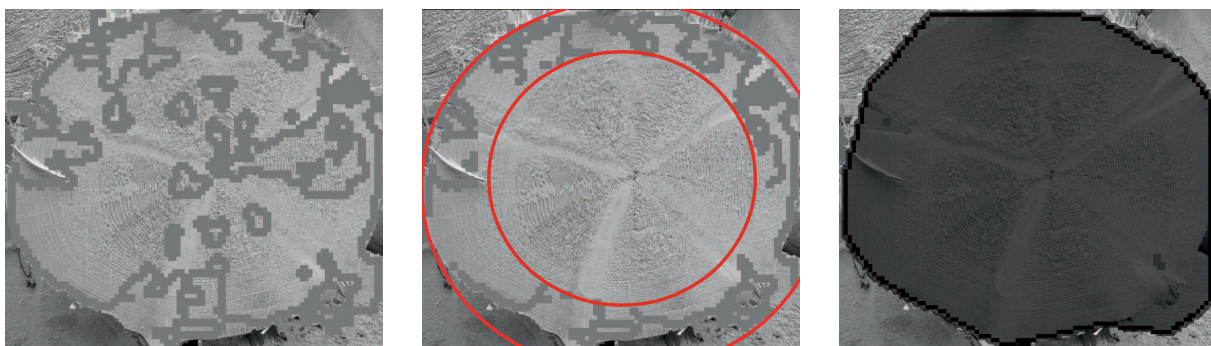
**Figure 6.9:** Cluster initialisation and cluster growing/merging result

16x16 and half-overlapping blocks and orientation-based seed point selection as well as cluster initialisation. The corresponding cluster growing and merging result is illustrated in Fig. 6.9b. It is clearly visible that the resulting cluster covers the entire cross section. Unfortunately, similar textured cross-sections in the background are difficult to distinguish from the main cross-section. This problem is visible in the bottom right of Fig. 6.9b .

### 6.4.3 Shape estimation

The blocks of the merged clusters are further used to compute an estimate of the cross-section boundary. The boundary is computed in four steps:

1. Select border blocks (see Fig. 6.10a).
2. Fit circle – remove all blocks within the fitted circle (see Fig. 6.10b).
3. Fit ellipse – cut off outliers (see Fig. 6.10b).
4. Fit alpha shape (see Fig. 6.10c).



**(a)** Step 1: Select border blocks      **(b)** Step 2/3: Fit circle - Fit ellipse and cut off outliers from wrong segmented blocks.      **(c)** Step 4: Cross-section boundary estimation building an alpha shape with  $\alpha = 50$ .

**Figure 6.10:** Illustration of the four steps to estimate the cross-section boundary

The first three steps are not mandatory and are intended to increase the accuracy and speed of the alpha shape fitting step. Subsequently, first the basic ideas of the first three steps are introduced and second the alpha shape fitting step is outlined.

The main goal of the first step is to reduce the amount of blocks for the alpha shape fitting step. For this reason, all blocks which have at least one neighbour that is not in the cluster

are selected. As illustrated in Fig. 6.10a this approach significantly reduces the amount of blocks and all of the blocks representing parts of the cross-section boundary still remain. The reduction of the amount of blocks leads to a significant speed up of the alpha shape fitting step.

The intention of the steps 2 and 3 is to remove blocks from wrong segmented parts and to cut off outliers. For that, it is assumed that cross-sections are approximately elliptical. In Step 2 a circle is fitted into the point cloud of the remaining blocks. Blocks within the circle are removed. This step is just performed to improve the accuracy of the ellipse fitting step. In Step 3 an ellipse is fitted into the point cloud. After ellipse fitting all blocks located outside of the ellipse are removed (see Fig. 6.10b). In the best case and especially for elliptical cross-sections this procedure decreases the probability of including wrongly segmented blocks (e.g. caused by neighbored cross-sections in the background). In the worst case the cross-section is not elliptical and parts of the cross-section boundary are cut-off and probably Step 4 fails due to this.

Step 4 is the only mandatory step which finally computes an estimate of the cross-section boundary. For this purpose, the alpha shape of all cluster blocks or the remaining blocks of the first three steps is computed. Alpha shapes were introduced by Edelsbrunner et al. (1983). Alpha shapes are an approach to compute concave hulls and are a generalisation of convex hulls. As opposed to convex hulls, the formation of a concave hull is not well defined. The computation of an alpha shape is based on the Delaunay triangulation. The exterior face of the Delaunay triangulation of a set of points is the convex hull of the points. The advantage of alpha shapes is that they can be tuned by the  $\alpha$  parameter which controls the level of detail. A disc with  $\alpha$  as radius is used to determine the outer and inner alpha shape defined by point pairs that can be touched by the disc. We are only interested on the outer alpha shape. The higher the  $\alpha$  value is, the better the alpha shape approximates the convex hull and details of the boundary are neglected. The lower the value of  $\alpha$  is, the more details are considered. In contrast, a lower value makes the alpha shape computation vulnerable to large gaps between the outermost blocks.

Finally, the result of Step 4 (see Fig. 6.10c) is used as a final estimate of the cross-section boundary and finishes the cross-section segmentation algorithm.

## 6.5 Experiments

Different experiments provide information about the performance of the proposed cross-section segmentation algorithm. For this purpose, the two introduced approaches are tested using different configurations. The two approaches only differ by the seed point selection and cluster initialisation approach. The first approach, named pith based approach (PBA) uses the pith-based seed block selection and the pith-based cluster initialisation procedure. For this purpose, four clusters close to the pith are initialised.

Approach two, the orientation-based approach (OBA) uses the orientation based seed block selection and the orientation-based cluster initialisation. For seed block selection  $T_o = 5$  is used as orientation threshold. As orientation deviation limit for the orientation-based cluster initialisation, a value of 0.05 radians is used. The values have been determined in preliminary investigations. They are very low and restrictive to avoid cluster initialisation in background regions.

Apart from the goal to assess the performance of OBA and PBA, experiments with different configurations are used to assess the impact of:

1. different block sizes and half-overlapping/ non-overlapping blocks,
2. using intensity or LBP histograms as texture features, different local histogram distances and different variance factors ( $V_f$ ),
3. different weighting factors for the gray scale conversions of the original color image,
4. Step 2/3 – circle and ellipse fitting.

For the experiments, the RLE-IS from the pith estimation experiments (see Section 5.3.1) is used. The accuracy for a particular approach (PBA, OBA) and a certain configuration is evaluated computing the mean segmentation accuracy (Mean) and the deviation (StDev) over all of the 108 images. R gives the span between the minimum and maximum segmentation error. Additionally, the computation time in milliseconds [ms] provides information on the timing performance.

The computation of the segmentation accuracy requires a segmentation ground truth. For this purpose, a cross-section mask was created manually for each image of the test set. The images in Fig. 6.11 show the ground-truth mask and the computed cross-section mask for image #1

of the RLE-IS. The percentage of difference between the pixels of the ground-truth mask (Fig. 6.11b) and the computed cross-section mask (Fig. 6.11c) is defined as the segmentation accuracy. All steps of the cross-section segmentation algorithm have been implemented in

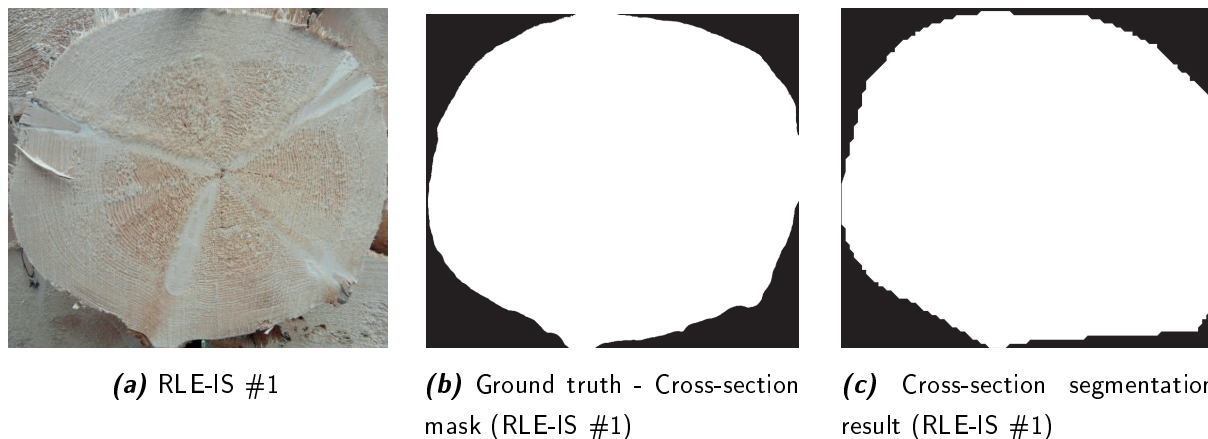


**Figure 6.11:** Illustration of the original image and the cross-section masks used to determine the segmentation accuracy

Java and all experiments have been performed on an Intel Core i7-2620M processor with 2.7 GHZ and 8 GB RAM, JRE 1.7.

To answer the questions noticed above, five experiments have been performed. The experimental settings and results are presented one after the other.

**Experiment #1 - Evaluation of intensity histograms as texture features** The first experiment evaluates the applicability of intensity histograms as texture features for the proposed cross-section segmentation algorithm. Furthermore, the impact of different local histogram distances, different block sizes and half-/ non-overlapping blocks is tested. All settings are tested for PBA and OBA. The experiments have been performed on grayscale images which have been converted using equal weighting factors for the RGB channels ( $R=0.33$ ,  $G=0.33$ ,  $B=0.33$ ). Block sizes of  $16 \times 16$  and  $32 \times 32$  pixels are evaluated half- and non-overlapping.

The set of evaluated histogram distances is described in Section 6.3.3. For the cluster growing procedure each histogram distance is tested with variance factors ( $V_f$ ) in a range between  $[-2.0, 2.0]$ . For the entropy and mean gray value comparisons a constant  $V_f = 1$  is used. The best result for a particular configuration is presented in Table 6.1.

First, the performance of the used histogram distances regarding their segmentation accuracies (Mean, StDev) for the different configurations are considered in detail. Results show, that for both configurations and half-/non-overlapping blocks the EMD achieves a good segmentation

Config.	$H_d$	$V_f$	Mean	StDev	R	[ms]	
PBA - Blocksize 16x16	non overlapping	$L_1$	0.9	7.29	3.74	17.0	312
		$L_2$	1.0	7.97	3.4	15.0	310
		H	0.9	7.72	4.16	17.0	312
		$X^2$	0.6	8.55	4.27	17.0	310
		<b>EMD</b>	<b>0.5</b>	<b>6.45</b>	<b>3.41</b>	<b>17.0</b>	<b>304</b>
	half overlapping	$L_1$	-0.5	10.04	5.64	20.0	2135
		$L_2$	-0.4	10.52	4.68	20	2175
		H	-0.3	11.11	5.99	21.0	2278
		$X^2$	-0.9	6.71	4.14	19.0	2000
		<b>EMD</b>	<b>-0.1</b>	<b>5.53</b>	<b>3.3</b>	<b>14.0</b>	<b>1867</b>
PBA - Blocksize 32x32	non overlapping	$L_1$	1.3	10.05	3.46	18.0	258
		$L_2$	1.7	11.13	3.87	17.0	261
		H	1.0	9.45	3.81	18.0	267
		$X^2$	0.6	10.88	4.11	19.0	260
		<b>EMD</b>	<b>1.2</b>	<b>9.34</b>	<b>3.49</b>	<b>16.0</b>	<b>262</b>
	half overlapping	$L_1$	-0.3	8.03	3.03	14.0	1103
		$L_2$	-0.2	8.44	3.12	15.0	1090
		<b>H</b>	<b>-0.3</b>	<b>7.13</b>	<b>3.16</b>	<b>14.0</b>	<b>1078</b>
		$X^2$	-0.6	8.12	3.05	15.0	1064
		<b>EMD</b>	<b>0.4</b>	<b>8.35</b>	<b>3.57</b>	<b>17.0</b>	<b>1043</b>
OBA - Blocksize 32x32	non overlapping	$L_1$	0.9	7.97	4.14	16.0	386
		$L_2$	1.3	9.1	3.84	17.0	372
		H	1.0	8.06	4.31	17.0	377
		$X^2$	0.9	10.24	4.6	17.0	371
		<b>EMD</b>	<b>0.7</b>	<b>7.06</b>	<b>3.38</b>	<b>15.0</b>	<b>360</b>
	half overlapping	$L_1$	-0.7	7.88	4.85	19.0	3622
		$L_2$	-1.0	7.15	3.53	15.0	3484
		H	-0.3	9.21	5.15	20.0	3502
		$X^2$	-0.8	7.21	4.42	18.0	3529
		<b>EMD</b>	<b>0.1</b>	<b>6.19</b>	<b>3.74</b>	<b>18.0</b>	<b>3657</b>
OBA - Blocksize 32x32	non overlapping	$L_1$	<b>1.3</b>	<b>11.6</b>	<b>5.04</b>	<b>31.0</b>	<b>265</b>
		$L_2$	1.4	12.2	5.15	34.0	267
		H	1.8	12.19	4.9	33.0	270
		$X^2$	0.5	13.79	7.68	37.0	278
		<b>EMD</b>	<b>1.6</b>	<b>11.53</b>	<b>5.72</b>	<b>31.0</b>	<b>260</b>
	half overlapping	$L_1$	-0.3	<b>8.47</b>	<b>2.94</b>	<b>13.0</b>	<b>1187</b>
		$L_2$	0.1	9.71	3.47	18.0	1274
		H	0.0	8.37	3.29	15.0	1122
		$X^2$	-0.5	8.83	3.11	13.0	1100
		<b>EMD</b>	<b>0.7</b>	<b>9.5</b>	<b>3.94</b>	<b>17.0</b>	<b>1111</b>

**Table 6.1:** Experiment #1: RLE-IS cross-section segmentation using intensity histograms as texture features – statistical analysis of the pith-based (PBA) and the orientation-based (OBA) segmentation approach using different configurations. The left table shows results for PBA using different block sizes, half- and non-overlapping blocks and different histogram distances  $H_d$ . The same is illustrated for OBA in the right table.

accuracy. In the case of 16x16 pixels blocks (half-/non-overlapping), the most accurate results for PBA and OBA are reached with the EMD (best result 16x16 blocks = PBA/EMD/half-overlapping – Mean: 5.55, StDev: 3.3). For 32x32 blocks the results using EMD are somewhat equal to the results of the other distances (best result 32x32 blocks = PBA/half-overlapping – Mean: 7.13, StDev: 3.16). Although the EMD is not the most accurate distance in all of the tested configurations, it reaches the most consistent results. This confirms that the EMD is a robust and appropriate histogram distance for all tested segmentation configurations.

Second, the impact of the block size and half-/non-overlapping blocks is analysed. For the EMD results, the accuracies of PBA and OBA are better for 16x16 blocks, as well as for half-overlapping blocks. As opposed to the EMD, for  $L_1$ ,  $L_2$  and H the accuracies are not increasing for PBA/16x16 blocks using half-overlapping blocks. Generally, it can be concluded that smaller block sizes and overlapping blocks increase the segmentation accuracy. Especially

for shape estimation, a smaller distance between the block-center points leads to a refinement and increases the accuracy of the cross-section shape estimation.

On the other hand, the block size and the overlapping-factor determine the amount of blocks which are involved in the region growing procedure. The timing measurements of the configurations using 16x16 blocks and/or half-overlapping blocks shows that the performance decreases. For example, PBA/EMD using 16x16 non-overlapping blocks requires 304 ms and with half-overlapping blocks 1867 ms for each image on average. For the different histogram distances no impact on the timing performance is recognizable. Furthermore, the results show that for non-overlapping blocks lower variance factors ( $V_f$ ) and for half-overlapping blocks higher variance factors are required. Overlapping and smaller blocks are more similar than larger sized ones which are not overlapping. Thus, the variance factors for larger sized blocks need to be higher and consequently less restrictive. Smaller block sizes and overlapping blocks require lower variance factors and enable a more accurate segmentation.

Finally, the differences between the results for PBA and OBA are considered. Results show, that the timing performance of all OBA configurations compared to the PBA configurations decreases slightly. This behaviour is caused by the more sophisticated cluster initialisation procedure. Comparing all Mean and StDev results between PBA and OBA it can be recognized that the sophisticated orientation-based cluster initialisation procedure also decreases the accuracy performance. This confirms the assumption that orientation-based cluster initialisation initialises clusters in background regions. PBA using pith-based cluster initialisation is not affected by clusters initialised in the background.

**Experiment #2 - Evaluation of LBP histograms as texture features** The second experiment evaluates the performance of the cross-section segmentation algorithm using LBP histograms as texture features. By analogy to the first experiment, the impact of different local histogram distances, different block sizes and half-/non-overlapping blocks is assessed. Due to the lower performance of OBA in the first experiment, only the PBA is tested. As opposed to the first experiment, the EMD is not evaluated because the bins of the LBP histograms are not ordered in a proper way. For the computation of the LBP histograms four different variations are evaluated. The first variation uses the basic LBP operator and a 3x3 neighbourhood. In the second variation only uniform LBPs are considered for the LBP histograms. As a third variation multiscale LBPs for the LBP histograms are computed. The LBPs are computed for three scales. In the last variation multiscale LBPs are computed and the uniform LBPs are used for the LBP histograms.

The other tested settings and parameters are equal to those from the first experiment. The best results for each configuration, local histogram distance and LBP variation are presented in Table 6.2 .

First, the performance of the different histogram distances regarding their segmentation accuracies (Mean, StDev) is examined. For many configurations no results are presented. In the implementation of the experiments the computation for a certain configuration terminates if the mean accuracy cannot achieve a value lower than 15%. As opposed to the first experiment, not all configurations achieve a mean value lower than 15% and no values are available. The most accurate results for each configuration and LBP variation in Table 6.2 are highlighted in bold.

For most of the configurations and LBP variations the  $L_1$  or  $L_2$  histogram distance achieved good results. Except for one configuration, all of the most accurate results for each configuration are computed using the  $L_2$  norm as local histogram distance. Generally, it seems that the Hellinger and Chiquadrat distance (H and  $X^2$ ) are less suitable for the proposed cross-section segmentation algorithm using LBP histograms.

A closer examination of the segmentation accuracies for different block sizes and half-/non-overlapping blocks is less meaningful. Contrary to the first experiment using intensity histograms, the use of smaller block sizes and overlapping blocks does not increase the segmentation accuracy. Additionally, the accuracies are strongly varying and it is not possible to draw specific conclusions about the impact of the block size and half-/ non-overlapping blocks on the accuracy. To the same extent as in the first experiment, a smaller block size and half-overlapping blocks deteriorate the timing performance.

Next, the differences between the LBP variations are considered in detail. The most accurate results are achieved using the  $L_1$  norm and multiscale or multiscale & uniform LBPs (best result 16x16 blocks = PBA/ $L_1$ /half-overlapping – Mean: 7.5, StDev: 3.41). It is difficult to conclude that using multiscale LBPs or uniform LBPs instead of normal 3x3 LBPs improves the segmentation accuracy. However, the two most accurate results are reached with the LBP extensions. At least, it can be stated that the two LBP extensions influence the timing performance differently. While for uniform LBPs the number of bins in the LBP histogram decreases, for multiscale LBPs the number of bins increases with each scale. Consequently, uniform LBPs increase the timing performance and multiscale LBPs cause a significant deterioration of the timing performance.

3x3 LBPs							
Config.	$H_d$	$V_f$	Mean	StDev	R	[ms]	
PBA - Blocksize 16x16	non	$L_1$	0.9	12.33	4.31	19.0	782
	over-lap-ping	$L_2$	<b>0.9</b>	<b>9.85</b>	<b>4.75</b>	<b>20.0</b>	<b>772</b>
		H	-	-	-	-	-
		$X^2$	0.5	12.94	3.9	18.0	800
	half	$L_1$	0.0	16.83	4.53	45.0	7617
	over-lap-ping	$L_2$	0.0	11.75	7.57	74.0	6887
		H	-	-	-	-	-
		$X^2$	-	-	-	-	-
PBA - Blocksize 32x32	non	$L_1$	0.7	10.96	3.65	19.0	712
	over-lap-ping	$L_2$	0.7	10.15	4.06	19.0	713
		H	1.5	14.98	2.72	14.0	721
		$X^2$	0.5	14.13	2.71	12.0	728
	half	$L_1$	-	-	-	-	-
	over-lap-ping	$L_2$	<b>-0.2</b>	<b>8.88</b>	<b>3.83</b>	<b>25.0</b>	<b>3273</b>
		H	0.0	14.36	2.82	22.0	3431
		$X^2$	-0.4	11.52	2.89	13.0	7155

3x3 uniform LBPs							
Config.	$H_d$	$V_f$	Mean	StDev	R	[ms]	
PBA - Blocksize 16x16	non	$L_1$	0.9	9.63	4.79	20.0	767
	over-lap-ping	$L_2$	1.1	11.41	4.42	20.0	781
		H	0.9	11.94	4.41	18.0	783
		$X^2$	0.3	9.33	4.31	19.0	799
	half	$L_1$	-0.2	10.24	3.57	16.0	7017
	over-lap-ping	$L_2$	0.0	10.86	4.6	32.0	6943
		H	-	-	-	-	-
		$X^2$	<b>-0.4</b>	<b>8.57</b>	<b>2.91</b>	<b>14.0</b>	<b>6636</b>
PBA - Blocksize 32x32	non	$L_1$	0.7	9.7	3.64	16.0	707
	over-lap-ping	$L_2$	<b>0.5</b>	<b>9.66</b>	<b>3.64</b>	<b>14.0</b>	<b>711</b>
		H	0.7	10.61	3.95	17.0	714
		$X^2$	0.1	10.55	3.13	17.0	719
	half	$L_1$	-0.1	13.44	4.07	18.0	2862
	over-lap-ping	$L_2$	0.0	8.67	4.05	25.0	3332
		H	-0.2	10.12	3.8	29.0	3321
		$X^2$	-	-	-	-	-

3x3 multiscale LBP							
Config.	$H_d$	$V_f$	Mean	StDev	R	[ms]	
PBA - Blocksize 16x16	non	$L_1$	1.1	12.32	4.32	19.0	1267
	over-lap-ping	$L_2$	<b>1.3</b>	<b>11.43</b>	<b>4.26</b>	<b>19.0</b>	<b>1294</b>
		H	-	-	-	-	-
		$X^2$	-	-	-	-	-
	half	$L_1$	-	-	-	-	-
	over-lap-ping	$L_2$	0.0	9.37	7.31	73.0	9545
		H	-	-	-	-	-
		$X^2$	0.0	14.48	9.16	71.0	8504
PBA - Blocksize 32x32	non	$L_1$	1.1	9.85	3.57	20.0	1271
	over-lap-ping	$L_2$	1.5	10.05	6.98	53.0	1218
		H	1.3	12.05	3.35	15.0	1308
		$X^2$	0.1	12.68	4.34	39.0	1335
	half	$L_1$	-	-	-	-	-
	over-lap-ping	$L_2$	<b>0.3</b>	<b>7.53</b>	<b>3.45</b>	<b>14.0</b>	<b>5084</b>
		H	-	-	-	-	-
		$X^2$	-	-	-	-	-

3x3 multiscale & uniform LBPs							
Config.	$H_d$	$V_f$	Mean	StDev	R	[ms]	
PBA - Blocksize 16x16	non	$L_1$	<b>0.9</b>	<b>8.89</b>	<b>4.29</b>	<b>16.0</b>	<b>1250</b>
	over-lap-ping	$L_2$	0.9	12.33	4.57	21.0	1312
		H	1.1	13.29	4.04	18.0	1245
		$X^2$	0.5	12.57	4.25	17.0	1263
	half	$L_1$	-	-	-	-	-
	over-lap-ping	$L_2$	0.0	12.31	3.18	14.0	9976
		H	-	-	-	-	-
		$X^2$	0.0	11.53	3.18	14.0	8284
PBA - Blocksize 32x32	non	$L_1$	0.9	9.21	4.93	32.0	1262
	over-lap-ping	$L_2$	1.5	9.32	4.02	34.0	1250
		H	1.5	11.18	3.35	16.0	1287
		$X^2$	0.3	11.6	3.4	22.0	1314
	half	$L_1$	-0.1	11.67	9.41	72.0	5154
	over-lap-ping	$L_2$	<b>0.1</b>	<b>7.5</b>	<b>3.41</b>	<b>15.0</b>	<b>5206</b>
		H	0.3	14.15	3.29	16.0	5383
		$X^2$	-	-	-	-	-

**Table 6.2:** Experiment #2: RLE-IS cross-section segmentation using LBP histograms as texture features – statistical analysis of the pith-based (PBA) using different configurations. The table shows results for PBA using different block sizes, half- and non-overlapping blocks, different histogram distances  $H_d$  and different LBP variations.

Finally, the results are compared to the results of the first experiment. Some results of the LBP configurations are somewhat equivalent to the results from the first experiment. Nevertheless, the results of the first experiment are more robust over all configurations and histogram distances. Furthermore, it is shown that the best results of the first experiment using intensity histograms remarkable outperform the segmentation accuracies and timing measurements of the second experiment using LBP histograms.

**Experiment #3 - Grayscale conversion** The third experiment is based on the insights from the first experiment and evaluates the impact of the different RGB weighting factors for the grayscale conversion on the segmentation accuracy. As in the first experiment intensity histograms are used as texture features. LBP histograms as texture features are not evaluated because it is assumed that they are less affected by the grayscale conversion. This assumption is based on the fact that LBPs are invariant to monotonic intensity changes.

In the experiment different gray scale conversions are tested using the pith based approach and the EMD as local histogram distance for cross-section segmentation. As blocks 16x16 blocks, half- and non-overlapping are tested.

Four different grayscale conversions are evaluated. Like in the previous experiments, the first conversion uses equal weighting factors ( $R=0.33$ ,  $G=0.33$ ,  $B=0.33$ ) for each color channel. The second grayscale conversion uses the weighting factors suggested by Norell and Borgefors (2008) - ( $R=0.2989$ ,  $G=0.5870$ ,  $B=0.1140$ ). Further two tested grayscale conversions are Lightness ( $= \frac{1}{2} \cdot (\max(R,G,B) + \min(R,G,B))$ ) and Luminosity ( $R=0.21$ ,  $G=0.72$ ,  $B=0.07$ ) which are used in GIMP (<http://docs.gimp.org/en/gimp-tool-desaturate.html>).

By analogy to the first experiment each configuration is tested with histogram distance variance factors ( $V_f$ ) in a range between  $[-2.0, 2.0]$ . The most accurate results for each configuration and grayscale conversion are presented in Table 6.3. Generally, it seems that the different grayscale conversion methods have a low impact on the segmentation accuracy. The differences between the results are minimal and no grayscale conversion method can be highlighted.

**Experiment #4** In this experiment the impact of circle and ellipse fitting (Step 2/3 - see Subsection 6.4.3) is evaluated. Circle and ellipse fitting are non-mandatory intermediate steps used in the shape estimation procedure. Furthermore, background corner segmentation is introduced and evaluated. Background corner segmentation is based on the knowledge of the present image structure. With the use of background corner segmentation, the applicability of

Configuration		Conversion	$V_f$	Mean	StDev	R	[ms]
PBA/ EMD Blocksize 16x16	non over- lapping	Equal Weights	0.5	6.45	3.41	17.0	304
		Norell	0.8	7.1	3.75	15.0	303
		Luminosity	0.5	6.66	3.45	17.0	332
		Lightness	0.4	6.25	3.15	14.0	316
	half over- lapping	Equal Weights	-0.1	5.53	3.3	14.0	1867
		Norell	-0.2	5.33	3.03	14.0	1856
		Luminosity	-0.1	5.55	3.41	14.0	1942
		Lightness	-0.1	5.51	3.53	17.0	1991

**Table 6.3:** Experiment #3 - Grayscale conversion: RLE-IS cross-section segmentation using intensity histograms – statistical analysis of the pith based segmentation approach (PBA) using EMD and 16x16 pixels blocks. The two configurations are tested using different grayscale conversions.

the cross-section segmentation approach is limited to a particular image structure. Background corner segmentation and circle-/ellipse fitting are assessed for PBA cross section segmentation using intensity histograms. Analogous to the third experiment, PBA with EMD as local histogram distance is used and 16x16 pixels blocks half-/ and non-overlapping are evaluated. The grayscale conversion uses equal weights.

For background corner segmentation, in each image edge a single cluster is initialized for which the region growing procedure is performed. Background edge segmentation is performed as preceding step to PBA or OBA. The background region growing procedure is performed with a restrictive histogram distance variance factor which is half of the value of the variance factor ( $V_f$ ) used for the subsequent PBA. Blocks which are assigned to one of the background corner clusters are not considered for the subsequent cross-section segmentation approach. Background corner segmentation is suitable for images where the entire cross-section of interest is in the image center. Due to the circular shape, it can be assumed that the image corners contain background information. Prior background corner segmentation can be used to prevent the algorithm from assigning blocks of background cross-sections to the cross-section of interest.

The results for experiment #4 are summarized in Table 6.4. The first row of each configuration shows the reference results (PBA/EMD/Equal Weights). The other results are achieved by using one or both improvement approaches. Results show that background corner segmentation as well as the circle-/ellipse fit step are increasing the segmentation accuracy. The most accurate results are reached when both improvements are applied. As opposed to the background corner segmentation approach, the circle-/ellipse fit approach is very time consuming.

Configuration		Improvement	$V_f$	Mean	StDev	R	[ms]
PBA/ EMD Blocksize 16x16	non over- lapping	(1) Equal Weights	0.5	6.45	3.41	17.0	304
		(1) + (2)Corner segmentation	0.5	5.32	2.3	10.0	317
		(1) + (3)Circle-/Ellipse Fit	0.4	5.99	2.83	12.0	610
		(1) + (2) + (3)	0.6	5.14	2.22	10.0	562
	half over- lapping	(1) Equal Weights	-0.1	5.53	3.3	14.0	1867
		(1) + (2)Corner segmentation	-0.2	4.53	2.38	12.0	1880
		(1) + (3)Circle-/Ellipse Fit	-0.1	5.1	2.85	13.0	2597
		(1) + (2) + (3)	-0.1	4.31	2.19	12.0	2582

**Table 6.4:** Experiment #4: RLE-IS cross-section segmentation – statistical analysis of two improvement approaches using intensity histograms as texture features. Both improvement approaches are tested using the pith based segmentation approach (PBA) with EMD and 16x16 blocks. As reference configuration the results from the previous experiment (#2) using equal weights are presented.

The segmentation accuracies for the most accurate configuration using both improvements (half-overlapping blocks: Mean=4.31, StDev=2.19) are illustrated in Fig.6.12. Both improvements are well suitable for cross-section segmentation in images where the rough log end is the main motive.

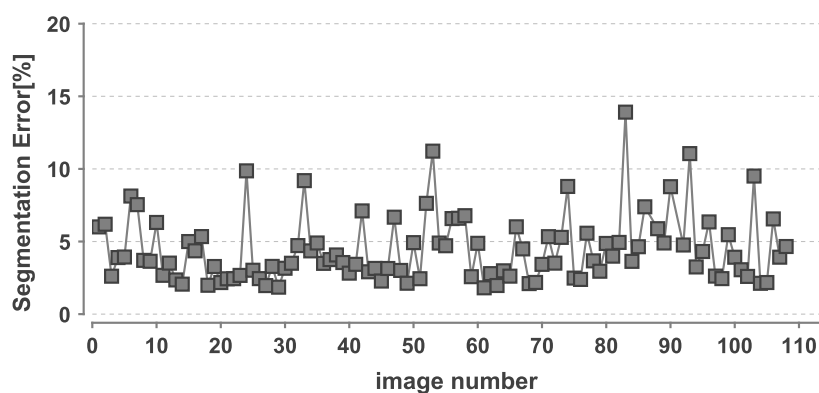


**Figure 6.12:** Segmentation accuracies for the pith based segmentation approach (PBA) using EMD/16x16 half-overlapping blocks and both improvement methods

**Experiment #5** Finally, this experiment evaluates the impact of the improvement steps (background corner segmentation and circle-/ellipse fitting) on cross section segmentation using LBP histograms as texture features. For this purpose, results for PBA using different LBP variations, 16x16 and 32x32 pixels blocks, half-/non-overlapping blocks and  $L_1$  and  $L_2$  as histograms distances were computed. Results from experiment #4 showed that the best

results are achieved using both improvements. Therefore, this experiment just evaluates the combination of both improvements.

For each LBP variation, the configuration with the most accurate results for  $L_1$  and  $L_2$  are presented in Table 6.5.

Configuration			LBP variation	$V_f$	Mean	StDev	R	[ms]
PBA & $L_1$	16x16	non overlapping	8x8 LBP	0.9	8.14	3.13	12.0	1194
	16x16	non overlapping	uniform LBP	0.9	6.54	2.66	11.0	1178
	16x16	non overlapping	multiscale LBP	1.1	7.41	2.47	10.0	1703
	16x16	non overlapping	uniform & multiscale LBP	0.9	6.29	2.34	11.0	1708
PBA & $L_2$	16x16	non overlapping	8x8 LBP	0.9	6.97	2.91	11.0	1203
	16x16	non overlapping	uniform LBP	1.1	7.89	3.06	13.0	1195
	16x16	non overlapping	multiscale LBP	1.3	8.33	3.17	18.0	2025
	16x16	non overlapping	uniform & multiscale LBP	1.3	11.46	3.2	16.0	2003

**Table 6.5:** Experiment #5: RLE-IS cross-section segmentation – statistical analysis of two improvement approaches. Both improvement approaches are tested using the pith based segmentation approach (PBA) and LBP histograms as texture features.

Except for the  $L_2$  – multiscale and multiscale&uniform LBP configurations, all accuracies increased significantly compared to the corresponding results from experiment #2 (see Table 6.3). Results again confirm that background corner segmentation and circle-/ellipse fitting are valuable approaches to increase the segmentation accuracy and on the other hand decrease the timing performance. As in experiment #4 the most accurate results are achieved using 16x16 pixels blocks. Based on all results using intensity histograms it seems that half-overlapping blocks are not crucial to improve the accuracy. All of the best results are achieved using configurations with non-overlapping blocks. Eventually, the most accurate result for all evaluated configurations using LBP histograms is achieved using both improvements, 16x16 non-overlapping pixels blocks, the  $L_1$  norm as histogram distance and the uniform LBP approach (Mean=6.51, StDev=2.66).

## 6.6 Summary

The experiments showed that the pith based segmentation approach (PBA) using intensity histograms is well-suited to segment cross-sections in images of rough log ends. The first experiment highlighted that the EMD is the most robust histogram distance over all evaluated configurations using intensity histograms. The results from the second experiment using LBP

histograms as texture features are very irregular and it is not possible to make statements about appropriate settings and configurations to improve the segmentation. In any case, results from experiment #1 and #2 show that intensity histograms and especially the EMD achieve more accurate results and are faster than the results from the experiments with LBP histograms and bin-by-bin distances. Additionally, the comparison between the results from experiment #1 and #2 leads to an interesting conclusion. For particular segmentation applications, simple texture features and a more sophisticated similarity measure can outperform matured texture features and a simple similarity measure.

Subsequently, some insights from cross-section segmentation using intensity histograms are summarized: Like in the pith estimation experiments, the most accurate segmentation results are reached with a blocks size of 16x16 pixels and half-overlapping blocks. This confirms that the block size and the overlapping between the blocks are very important for cross-section segmentation. Cross-section segmentation using intensity histograms is very fast and the timing performance mainly depends on the block parameters.

Against all expectations, experiment #3 indicates that different weighting factors for the grayscale conversion have less impact on the segmentation accuracy. In the fourth and fifth experiment it is shown that in case of a certain image structure, background corner segmentation and the circle- /ellipse fit approach are helpful extensions to increase the segmentation accuracy.

Future research should use color information for cross-section segmentation. The EMD can be used to compare local color histograms. First investigations indicated that local color histograms can improve the proposed segmentation approach. Further research is required to present results on cross-section segmentation using local color histograms. Furthermore, more investigations on using LBPs and further texture analysis methods are required.

# Chapter 7

## Discussion

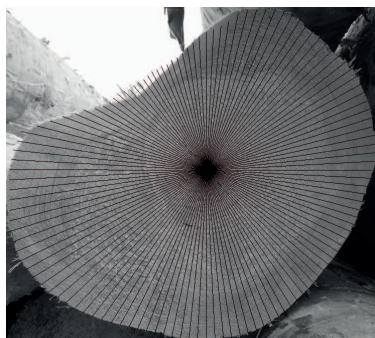
This thesis provides a basis for the further development of the TreeBio framework. The theoretical part serves as introduction into the topic and forms a solid basis for the theoretical considerations to the TreeBio framework. The idea of using log end faces as biometric characteristic to enable log traceability is appealing at first. Biometric recognition has many advantages and the log-processing industries would take a working system with open arms. Unfortunately, there still remain open issues. Future efforts should address these issues to promote the development of a TreeBio framework.

It soon became obvious that it will not be possible to edit and implement all the components which are required for the TreeBio framework. The main issues when using log end faces are caused by disturbances due to cutting or dirt. The TreeBio framework has to be capable of processing images of rough log ends. In the past, only a few works have contributed to the development of cross-section analysis methods treating real world images of log ends.

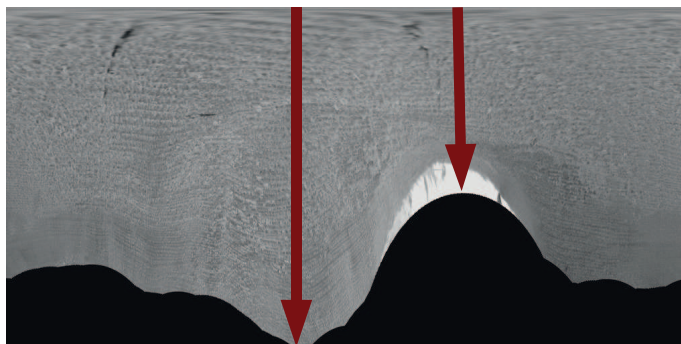
For several reasons, the practical part of this work focuses on the development and evaluation of approaches for pith estimation. These tasks are required as initial image analysis prior to feature extraction. Segmented cross-sections and their pith positions serve as basis for the evaluation of different feature extraction methods used in fingerprint and iris recognition.

Such methods require an alignment/registration of the cross-section surface. For example, iris feature extraction techniques require a polar transformed representation of the cross-section. The pith position and the cross-section boundary are required to polar-transform the cross-section. Figure 7.1a illustrates the sampling (black lines) of the cross-section using the estimated pith position and cross-section boundary. Figure 7.1b illustrates the polar transformed

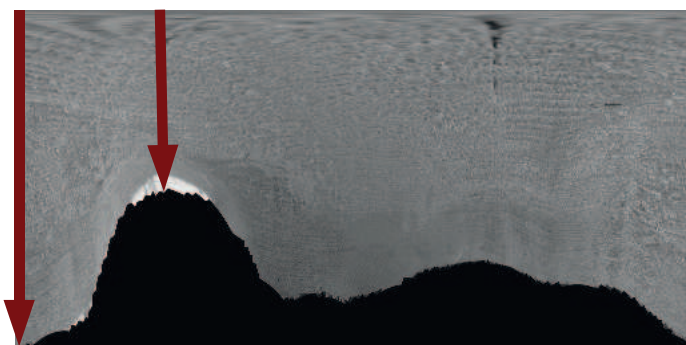
cross-section. By transforming all cross-sections into equally sized polar images, the system becomes scale-invariant. Further, solutions to handle different cross-section rotations and capturing angles are required. In case of rotation invariance in Fig. 7.1b and Fig. 7.1c, a possible solution is depicted. For this purpose, the maximum and minimum pith-to-boundary distances can be used to align the cross-section or the polar transformed cross-section.



(a) Rough log end image – the black lines illustrate the sampling for the polar transformation



(b) Polar transformed cross-section of Fig.7.1a. The two red arrows depict the min. and max. boundary distances.



(c) The min. and max. boundary distances can be used to align the image. Such a procedure may be used to enable a rotation invariant system.

**Figure 7.1:** Polar transformation and image alignment

Besides the requirement for image registration, the evaluation of different feature extraction methods requires appropriate image test sets. One promising approach is the generation of synthetic log end images. The work of Norell (2009b) provides a solution for this. The proposed approach enables creating different images of a certain synthetic cross-section. These images can be simulated with camera positions/lighting conditions and different disturbances. Synthetic images could be used to draw basic conclusions about the applicability of different feature extraction methods to cross-section images.

Conversely, real world image sets captured at different places in the processing chain are

required. Real world image sets exhibit more problems which are relevant for industrial use. In other words, methods and techniques to overcome problems caused by disturbances are necessary.

Until now, only computational and image processing issues have been discussed. Finally, questions regarding the biometric characteristic quality (see Section 2.4.1) of cross-sections are still open. An important question concerns the stability/change of the cross-section and its biometric features along the longitudinal axis of the log. In an industrial application, logs are cross-cut at both log ends before they are sorted in the sawmill. Usually, thin slices are cut off. Consequently, a biometric system requires a certain stability of the biometric features in a small range along the longitudinal axis. It can be assumed that the biometric features at the two ends of a log are completely different.

This discussion showed up several issues and ideas for future work on biometric log traceability of wood logs using log end images. Although the realization of an biometric log recognition approach is very ambitious and many questions remain open, it will be worthwhile to keep on working on it.

# Bibliography

- Andreu, J.-P. and Rinnhofer, A. (2001). Automatic detection of pith and annual rings on industrial computed tomography log images. In *Procs. of the 9th International Conference on Scanning Technology and Process Optimization for the Wood Industry*, pages 37–47, Washington, USA.
- Andreu, J. P., Rinnhofer, A., and Petutschnigg, A. (2002). Enhancement of annual rings on industrial CT images of logs. In *Proceedings of the 16th International Conference on Pattern Recognition (ICPR'02)*, pages 261–264, Washington, USA. IEEE Computer Society.
- Arivazhagan, S., Nidhyandhan, R. S. S., and L.Ganesan (2010). Fruit recognition using color and texture features. *Journal of Emerging Trend in Computing and Information Sciences*, 1:90–94.
- Baumgartner, R., Brüchert, F., and Sauter, U. (2010). Knots in ct scans of scots pine logs. In *Proceedings of the Final Conference on The Future of Quality Control for Wood & Wood Products (COST Action E53)*, Edingburgh, UK.
- Baumgartner, R., Brüchert, F., Staudenmaier, J., and Sauter, U. (2007). Bark measurements with x-ray technology. In *Proceedings of the Conference on Quality Control for Wood and Wood Products (COST E 53)*, pages 13–16, Warsaw, PL.
- Bhandarkar, S., Faust, T., and Tang, M. (1996). A system for detection of internal log defects by computer analysis of axial ct images. In *Proceedings of the 3rd Workshop on Applications of Computer Vision (WACV '96)*, pages 258–263.
- Bhandarkar, S., Luo, X., Daniels, R., and Tollner, E. (2008). Automated planning and optimization of lumber production using machine vision and computed tomography. *IEEE Transactions on Automation Science and Engineering*, 5(4):677–695.
- Bhandarkar, S. M., Faust, T. D., and Tang, M. (1999). Catalog: a system for detection

- and rendering of internal log defects using computer tomography. *Machine Vision and Applications*, 11(4):171–190.
- Bhandarkar, S. M., Luo, X., Daniels, R., and Tollner, E. W. (2005). Detection of cracks in computer tomography images of logs. *Pattern Recognition Letters*, 26(14):2282–2294.
- Bhandarkar, S. M., Luo, X., Daniels, R., and Tollner, E. W. (2006). A novel feature-based tracking approach to the detection, localization, and 3-d reconstruction of internal defects in hardwood logs using computer tomography. *Pattern Analysis Applications*, 9(2):155–175.
- Bhardwaj, A. and Kaur, M. (2013). A review on plant recognition and classification techniques using leaf images. *International Journal of Engineering Trends and Technology*, 4:86–91.
- Bigun, J. (1992). Frequency and orientation sensitive texture measures using linear symmetry. *Signal Processing*, 29:1–16.
- Bigun, J. and Granlund, G. H. (1987). Optimal Orientation Detection of Linear Symmetry. In *Proceedings of the IEEE First International Conf. on Computer Vision*, pages 433–438, London, GB.
- Boukadida, H., Longuetaud, F., Colin, F., Freyburger, C., Constant, T., Leban, J. M., and Mothe, F. (2012). Pithextract: A robust algorithm for pith detection in computer tomography images of wood - application to 125 logs from 17 tree species. *Computers and Electronics in Agriculture*, 85:90–98.
- Breinig, L., Brüchert, F., Baumgartner, R., and Sauter, U. H. (2012). Measurement of knot width in ct images of norway spruce (*picea abies* [l.] karst.)-evaluating the accuracy of an image analysis method. *Computers and Electronics in Agriculture*, 85:149–156.
- Buchanon, J., Cowburn, R., Jausovec, A.-V., Petit, D., S., P., Xiong, G., Atkinson, D., Fenton, K., Allwood, D., and Bryan, T. (2005). Forgery: Fingerprinting documents and packaging. *Nature*, 436:475.
- Canny, J. (1986). A computational approach to edge detection. *IEEE Transactions on Pattern Analysis and Machine Vision*, 8(6):679–698.
- Cerda, M., Hirschfeld-Kahler, N., and Mery, D. (2007). Robust tree-ring detection. In Mery, D. and Rueda, L., editors, *Procs. of Advances in Image and Video Technology*, volume 4872 of *LNCS*, pages 575–585. Springer Berlin / Heidelberg.
- Cha, S.-H. and Srihari, S. N. (2002). On measuring the distance between histograms. *Pattern Recognition*, 35(6):1355–1370.

- Chalifour, A., Nouboud, F., Deprost, B., and Okana, S. (2001). Automatic detection of tree-rings on wood disc images. In *Proceedings of the 5th International Conference on Quality Control by Artificial Vision*, pages 348–352.
- Chan, T., Esedoglu, S., and Ni, K. (2007). Histogram based segmentation using wasserstein distances. In *Proceedings of the 1st international conference on Scale space and variational methods in computer vision, SSVM'07*, pages 697–708, Ischia, ITA. Springer Berlin / Heidelberg.
- Chan, T. and Vese, L. (2001). Active contours without edges. *IEEE Transactions on Image Processing*, 10(2):266–277.
- Chiorescu, S. and Grönlund, A. (2003). The fingerprint approach: using data generated by a 2-axis log scanner to accomplish traceability in the sawmill's log yard. *Forest products journal*, 53:78–86.
- Chiorescu, S. and Grönlund, A. (2004). The fingerprint method: Using over-bark and under-bark log measurement data generated by three-dimensional log scanners in combination with radiofrequency identification tags to achieve traceability in the log yard at the sawmill. *Scandinavian Journal of Forest Research*, 19(4):374–383.
- Clarkson, W., Weyrich, T., Finkelstein, A., Heninger, N., Halderman, J., and Felten, E. (2009). Fingerprinting blank paper using commodity scanners. In *Proceedings of the 30th IEEE Symposium on Security and Privacy*, pages 301–314.
- Conner, W. (1999). A computer vision based tree ring analysis and dating system. Master's thesis, University of Arizona, Department of Electrical & Computer Engineering.
- Conner, W., Schowengerdt, R., Munro, M., and Hughes, M. (1998). Design of a computer vision based tree ring dating system. In *Proceedings of IEEE Southwest Symposium on Image Analysis and Interpretation*, pages 256–261.
- Conner, W. S., Schowengerdt, R. A., Munro, M., and Hughes, M. K. (2000). Engineering design of an image acquisition and analysis system for dendrochronology. *Optical Engineering*, 39(2):453–463.
- Corkery, G., Gonzales Barron, U., Ayalew, G., Ward, S., , and McDonnell, K. (2009). A preliminary investigation of avian comb as a potential biometric marker for identification of poultry. In *Transactions of the ASABE*, volume 52, pages 991–998.

- Cristhian A. Aguilera, Mario A. Ramos, A. D. S. (2012). *Simulated Annealing - Advances, Applications and Hybridizations*, chapter Simulated Annealing: A Novel Application of Image Processing in the Wood Area, pages 91–104. INTECHOPEN.
- Davis, E. R. (2008). *Handbook of Texture Analysis*, chapter Introduction to Texture Analysis, pages 1–33. Imperial College Press.
- Deere, J. (2011). Forest machines - forest heads. [http://www.deere.co.uk/en\\_GB/forestry/forestry\\_equipment/downloads/attachments/harvesting\\_heads\\_brochure.pdf](http://www.deere.co.uk/en_GB/forestry/forestry_equipment/downloads/attachments/harvesting_heads_brochure.pdf). [last accessed: 28.07.2011].
- Dykstra, D. P., Kuru, G., Taylor, R., Nussbaum, R., Magrath, W. B., and Story, J. (2003). Technologies for wood tracking. Technical report, World Bank - WWF Alliance report.
- Edelsbrunner, H., Kirkpatrick, D., and Seidel, R. (1983). On the shape of a set of points in the plane. *Information Theory, IEEE Transactions on*, 29(4):551–559.
- Ekevad, M. (2004). Method to compute fiber directions in wood from computed tomography images. *Journal of Wood Science*, 50(1):41–46.
- Engle, J. B. (2000). A computer-assisted tree-ring chronology composition system. Master's thesis, University of Arizona, Department of Electrical & Computer Engineering.
- Entacher, K., Hegenbart, S., Kerschbaumer, J., Lenz, C., Planitzer, D., Seidel, M., Uhl, A., and Weiglmaier, R. (2008). Pith detection on ct-cross-section images of logs: An experimental comparison. In *Proceedings of the 3rd International Symposium on Communications, Control and Signal Processing*, pages 478–483, St.Julians, MT.
- Entacher, K., Lenz, C., Seidel, M., Uhl, A., and Weiglmaier, R. (2007). Applicability of motion estimation algorithms for an automatic detection of spiral grain in ct cross-section images of logs. In *CAIP*, pages 36–44.
- Fellner, J., Teischinger, A., and Zschokke, W. (2006). *Holzspektrum*. proHolz Austria.
- Flodin, J., Oja, J., and Grönlund, A. (2007). Fingerprint traceability of sawn products using x-ray log scanning and sawn timber surface scanning. In *Proceedings of Quality control for wood and wood products: COST Action E 53 the first conference*.
- Flodin, J., Oja, J., and Grönlund, A. (2008a). Fingerprint traceability of logs using the outer shape and the tracheid effect. *Forest Products Journal*, 58(4):21–27.

- Flodin, J., Oja, J., and Grönlund, J. (2008b). Fingerprint traceability of sawn products using industrial measurement systems for x-ray log scanning and sawn timber surface scanning. *Forest Products Journal*, 58:11.
- Flood, K., Danielsson, P.-E., and Seger, A. M. (2003). On 3d segmentation of knots in 3d-volume data acquired from x-ray linear cone-beam scanning. In Rinnhofer, A., editor, *Proceedings of the 5th International Conference on Image Processing and Scanning of Wood*, pages 151–159.
- Fraunhofer (2010). Rundholz mit Antenne. <http://www.fraunhofer.de/de/presse/presseinformationen/2010/08/rundholz-mit-antenne.html>. [last accessed: 28.07.2011].
- Funt, B. (1985). A computer vision system that analyzes ct-scans of sawlogs. In *Proceedings of IEEE Conference on Computer Vision and Pattern Recognition*, pages 175–177, San Francisco, USA.
- Funt, B. and Bryant, E. (1987). Detection of internal log defects by automatic interpretation of computer tomography images. *Forest Products Journal*, 37(1):56–62.
- Giribalan, G. (2000). An interactive image analysis system for dendrochronology. Master's thesis, University of Arizona, Department of Electrical & Computer Engineering.
- Gjerdrum, P. and Høibø, O. (2004). Heartwood detection in scots pine by means of heat-sensitive infrared images. *Holz als Roh- und Werkstoff*, 62(2):131–136.
- Gonzales-Barron, U., Barry, B., Corkery, G., Donnell, K. M., Butler, F., and Ward, S. (2008). A longitudinal study of the effect of time on the matching performance of a retinal recognition system for lambs. *Computers and Electronics in Agriculture*, 64(2):202–211.
- Gonzales Barron, U., Corkery, G., Barry, B., Butler, F., McDonnell, K., and Ward, S. (2008). Assessment of retinal recognition technology as a biometric method for sheep identification. *Computers and Electronics in Agriculture*, 60(2):156–166.
- Gonzales-Barron, U., Corkery, G., Butler, F., McDonnell, K., and Ward, S. (2007a). A preliminary investigation on face recognition as a biometric identifier of sheep. In *Transactions of the ASABE*, volume 50, pages 313–320.
- Gonzales-Barron, U., Corkery, G., Butler, F., McDonnell, K., and Ward, S. (2007b). Using muzzle pattern recognition as a biometric approach for cattle identification. In *Transactions of the ASABE*, volume 50, pages 1073–1080.

- Gonzalez, R. C. and Woods, R. E. (2001). *Digital Image Processing*. Addison-Wesley, Boston, MA, USA, 2nd edition.
- Granlund, G. H. and Knutsson, H. (1995). *Signal Processing for Computer Vision*. Dordrecht: Kluwer Academic Publishers.
- Hanning, T., Kickingereeder, R., and Casasent, D. (2003). Determining the average annual ring width on the front side of lumber. In Osten, W., Kujawinska, M., and Creath, K., editors, *Proceedings of SPIE: Optical Measurement Systems for Industrial Inspection*, volume 5144, pages 707–716, Munich, Germany.
- Jähne, B. (2005). *Digital Image Processing*. Springer Berlin / Heidelberg, 5th edition.
- Josso, B., Burton, D. R., and Lalor, M. J. (2005). Texture orientation and anisotropy calculation by fourier transform and principal component analysis. *Mechanical Systems and Signal Processing*, 19(5):1152–1161.
- Knutsson, H. and Granlund, G. H. (1983). Texture analysis using two-dimensional quadrature filters. In *IEEE Computer Society Workshop on Computer Architecture for Pattern Analysis and Image Database Management*, Pasadena, USA.
- Korten, S. and Kaul, C. (2008). Application of RFID (Radio frequency identification) in the timber supply chain. *Croatian Journal of Forest Engineering*, 29(1).
- Kvarnström, B. and Oghazi, P. (2008). Methods for traceability in continuous processes—experience from an iron ore refinement process. *Minerals Engineering*, 21(10):720–730.
- Kvarnström, B. and Oja, J. (2008). *Applications of RFID to Improve Traceability in Continuous Processes*, chapter Sustainable Radio Frequency Identification Solutions, page 19. InTech.
- Laggoune, H., Sarifuddin, and Guesdon, V. (2005). Tree ring analysis. In *Procs. of the Canadian Conference on Electrical and Computer Engineering*, pages 1574–1577.
- Lahiri, M., Tantipathananandh, C., Warungu, R., Rubenstein, D. I., and Berger-Wolf, T. Y. (2011). Biometric animal databases from field photographs: identification of individual zebra in the wild. In *Proceedings of the 1st ACM International Conference on Multimedia Retrieval, ICMR '11*, pages 61–68, New York, USA. ACM.
- Li, L. and Qi, D. (2007). Detection of cracks in computer tomography images of logs based on fractal dimension. In *Proceedings of the IEEE International Conference on Automation and Logistics*, pages 2259–2264.

- Li, P., Abbott, A., and Schmoldt, D. (1996). Automated analysis of ct images for the inspection of hardwood logs. In *Proceedings of the IEEE International Conference on Neural Networks*, volume 3, pages 1744–1749.
- Longuetaud, F., Leban, J.-M., Mothe, F., Kerrien, E., and Berger, M.-O. (2004). Automatic detection of pith on ct images of spruce logs. *Computers and Electronics in Agriculture*, 44(2):107–119.
- Longuetaud, F., Mothe, F., Kerautret, B., Krähenbühl, A., Hory, L., Leban, J. M., and Debled-Renneson, I. (2012). Automatic knot detection and measurements from x-ray ct images of wood: A review and validation of an improved algorithm on softwood samples. *Computers and Electronics in Agriculture*, 85:77–89.
- Longuetaud, F., Mothe, F., and Leban, J.-M. (2007). Automatic detection of the heartwood/sapwood boundary within norway spruce (*picea abies* (l.) karst.) logs by means of ct images. *Computers in Electronics and Agriculture*, 58(2):100–111.
- Mäenpää, T. (2003). *The Local Binary Pattern Approach to Texture Analysis - Extensions and Applications*. PhD thesis, University of Oulu.
- Mäenpää, T. and Pietikäinen, M. (2003). Multi-scale binary patterns for texture analysis. In *Proceedings of the 13th Scandinavian conference on Image analysis, SCIA'03*, pages 885–892, Berlin, Heidelberg. Springer-Verlag.
- Maes, R. (2012a). *Physically Unclonable Functions: Constructions, Properties and Applications*. PhD thesis, KU Leuven, <http://www.cosic.esat.kuleuven.be/publications/thesis-211.pdf>. [last accessed: 01.03.2013].
- Maes, R. (2012b). Pufs: Physical(ly) unclonable functions. [homes.esat.kuleuven.be/~rmaes/puf.html](http://homes.esat.kuleuven.be/~rmaes/puf.html). [last accessed: 10.03.2012].
- Maes, R. and Verbauwhede, I. (2010). Physically Unclonable Functions: A Study on the State of the Art and Future Research Directions. In Sadeghi, A.-R. and Naccache, D., editors, *Towards Hardware-Intrinsic Security*, Information Security and Cryptography, pages 3–37. Springer Berlin / Heidelberg.
- Maltoni, D., Maio, D., Jain, A. K., and Prabhakar, S. (2009). *Handbook of fingerprint recognition*. Springer New York.
- Materka, A. and Strzelecki, M. (1998). Texture analysis methods - a review. Technical report, Institute of Electronics, Technical University of Lodz.

- McMillin, C. W. (1982). Application of automatic image analysis in wood science. *Wood Science*, 14:97–105.
- Metois, E., Yarin, P., Salzman, N., and Smith, J. (2002). Fiberfingerprint identification. In *Proceedings of the 3rd Workshop on Automatic Identification*, New York City, USA.
- Norell, K. (2009a). An automatic method for counting annual rings in noisy sawmill images. In *Proceedings of the Conference on Image Analysis and Processing (ICIAP)*, number 5716 in LNCS, pages 307–316. Springer Berlin / Heidelberg.
- Norell, K. (2009b). Creating synthetic log end face images. In *Proceedings of 6th International Symposium on Image and Signal Processing and Analysis (ISPA'09)*, pages 353–358.
- Norell, K. (2010). Counting annual rings on pinus sylvestris end faces in sawmill industry. *Computers and Electronics in Agriculture*, 75(2):231–237.
- Norell, K. and Borgefors, G. (2008). Estimation of pith position in untreated log ends in sawmill environments. *Computers and Electronics in Agriculture*, 63(2):155–167.
- Norell, K. and Lindblad, J. (2008). Spatially-variant morphological operations on binary images based on the polar distance transform. In *Proceedings of 19th International Conference on Pattern Recognition (ICPR'08)*, IEEE Proceedings. IEEE Computer Society.
- Norell, K., Lindblad, J., and Svensson, S. (2007). Grey weighted polar distance transform for outlining circular and approximately circular objects. In *Procs. of 14th International Conference on Image Analysis and Processing (ICIAP'07)*, pages 647–652.
- Nylinder, M., Kuběnka, T., and Hultnäs, M. (2008). Roundwood measurement of truck loads by laser scanning. <http://www.woodtechms.com/paper-logmeter4000.pdf>. [last accessed: 28.07.2011].
- Nystrom, J. and Hagman, O. (1999). Methods for detecting compression wood in green and dry conditions. In *Proceedings of the Conference on Polarization and Color Techniques in Industrial Inspection (SPIE)*, pages 287–294, Bellingham, Wash.
- Ojala, T. and Pietikäinen, M. (2012). Texture classification, machine vision and media processing unit, university of oulu, finland. [http://homepages.inf.ed.ac.uk/rbf/CVonline/LOCAL\\_COPIES/OJALA1/texclas.html](http://homepages.inf.ed.ac.uk/rbf/CVonline/LOCAL_COPIES/OJALA1/texclas.html). [last accessed: 20.05.2013].
- Ojala, T., Pietikäinen, M., and Harwood, D. (1996). A comparative study of texture measures with classification based on featured distributions. *Pattern Recognition*, 29(1):51–59.

- Ojala, T., Pietikainen, M., and Maenpaa, T. (2002). Multiresolution gray-scale and rotation invariant texture classification with local binary patterns. *IEEE Transactions on Pattern Analysis and Machine Intelligence*, 24(7):971–987.
- Österberg, P. (2009). *Wood Quality and Geometry Measurements Based on Cross Section Images*. PhD thesis, Tampere University of Technology, Department of Automation Science and Engineering.
- Österberg, P., Ihalainen, H., and Ritala, R. (2004). Method for analyzing and classifying wood quality through local 2d-spectrum of digital log end images. In *Proceedings of International Conference on Advanced Optical Diagnostics in Fluids*, Tokyo, JP.
- Päivinen, R. and Lindner, M. (2006). Assessment of sustainability of forest-wood chains. Technical report, EFI Technical Report 23.
- Pappu, R. S. (2001). *Physical one-way functions*. PhD thesis, Massachusetts Institute of Technology.
- Pappu, R. S., Recht, B., Taylor, J., and Gershenfeld, N. (2002). Physical one-way functions. *Science*, 297:2026–2030.
- Pele, O. and Werman, M. (2010). The quadratic-chi histogram distance family. In *Proceedings of the 11th European conference on Computer vision: Part II, ECCV'10*, pages 749–762. Springer Berlin / Heidelberg.
- Peterson, G. (2009). The potential of using log biometrics to track sawmill flow. Master's thesis, Oregon State University.
- ProHolz (2007). Dendrochronologie. <http://www.proholz.at/zuschnitt/27/dendrochronologie/>. [last accessed: 28.07.2011].
- Rauschkolb, M. R. (1994). Algorithms for automatic tree ring identification and measurement. Master's thesis, Mississippi State University.
- Rojas, G., Condal, A., Beauregard, R., Verret, D., and Hernández, R. E. (2006). Identification of internal defect of sugar maple logs from ct images using supervised classification methods. *Holz als Roh- und Werkstoff*, 64(4):295–303.
- Rubner, Y., Tomasi, C., and Guibas, L. (1998). A metric for distributions with applications to image databases. In *Computer Vision, 1998. Sixth International Conference on*, pages 59–66.

- Sarigul, E., Abbott, A., and Schmoldt, D. (2003a). Progress in analysis of computed tomography (ct) images of hardwood logs for defect detection. In *Proceedings of the Tenth International Conference on Scanning Technology and Process Optimization in the Wood Industry (ScanTech'03)*, pages 19–30.
- Sarigul, E., Abbott, A., and Schmoldt, D. (2003b). Rule-driven defect detection in ct images of hardwood logs. *Computers and Electronics in Agriculture*, 41:101–119.
- Schmoldt, D., Daniel, L., He, J., and Lynn, A. (1998). A comparison of several artificial neural network classifiers for ct images of hardwood logs. In *Proceedings of Machine Vision Applications in Industrial Inspection VI*, volume 3306, pages 34–43, SPIE.
- Schmoldt, D., He, J., and Abbott, A. (2000). Automated labeling of log features in ct imagery of multiple hardwood species. *Wood and Fiber Science*, 32(3):287–300.
- Schmoldt, D., Li, P., and Abbott, A. (1997). Machine vision using artificial neural networks with local 3d neighborhoods. *Computers and Electronics in Agriculture*, 16(3):255–271.
- Schraml, R. and Uhl, A. (2013). Pith estimation on rough log end images using local fourier spectrum analysis. In *Proceedings of the 14th Conference on Computer Graphics and Imaging (CGIM'13)*, Innsbruck, AUT.
- Sepúlveda, P. (2001). Measurement of spiral grain with computed tomography. *Journal of Wood Science*, 47(4):289–293.
- Sepúlveda, P., Oja, J., and Grönlund, A. (2002). Predicting spiral grain by computed tomography of norway spruce. *Journal of Wood Science*, 48(6):479–483.
- Sliwa, T., Brunet, P., Voisin, Y., C., O. M., Stolz, C., and A. Diou, A. (2003). Détection automatique des stries de croissance des arbres par transformée en ondelettes (automatic detection of growth rings of trees by wavelet transforms). In *Proceedings of the 16th International Conference on Vision Interface*, Halifax, CAN.
- Smith, W. R. (1995a). A prototype and algorithms for tree ring area measurement. In *Proceedings of the 33rd annual on Southeast regional conference*, ACM-SE 33, pages 254–259, New York, USA. ACM.
- Smith, W. R. (1995b). A prototype and algorithms for tree ring area measurement. In *Proceedings of the 33rd annual on Southeast regional conference*, ACM-SE 33, pages 254–259, New York, USA. ACM.

- Som, S., Davis, J., Wells, P., and Svalbe, I. (1993). Morphology methods for processing tomographic images of wood. In *Digital Image Computing: Techniques and Applications (DICTA'93)*, volume 2, pages 564–571, Sydney, AU.
- Som, S., Svalbe, I., Davis, J., Grant, J., Gold, E., Tsui, K., and Wells, P. (1995). Internal scanning of logs for grade evaluation and defect location. In *Digital Image Computing: Techniques and Applications (DICTA'95)*, pages 408–413, Brisbane AU.
- Töyrylä, I. (1999). *Realising the Potential of Traceability – A Case Study Research on Usage and Impacts of Product Traceability*. PhD thesis, Helsinki University of Technology.
- Uusijärvi, R. (2010a). Forest rfid transponder and reader design - indisputable key project. Technical report, IST - ICT for Networked Businesses - Extended products and services. [last accessed: 22.03.2012].
- Uusijärvi, R. (2010b). Indisputable key project. [http://interop-vlab.eu/ei\\_public\\_deliverables/indisputable-key](http://interop-vlab.eu/ei_public_deliverables/indisputable-key). [last accessed: 28.07.2011].
- Vaz, C., Carvalho, P., Duarte, F., and Dourado, A. (2004). A vision-based system for automatic growing ring detection and measurement. *Comput. Ind. Eng.*, 46(2):347–354.
- VirginiaTech - SES Lab (2013). Background on physical unclonable functions. <http://rijndael.ece.vt.edu/puf/background.html>. [last accessed: 01.03.2013].
- Ward, S., McDonnell, K., and F. Butler (2009). Ucd biometrics and food chain - e-tracking group, compendium of recent publications. [http://www.ucd.ie/bioresources/pdfs/Biometric\\_Final%20Document.pdf](http://www.ucd.ie/bioresources/pdfs/Biometric_Final%20Document.pdf). [last accessed: 28.07.2011].
- Wayman, J., Jain, A., and Maltoni, D. (2005). *Biometric Systems*. Springer Berlin / Heidelberg.
- Wehrhausen, M., Norvin, N., Bruchert, F., and Sauter, U. (2012). Crack detection in computer tomographic scans of softwood tree discs. *Forest Products Journal*, 62(6):434–?
- Wei, Q., Chui, Y., Leblon, B., and Zhang, S. (2009). Identification of selected internal wood characteristics in computed tomography images of black spruce: a comparison study. *Journal of Wood Science*, 55(3):175–180.
- Wells, P., Som, S., and Davis, J. (1991). Automated feature extraction from tomographic images of wood. In *Digital Image Computing: Techniques and Applications (DICTA'91)*, volume 2, pages 564–571, Melbourne, AU.

- Wiedenhoeft, A. (2010). *Wood Handbook - Wood as an Engineering Material*, chapter Structure and Function of Wood. Forest Products Laboratory. Wood handbook U.S. Department of Agriculture.
- Wu, J. and Liew, D. (2000). A computer vision method for detection of external log cracks and pith in log cross-section images. In *Procs. of the World Automation Congress: International Symposium on Intelligent Automation and Control (ISIAC'00)*, Hawaii, USA.
- Zhu, D. (1993). *A feasibility study on using ct image analysis for hardwood log inspection*. PhD thesis, Virginia Polytechnic Institute and State University. AA19323799.
- Zhu, D., Conners, R., Schmoldt, D., and Araman, P. (1996). A prototype vision system for analyzing ct imagery of hardwood logs. *IEEE Transactions on Systems, Man, and Cybernetics, Part B: Cybernetics*, 26(4):522–532.